TARGETED CO-DELIVERY OF DOXORUBICIN AND TPGS TO BREAST CANCER CELLS BY PLGA COATED MAGNETIC NANOPARTICLES

A THESIS SUBMITTED TO
THE GRADUATE SCHOOL OF NATURAL AND APPLIED SCIENCES
OF
MIDDLE EAST TECHNICAL UNIVERSITY

BY

ESRA METİN

IN PARTIAL FULFILLMENT OF THE REQUIREMENTS
FOR
THE DEGREE OF MASTER OF SCIENCE
IN
BIOTECHNOLOGY

JANUARY 2017

Approval of the thesis

TARGETED CO-DELIVERY OF DOXORUBICIN AND TPGS TO BREAST CANCER CELLS BY PLGA COATED MAGNETIC NANOPARTICLES

submitted by **ESRA METİN** in partial fulfillment of the requirements for the degree of **Master of Science in Biotechnology Department, Middle East Technical University** by,

Prof. Dr. Gülbin Dural Ünver _____
Dean, Graduate School of **Natural and Applied Sciences**

Assoc. Prof. Dr. Çağdaş Devrim Son _____
Head of Department, **Biotechnolog**

Prof. Dr. Ufuk Gündüz _____
Supervisor, **Biology Dept., METU**

Assoc. Prof. Dr. Pelin Mutlu _____
Co-Supervisor**, Central Laboratory, Mol Bio and Biotech R&D Center, METU**

Examining Committee Members:

Assoc. Prof. Dr. Çağdaş Devrim Son _____
Biology Dept, METU

Prof. Dr. Ufuk Gündüz _____
Biology Dept, METU

Assoc. Prof. Dr. Dilek Keskin _____
Engineering Sciences Dept., METU

Assoc. Prof. Dr. Serap Yalçın Azarkan _____
Molecular Biology and Genetics Dept, Ahi Evran University

Assist. Prof. Dr. Bala Gür Dedeoğlu _____
Biotechnology Institute, Ankara University

Date: 24.01.2017

I hereby declare that all information in this document has been obtained and presented in accordance with academic rules and ethical conduct. I also declare that, as required by these rules and conduct, I have fully cited and referenced all material and results that are not original to this work.

Name, Last name: Esra Metin

Signature:

ABSTRACT

TARGETED CO-DELIVERY OF DOXORUBICIN AND TPGS TO BREAST CANCER CELLS BY PLGA COATED MAGNETIC NANOPARTICLES

Metin, Esra

M.S., Department of Biotechnology

Supervisor: Prof. Dr. Ufuk Gündüz

Co-Supervisor: Assoc. Prof. Dr. Pelin Mutlu

January 2017, 113 pages

Although conventional chemotherapy is the most common method for cancer treatment, it has several side effects such as neuropathy, alopecia and cardiotoxicity. Since the drugs are given to body systemically, normal cells also effect as cancer cells. However, in recent years, targeted drug delivery has been developed to overcome these drawbacks.The targeting strategy can be changed depending on carrier types, but magnetic nanoparticles are commonly preferred due to their easy targetable features by using external magnetic field.

In this study, poly(dl-lactic-co-glycolic acid) (PLGA) coated magnetic nanoparticles were synthesized for targeted co-delivery of doxorubicin and vitamin E TPGS to breast cancer cells. TPGS is known as an inhibitor of multidrug resistance, enhancer of cellular drug uptake and drug release rate. The magnetic nanoparticles were synthesized by co-precipitation method, and then coated with oleic acid. Coated nanoparticles were encapsulated in PLGA and TPGS polymer and drug loaded form of this polymeric magnetic nanoparticle was also produced.

Synthesized nanoparticles were characterized by using FTIR, zeta-potential, XPS, VSM, DLS, TGA, SEM, TEM and spectrophotometric analyses. The results showed that the nanoparticles were spherical, superparamagnetic and drug loaded nanoparticle (NP) size was 121 nm which is in the range for successful targeting. Moreover, TPGS and doxorubicin loading were confirmed by TGA and FTIR analysis. Drug loading and release profiles were studied. It was found that 177 µg doxorubicin was loaded on 1 mg Dox-PLGA-TPGS-MNP (Dox NPT20) nanoparticle and 155 µg on Dox PLGA-MNP (Dox NPT0). In both types of nanoparticles, a sustained release profile was obtained.

Internalization of magnetic polymeric nanoparticles was detected by Prussian blue staining technique. The NPs were taken by cells in 5 hours. Presence of TPGS on core material increased the cellular internalization of nanoparticles in human breast adenocarcinoma cell lines (drug sensitive MCF-7 and doxorubicin resistant MCF-7/Dox cells). Moreover, the targetable properties of magnetic polymeric nanoparticles were shown by applying an external magnetic field. XTT cell proliferation assay indicated that drug free nanoparticles did not killed the cells (MCF-7 and MCF-7/Dox) and the cytotoxic effects of drug loaded nanoparticles on drug sensitive and drug resistant cell lines were shown. The cytotoxic effects of drug loaded nanoparticles increased in the presence of TPGS in core. In addition, TPGS increased the drug accumulation in drug resistant cells.

Doxorubicin and TPGS loaded magnetic polymeric nanoparticles due to their size, biocompatibility, cytotoxicity and targetable properties could be used in new generation targeted chemotherapy.

Keywords: MNP, PLGA, vitamin E TPGS, doxorubicin, MCF-7, drug resistance, targeted drug delivery

ÖZ

PLGA KAPLI MANYETİK NANOPARÇACIKLAR KULLANILARAK DOKSORUBİSİN VE TPGS'İN MEME KANSERİ HÜCRELERİNE HEDEFLENMESİ

Metin, Esra

Yüksek Lisans, Biyoteknoloji Bölümü

Tez Yöneticisi: Prof. Dr. Ufuk Gündüz

Ortak Tez Yöneticisi: Doç. Dr. Pelin Mutlu

Ocak 2017, 113 sayfa

Geleneksel kemoterapi kanser tedavisinde yaygın olarak kullanılmasına rağmen nöropati, saç dökülmesi ve kardiyotoksisite gibi bir çok yan etkisi olan bir yöntemdir. Kemoterapatik ilaç vücuda sistemik olarak verildiği için tüm vücuda yayılır, normal hücreler de kanser hücresi gibi etkilenir. Bu nedenle son yıllarda kemoterapinin yan etkilerini engellemek için ilaç hedefleme sistemleri geliştirilmiştir. Hedefleme stratejisi, kullanılacak olan taşıyıcı sistemin türüne göre değişmektedir. Dışarıdan manyetik alan kullanılarak kolayca hedeflenebilme özelliklerinden dolayı manyetik nanoparçacıklar tercih edilmektedir.

Bu çalışmada, doksorubisin ve E vitaminini meme kanseri hücrelerine hedeflemek için poli(dl-laktik-ko-glikolik asit) (PLGA) kaplı manyetik nanoparçacıklar sentezlenmiştir. TPGS'in çoklu ilaç dirençliliğini azalttığı, ilacın hücre içine alınması ve parçacıktan salınmasını kolaylaştırdığı bilinmektedir, bu nedenle ilaçla birlikte TPGS de nanoparçacıklara yüklenmiştir. Manyetik nanoparçacıklar (MNP) ko-presipitasyon metodu ile sentezlenmiş ve oleik asit (OA) ile kaplanmıştır. Kaplı nanoparçacıklar PLGA ve TPGS polimerleri içine hapsedilmiş ve bu parçacıklara doksorubisin yüklenmiştir.

Sentezlenen nanoparçacıklar FTIR, zeta potansiyel, XPS, VSM, DLS, TGA, SEM, TEM ve spektrofotometrik analizlerle karakterize edilmiştir. Üretilen parçacıkların küresel yapıya ve süperparamanyetik özelliğe sahip olduğu, ilaç yüklü nanoparçacık boyutunun 121 nm olduğu gösterilmiştir. Ayrıca ilaç yüklü PLGA nanoparçacıklarda TPGS ve doksorubisinin varlığı FTIR ve TGA analizleriyle gösterilmiştir. İlaç yükleme ve salım çalışmaları yapılmıştır. 1 mg Dox-PLGA-TPGS-MNP (Dox NPT20)de 177 µg ilacın yüklenirken bu değerin Dox-PLGA-MNP (Dox NPT0)de 155 µg olduğu gözlemlenmiştir. Diğer yandan her iki nanoparçacık türünde de ilaç salımının uzun süreli (35 gün) olduğu saptanmıştır.

Manyetik polimerik nanoparçacıkların hücre içine alımı Prussian mavi boyama tekniğiyle incelenmiş, 5 saat içinde hücrelerin içine alındıkları görülmüştür. TPGS içeren nanoparçacıkların hücre içine alımının daha fazla olduğu belirlenmiştir. Polimer kaplı manyetik nanoparçacıkların hedeflenebilme özelliği manyetik alan kullanılarak gösterilmiştir. Diğer yandan, yapılan XTT analizi sonucunda ilaç içermeyen parçacıkların ilaca duyarlı ve dirençli hücrelerde ölüme neden olmadığı görülmüştür. İlaç yüklü parçacıkların MCF-7 ve MCF-Dox hücreleri üzerindeki sitotoksik etkileri de incelenmiştir.

Nanoparçacık yapısında TPGS'in bulunmasının sitotoksik etkiyi arttırdığı gösterilmiştir. Ayrıca, TPGS'in ilaca dirençli hücre hattında hücre içi ilaç birikimini de arttırdığı görülmüştür.

Doksorubisin ve TPGS yüklü manyetik polimerik nanoparçacıklar boyut, biyouyumluluk, sitotoksisite ve hedeflenebilme özellikleri açısından yeni nesil hedefli kemoterapide kullanılmaya uygundur.

Anahtar sözcükler: MNP, PLGA, vitamin E TPGS, doksorubisin, MCF-7, ilaç dirençliliği, hedefli ilaç iletimi

To my precious family,

ACKNOWLEDGEMENTS

Firstly, I would like to express my gratitude to my supervisor Prof. Dr. Ufuk Gündüz for her advices, supports and encouragements throughout this study. I also would like to convey my thanks to Assoc. Prof. Dr. Pelin Mutlu for her valuable comments on my study and endless encouragements.

I thank to the members of examining committee, Assoc. Prof. Dr. Çağdaş Devrim Son, Assoc. Prof. Dr. Dilek Keskin, Assoc. Prof. Dr. Serap Yalçın Azarkan and Assist. Prof. Dr. Bala Gür Dedeoğlu.

I am obliged to Assoc. Prof. Dr. Bora Maviş for providing the opportunity to use the FTIR and zeta potential instruments in his laboratory.

I am grateful to Maryam Parsian for her advices, endless help and encouragements. I would like to convey my thanks to her for especially invaluable friendship on the outside of the laboratory, too.

I would like to thank my other lab mates Çağrı Urfalı, Negar Taghavi, Ayça Nabioğlu, Hasan Hüseyin Kazan and Gözde Ünsoy for their friendship, helps and sharing their experiences.

My deepest gratitude goes to my mother Fatma, my father Abdullah and my brothers Ersin and Ender for their endless love, support and hand holdings in my life. My sister-in law Selin deserves my special thanks for her moral support in my stressful times.

My warmest thanks to Enes Yurdakul for his helps to overcome in my all disappointments, favour and encouragements in all time.

This study is supported by METU Research Fund (Grant ID: BAP-07-02-2014-007-339).

TABLE OF CONTENTS

ABSTRACT …….....v

ÖZ……...…..vii

ACKNOWLEDGEMENTS…….…..xi

LIST OF FIGURES……...xvii

LIST OF TABLES…….…...xx

LIST OF ABBREVIATIONS…….....xxi

CHAPTERS

1 INTRODUCTION……1

1.1 Cancer……...1

1.1.1 The Hallmarks of Cancer Cells……1

1.1.2 The Characteristics of Tumor Tissue……2

1.1.3 Breast Cancer……4

1.2 Therapy Types for Breast Cancer……6

1.2.1 Surgery……..7

1.2.2 Radiotherapy……..…7

1.2.3 Hormone Therapy……..…7

1.2.4 Chemotherapy……...8

1.2.4.1 Types of Chemotherapy Drugs……..9

1.2.4.1.1 Doxorubicin……....10

1.2.4.2 Multidrug Resistance……...11

1.2.5 Targeted Therapy…….. .13

1.2.5.1 Principles of Drug Targeting……...13

1.2.5.2 Nanocarriers for Targeted Therapy……14
1.3 Magnetic Nanoparticles (MNPs)……14
1.3.1 Types of Magnetization……..15
1.3.2 Biomedical Applications of Magnetic Nanoparticles…….17
1.3.3 Magnetic Nanoparticles for Drug Delivery in Cancer Therapy……..….17
1.3.4 The Principle of Magnetically Targeted Drug Delivery……..…18
1.3.5 The Synthesis Methods for MNP……...19
1.3.5.1 The Co-precipitation Method……..19
1.3.5.2 Surface Modifications of MNPs…….20
1.3.5.2.1 Poly(dl-lactic-co-glycolic acid) (PLGA)……...21
1.3.5.2.1.1 Nanoprecipitation Method……..23
1.3.5.2.2 D-alpha-tocopheryl Polyethylene Glycol 1000 Succinate (TPGS or Vitamin E TPGS)……...24
1.4 Aim of the Study……....25
2 MATERIALS AND METHODS……..27
2.1 MATERIALS…….27
2.1.1 Materials for Nanoparticle Synthesis and Drug Loading Studies……27
2.1.2 Materials for Cell Culture Studies……27
2.2 METHODS…….28
2.2.1 Synthesis of Magnetic Nanoparticles……...28
2.2.2 Coating of Magnetic Nanoparticles with Oleic Acid……...29
2.2.3 Synthesis of Polymeric Magnetic Nanoparticles Containing TPGS…….. .29
2.2.4 Conversion of Water Soluble Dox-HCl to Water Insoluble Dox…….30
2.2.5 Synthesis of Doxorubicin Loaded TPGS Containing Polymeric Magnetic Nanoparticles…….30

2.2.6 Drug Loading……31

2.2.7 Drug Release……....32

2.2.8 Characterization of Nanoparticles……....32

2.2.8.1 Fourier Transform Infrared (FTIR) Spectroscopy…….....33

2.2.8.2 Zeta-Potential Analysis.…….33

2.2.8.3 Scanning Electron Microscopy (SEM)……..33

2.2.8.4 Transmission Electron Microscopy (TEM)……...33

2.2.8.5 Vibrating Sample Magnetometer (VSM)……. 34

2.2.8.6 Dynamic Light Scattering (DLS) Analysis.……. 34

2.2.8.7 UV Spectrophotometer……. 34

2.2.8.8 Thermal Gravimetric Analyses (TGA)……. 34

2.2.8.9 X-ray Photoelectron Spectroscopy (XPS)…… 34

2.2.8.10 Hydrophobicity and Magnetic Sensitivity Test……...35

2.2.9 Cell Culture Studies……..35

2.2.9.1 Cell Lines and Culture Conditions…….35

2.2.9.2 Cell Passaging……....36

2.2.9.3 Cell Freezing……..36

2.2.9.4 Cell Thawing……..37

2.2.9.5 Viable Cell Counting…….37

2.2.9.6 Prussian Blue Staining for Detection of Nanoparticle Internalization..38

2.2.9.7 Magnetic Targeting of NPT20 with an External Field……..39

2.2.9.8 Determination of Drug Accumulation……...39

2.2.9.9 XTT Cell Proliferation Assay……....39

2.2.9.10 Stability of Dox NPT20s……...41

3 RESULTS & DISCUSSION……..41
3.1 Synthesis and Characterization of Magnetic Nanoparticles……41
3.1.1 Hydrophobicity and Magnetic Sensitivity Test……42
3.1.2 Transmission Electron Microscopy (TEM)……..44
3.1.3 Fourier Transform Infrared Spectroscopy (FTIR)……46
3.1.4 Vibrating Sample Magnetometer (VSM)……47
3.1.5 X-ray Photoelectron Spectroscopy (XPS)……48
3.1.6 Zeta Potential Analysis.……50
3.2 Synthesis and Characterization of Magnetic Polymeric Nanoparticles……..51
3.2.2 Zeta Potential Analysis.……52
3.2.3 Dynamic Light Scattering (DLS) Analysis.……53
3.2.4 Thermal Gravimetric Analysis (TGA)……54
3.2.5 Scanning Electron Microscopy……56
3.3 Synthesis and Characterization of Drug Loaded Magnetic Polymeric …….
Nanoparticles……57
3.3.1 UV-Vis Absorption Spectroscopy……....57
3.3.2 Fourier Transform Infrared Spectroscopy (FTIR)……...58
3.3.3 Scanning Electron Microscopy (SEM)……59
3.3.5 Dynamic Light Scattering (DLS) Analysis.……61
3.3.6 Thermal Gravimetric Analysis (TGA)……62
3.4 Drug Loading…… 63
3.5 Drug Release……...66
3.6 Cell Culture Studies……69
3.6.1 Development of Drug Resistant Cell Line……...69

3.6.2 Prussian Blue Staining for Detection of Nanoparticle Internalization…….71

3.6.3 Magnetic Targeting of NPT20 by External Field…….72

3.6.4 Determination of Drug Accumulation……..74

3.6.5 Anti-proliferative Effect of Nanoparticles on Cells……..…...75

3.6.5.1 In Vitro Cytotoxicity of NPT20 and Dox NPT20 on MCF-7 Cells…..76

3.6.5.2 In Vitro Cytotoxicity of NPT0 and Dox NPT0 on MCF-7 Cells……..77

3.6.5.3 In Vitro Cytotoxicity of NPT20 and Dox NPT20 on MCF-7/Dox……...
Cells……...79

3.6.5.4 In Vitro Cytotoxicity of NPT0 and Dox NPT0 on MCF-7/Dox Cells .80

3.6.6 Stability of Dox NPT20s.…….85

4 CONCLUSION…….84

REFERENCES…….87

APPENDICES……102

A. Calibration Curves and Cumulative Drug Releases……..100

B. Drug Loading…….....104

C.Cytotoxicity of Doxorubicin on MCF-7 and MCF-7/Dox Cells……105

D. Cytotoxicity of NPT20 and Dox NPT20 on MCF-7 Cells…….…...107

E. Cytotoxicity of NPT0 and Dox NPT0 on MCF-7 Cells…….…107

F. Cytotoxicity of NPT20 and Dox NPT20 on MCF-7/Dox Cells:…….....109

G. Cytotoxicity of NPT0 and Dox NPT0 on MCF-7/Dox Cells…….110

LIST OF FIGURES

FIGURES

Figure 1.1 Hallmarks of cancer cells…….2
Figure 1.2 Vascular pathophysiology and EPR effect in nanoparticle delivery……4
Figure 1.3 Anatomy of breast……4
Figure 1.4 Some symptoms of breast cancer…….5
Figure 1.5 Ten leading cancer types for the estimated new cancer cases and deaths by sex……6
Figure 1.6 Side effects of chemotherapy……...8
Figure 1.7 Chemical structure of Doxorubicin (Hydrochloride)…….11
Figure 1.8 Contributing factors of MDR…….11
Figure 1.9 (a) Passive , (b) active and (c) triggered targeting…….13
Figure 1.10 Nanocarrier types …….13
Figure 1.11 a) diamagnetic state b) paramagnetic state c) ferromagnetic state..…..15
Figure 1.12 Biomedical applications of magnetic nanoparticles……..17
Figure 1.13 Drug delivery process by using MNPs……..18
Figure 1.14 The structure of oleic acid…….20
Figure 1.15 Chemical structure of PLGA …….....21
Figure 1.16 Internalization of PLGA nanoparticles by the cell……22
Figure 1.17 Nanoprecipitation method for nanoparticle synthesis …….24
Figure 1.18 Chemical structure of TPGS…….24
Figure 2.1 Synthesis of MNP by co-precipitation method…..…….29
Figure 2.2 Synthesis of Dox-PLGA-TPGS-MNP by nanoprecipitation method….31
Figure 3.1 MNP in water (a) in the absence of magnet and (b) in the presence of magnet…..……..44
Figure 3.2 OA-MNP in DCM (a) in the absence of magnet and (b) in the presence of magnet……...44

Figure 3.3 OA-MNP in water and DCM (a) in the absence of magnet and (b) in the presence of magnet ……..45
Figure 3.4 TEM images of the MNP in water……46
Figure 3.5 TEM images of the OA-MNP in ethanol……..46
Figure 3.6 FTIR spectra for (a) MNP and (b) OA-MNP ……...…..……47
Figure 3.7 Chelating bidentate interaction between the COO- group of oleic acid and the iron atom……48
Figure 3.8 VSM analysis of OA-MNP MNP (a) at 25°C and (b) at 37°C…..……..49
Figure 3.9 X-ray photoelectron spectra of the synthesized MNPs (Fe2p spectrum was expanded.)……...50
Figure 3.10 X-ray photoelectron spectra of OA-MNPs (Fe2p and C1s spectra were expanded.)…….50
Figure 3.11 Zeta potential of (a) MNP and (b) OA-MNP…..……...52
Figure 3.12 FTIR spectrum of (a) PLGA-TPGS NP and (b) PLGA-TPGS-MNP....53
Figure 3.13 Zeta potential of (a) PLGA NP, (b) PLGA-TPGS NP and (c) PLGA-TPGS-MNP…….……..…….45
Figure 3.14 Hydrodynamic size distribution of PLGA-TPGS-MNP…..……..55
Figure 3.15 Thermal gravimetric analysis of TPGS…..……56
Figure 3.16 Thermogram for the weight loss of PLGA-TPGS NP……..…….56
Figure 3.17 Thermogram for weight loss of PLGA-TPGS-MNP (NPT20)……..…57
Figure 3.18 SEM image of PLGA-TPGS-MNPs……..……58
Figure 3.19 UV-Vis absorption spectra of Dox-PLGA-TPGS-MNP, PLGA-TPGS-MNP and doxorubicin dissolved in DCM, respectively……59
Figure 3.20 The FTIR spectra of (a) free doxorubicin and (b) Dox NPT20…….…60
Figure 3.21 The FTIR spectra of (a) free doxorubicin, (b) Dox NPT20, (c) PLGA-TPGS-MNP and (d) PLGA-TPGS NP…..……..61
Figure 3.22 SEM images of Dox NT20……...……..61
Figure 3.23 Zeta potential of Dox NPT20…...……..62
Figure 3.24 Hydrodynamic size distribution of Dox NPT20……..……..63
Figure 3.25 Thermogram of Dox NPT20 at 25-650°C…...……...64

Figure 3.26 The drug loading efficiency depending on added drug amount…….....66
Figure 3.27 Calibration curve for doxorubicin in pH 7.4 buffer……..…….68
Figure 3.28 Cumulative drug release profile of Dox NPT20 at pH 7.4……..…..69
Figure 3.29 Cumulative drug release of Dox NPT20 at pH 4.2, 5.2 and 7.4 in 24 hour ……...70
Figure 3.30 Cumulative drug release profile of Dox NPT0 at pH 7.4..……..…71
Figure 3.31 Cell proliferation profile of sensitive MCF-7 cells treated with increased concentration of doxorubicin...……..72
Figure 3.32 Cell proliferation profile of resistant MCF-7/Dox cells treated with increased concentration of doxorubicin……72
Figure 3.33 Light microscope imaging of MCF-7 cells (a) non-treated, (b) treated with NPT0 and (c) NPT20…..……74
Figure 3.34 Light microscope imaging of MCF-7/Dox cells (a) non-treated, (b) treated with NPT0 and (c) NPT20…..……74
Figure 3.35 Magnetic targeting of NPT20; (a) injection NPs to the canal, (b) and (c) accumulation of NPs, (d) removal of magnetic field, (e) dispersion of NPs and (f) re-accumulation of NPs when magnetic field returned…..…….68
Figure 3.36 Light microscope images of the cells (a) on the left, (b) middle and (c) right well……..…….69
Figure 3.37 Florescence microscope images of MCF-7/Dox cells (a) treated with 5µM Dox, (b) 5µM Dox and 20µg/ml NPT0, (c) 5µM Dox and 20µg/ml NPT20, (d) 5µM Dox and 200 µg/ml NPT20 and (e) 5µM Dox and 10 µg/ml TPGS……70
Figure 3.38 Cell proliferation profile of MCF-7 cells treated with NPT20 and Dox NPT20……79
Figure 3.39 Cell proliferation profile of MCF-7 treated with Dox NPT0…..……...80
Figure 3.40 Cell proliferation profile of MCF-7 treated with Dox NPT20 and Dox NPT0 containing the same amount of loaded doxorubicin…….81
Figure 3.41 Cell proliferation profile of MCF-7/Dox cells treated with NPT20 and Dox NPT20…….81
Figure 3.42 Cell proliferation profile of MCF-7/Dox treated with Dox NPT0..…...83

Figure 3.43 Cell proliferation profile of MCF-7/ Dox cells treated with Dox NPT0 and Dox NPT20 containing the same amount of loaded doxorubicin……...84
Figure A.1 Calibration curve for doxorubicin in pH 4.2 buffer……..……105
Figure A.2 Cumulative drug release at pH 4.2……....105
Figure A.3 Calibration curve for doxorubicin in pH 5.2 buffer……..……....106
Figure A.4 Cumulative drug release at pH 5.2……....106
Figure A.5 Calibration curve for doxorubicin in water……..……....107
Figure B.1 Drug loading to nanoparticles depending on added drug amount.....…108
Figure C.1 Cell proliferation profile of MCF-7 treated with doxorubicin…....….109
Figure C.2 Cell proliferation profile of MCF-7/Dox treated with doxorubicin.....109
Figure D.1 Cell proliferation profile of MCF-7 treated with Dox NPT20…..…....110
Figure D.2 Cell proliferation profile of MCF-7 treated with NPT20…..…..……..110
Figure E.1 Cell proliferation profile of MCF-7 treated with Dox NPT0.…..…….111
Figure E.2 Cell proliferation profile of MCF-7 treated with Dox NPT0 containing same amount Dox with Dox NPT20…….……111
Figure E.3 Cell proliferation profile of MCF-7 treated with NPT0.……112
Figure F.1 Cell proliferation profile of MCF-7/Dox treated with NPT20.……..…113
Figure F.2 Cell proliferation profile of MCF-7/Dox treated with Dox NPT20.....113
Figure G.1 Cell proliferation profile of MCF-7/Dox treated with Dox NPT0.…..…114
Figure G.2 Cell proliferation profile of MCF-7/Dox treated with NPT0……..…114
Figure G.3 96-well plate image at the end of XTT cell proliferation assay……..…115

LIST OF TABLES

TABLES

Table 1.1 Comparison of different methods for MNP synthesis……...16
Table 3.1 Entrapment efficiency, loading content and loading efficiency depending on the drug added during synthesis……...55
Table 3.2 Comparison of Dox NPT0 and Dox NPT20 in terms of EE (%), loading content and loading efficiency (%)……56
Table 3.3 Comparison of IC_{50} values of MCF-7 and MCF-7/Dox cells treated with Dox NPT20 and Dox NPT0…….……..68

LIST OF ABBREVIATIONS

ACS	American Cancer Society
BT	Body temperature
dH_2O	Distilled water
diH_2O	Deionized water
DCM	Dichloromethane
DMSO	Dimethyl sulfoxide
Dox	Doxorubicin
Dox NPT0	Doxorubicin loaded magnetic PLGA nanoparticle (0% TPGS, 100% PLGA)
Dox NPT20	Doxorubicin loaded magnetic PLGA nanoparticle (20% TPGS, 80% PLGA)
Dox-PLGA-TPGS-MNP	Dox and TPGS loaded magnetic PLGA nanoparticle
EE	Encapsulation efficiency
FBS	Fetal bovine serum
HCl	Hydrochloric acid
OA-MNP	Oleic acid coated Fe_3O_4 nanoparticle
PLGA	Poly(dl-lactic-co-glycolic acid)
PLGA-TPGS- MNP nanoparticle	TPGS loaded and magnetic nanoparticle encapsulated PLGA
M-H	Magnetization versus applied magnetic field

MNP	Fe_3O_4 nanoparticle
MRI	Magnetic Resonance Imaging
NCI	National Cancer Institute
NPT0	Magnetic PLGA nanoparticle (0% TPGS, 100% PLGA)
NPT20	Magnetic PLGA nanoparticle (20% TPGS, 80% PLGA)
RES	Reticuloendothelial System
RT	Room temperature
TEA	Triethylamine
TPGS	D-alpha-tocopheryl polyethylene glycol 1000 succinate
XTT	Sodium(2,3-bis(2-methoxy-4-nitro-5-sulphophenyl)-2 Htetrazolium-5-carboxanilide proliferation assay

CHAPTER 1

INTRODUCTION

1.1 Cancer

Cancer is a collection of diseases where some cells of the body proliferate irregularly and continuously, also spread into other parts of the body. Normal cells in human body proliferate in limited number which is controlled with growth factors. If the cells are damaged, they are repaired or go to apoptosis. On the other hand, cancer cells have defects in the control mechanisms related with cell division, cell repair or cell death process. Hence, they proliferate continuously (National Cancer Institute, 2016).

Normal cells can be converted to cancer cells owing to development of abnormal properties resulted from some mutations with chemicals, radiation, UV light and errors during chromosome replication. These mutagens can alter the structure of the DNA by affecting on nucleotides or bases, some errors occur in protein synthesis process due to DNA damage (Ruddon, 2007).

1.1.1 The Hallmarks of Cancer Cells

The cancer cells (malignant cells) which are transformed from normal cell have some common characteristics (Figure 1.1); evading growth suppressors, sustaining proliferative signaling, resisting cell death, deregulating cellular energetics, genome instability and mutation, inducing angiogenesis, activating invasion and metastasis, tumor promoting inflammation, enabling replicative immortality (Hanahan & Weinberg, 2011).

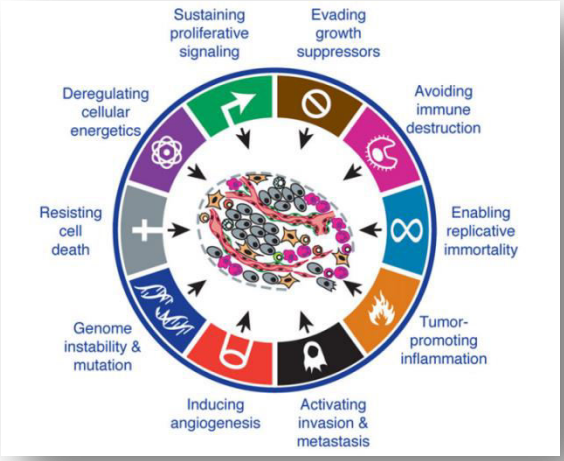

Figure 1.1 Hallmarks of cancer cells (Hanahan & Weinberg, 2011)

1.1.2 The Characteristics of Tumor Tissue

Acidic Microenvironment

The intracellular pH is neutral (pH 7.2 in normal breast duct cell) if oxygen and energy are available while extracellular pH is more alkaline (pH 7.4). On the other hand, tumor cells prefer glycolysis to produce energy even if in the absence of oxygen; thus, glycolytic acidosis is formed. However, in tumor cells, intracellular pH is maintained (pH 7.4 in breast duct cancer cell) via lactate efflux by monocarboxylate transporters and H^+ efflux by Na^+ driven proton pump, so extracellular pH is maintained as more acidic (pH 6.8). Thus, a pH gradient is formed through cell membrane in tumor cells. However, this gradient is opposite of the gradient in normal cells where intracellular pH is lower than extracellular pH. The slightly acidic extracellular pH in cancer cells provides an advantage for migration and angiogenesis (Damaghi, Wojtkowiak, & Gillies, 2013).

In addition to this, cancer cells perform lactic acid fermentation by splitting glucose to lactic acid which is another reason of acidic pH at the extracellular part of the tumor cells. The generated lactic acid increases proton accumulation and elevates respiratory quotients (respiratory quotient = CO_2 output/O_2 uptake) to higher than 1.5 in tumor cells (Vaupel, 2004)**.** It has been showed that cancer cells can produce the same amount of energy from fermentation and respiration, while in normal cells the energy obtained from respiration is higher than that of obtained from fermentation (Seyfried & Huysentruyt, 2013).

Enhanced Permeability and Retention (EPR)

In most solid tumors, there are newly formed micro vessels having several functional and structural abnormalities such that they are dilated, tortuous, saccular and elongated. The hydrostatic pressure which leads to viscous resistance to flow and the vascular permeability in tumor tissue increased due to incomplete endothelial lining and interrupted basement membranes. This phenomenon is called EPR effect (Vaupel, 2004).

Although the permeability of the vessels is increased in tumors, not all the blood vessels are leaky. The vascular permeability can be altered in the tumors of the same body, also it can vary in the same tumor tissue during tumor growth, regression and relapse (Fukumura & Jain, 2007).

In Figure 1.2, the vascular structure in normal and tumor tissue is shown. Leaky vascularization in tumor tissue allows the extravasation and accumulation of nanoparticles in solid tumor site. In contrast, nanoparticles cannot leak through intact vessels belonging to normal tissue, so systemic toxicity is prevented (Prabhakar *et al*., 2013).

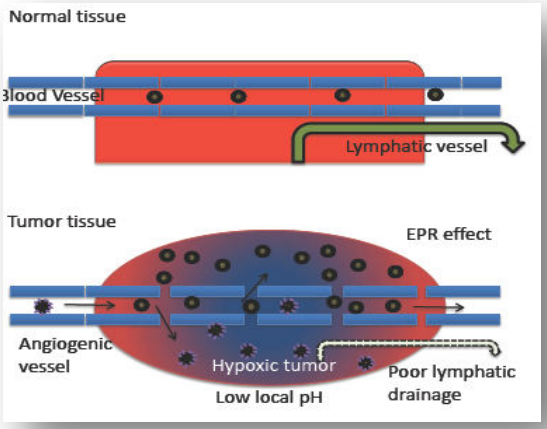

Figure 1.2 Vascular pathophysiology and EPR effect in nanoparticle delivery (Upreti, Jyoti, & Sethi, 2013)

1.1.3 Breast Cancer

Breast cancer is the most common type of cancer among women, but also it can be developed in men. It is a heterogeneous disease which have two main types; ductal carcinoma (ducts are the part of breast carrying milk to nipple) and lobular carcinoma (lobules glands where milk made). The normal breast anatomy is shown in Figure 1.3.

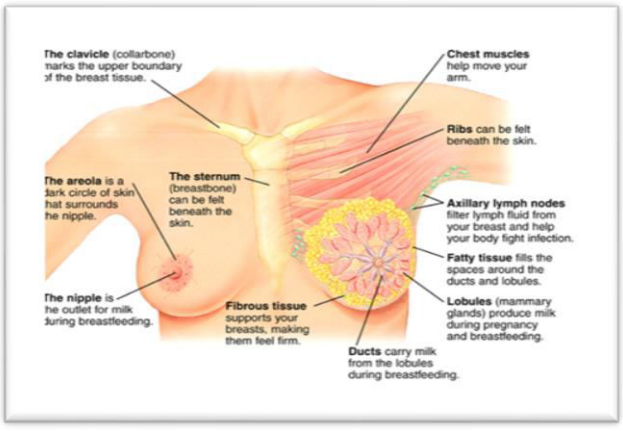

Figure 1.3 Anatomy of breast (Gabriel & Maxwell, 2016)

The woman especially who are under breast cancer risk and having symptoms should be checked in certain time intervals. Some of the symptoms are seen in Figure 1.4. In order to be sure, some imaging tests could be used; mammograms, breast ultrasound, magnetic resonance imaging (MRI) of the breast, ductogram (in nipple discharge cases) and biopsy (Institute, 2016).

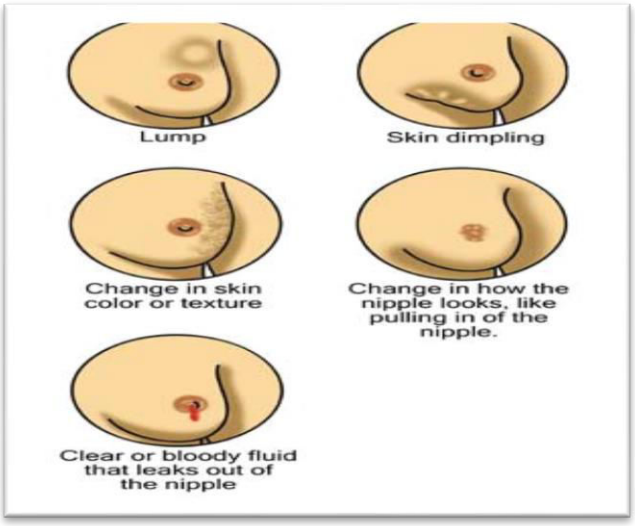

Figure 1.4 Some symptoms of breast cancer (Nordqvist, 2016)

There are some risk factors for developing breast cancer; getting older, genetics (familial tendency), having a history of the breast cancer, having had certain types of breast lumps, dense breast tissue, estrogen exposure (having earlier period starting or later menopause), obesity, alcohol consumption (Nordqvist, 2016). In 2016, breast cancer is at top of the cancer types are developed in woman in the USA (Figure 1.5.).

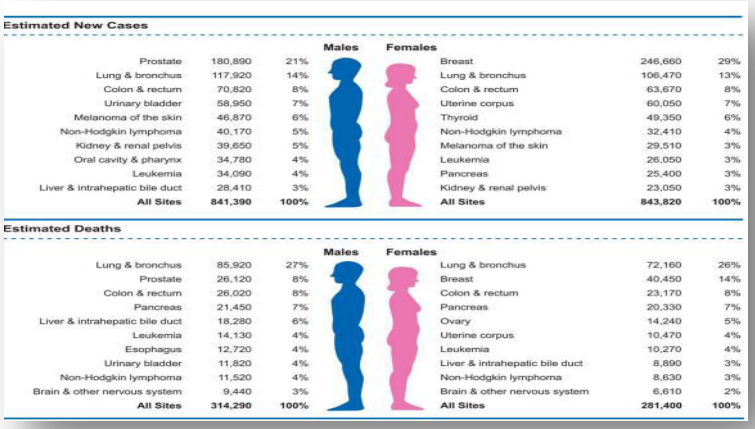

Estimated New Cases

Males			Females		
Prostate	180,890	21%	Breast	246,660	29%
Lung & bronchus	117,920	14%	Lung & bronchus	106,470	13%
Colon & rectum	70,820	8%	Colon & rectum	63,670	8%
Urinary bladder	58,950	7%	Uterine corpus	60,050	7%
Melanoma of the skin	46,870	6%	Thyroid	49,350	6%
Non-Hodgkin lymphoma	40,170	5%	Non-Hodgkin lymphoma	32,410	4%
Kidney & renal pelvis	39,650	5%	Melanoma of the skin	29,510	3%
Oral cavity & pharynx	34,780	4%	Leukemia	26,050	3%
Leukemia	34,090	4%	Pancreas	25,400	3%
Liver & intrahepatic bile duct	28,410	3%	Kidney & renal pelvis	23,050	3%
All Sites	**841,390**	**100%**	**All Sites**	**843,820**	**100%**

Estimated Deaths

Males			Females		
Lung & bronchus	85,920	27%	Lung & bronchus	72,160	26%
Prostate	26,120	8%	Breast	40,450	14%
Colon & rectum	26,020	8%	Colon & rectum	23,170	8%
Pancreas	21,450	7%	Pancreas	20,330	7%
Liver & intrahepatic bile duct	18,280	6%	Ovary	14,240	5%
Leukemia	14,130	4%	Uterine corpus	10,470	4%
Esophagus	12,720	4%	Leukemia	10,270	4%
Urinary bladder	11,820	4%	Liver & intrahepatic bile duct	8,890	3%
Non-Hodgkin lymphoma	11,520	4%	Non-Hodgkin lymphoma	8,630	3%
Brain & other nervous system	9,440	3%	Brain & other nervous system	6,610	2%
All Sites	**314,290**	**100%**	**All Sites**	**281,400**	**100%**

Figure 1.5 Ten leading cancer types for the estimated new cancer cases and deaths by sex (Siegel, Miller, & Jemal, 2016)

1.2 Therapy Types for Breast Cancer

There are some factors affecting the decision for what type of therapy used in breast cancer: The stage and grade of the cancer (size, localization and spreading of the tumor), hormone sensitivity of the cancer cells, other diseases on the patient, sex and age of the patient, the preferences of the patient (Coates *et al.*, 2015).

1.2.1 Surgery

Surgery is applied to most of the women having breast cancer for treatment. However, the reason of the surgery may differ among patients; thus, doctors could perform different types of surgery depending on situation (Harmer, 2011). If tumor is small and could be removed easily from the tissue, tumor and a thin layer of normal tissue around tumor are removed by surgery which is lumpectomy (breast conserving surgery). The other operation which is called as mastectomy is removing of the breast. This type of surgery involves removal of lobules, ducts, nipple, fatty tissue and some part of the skin

(in radical cases also muscle of the chest wall and lymph nodes in the armpit). If breast cancer reaches to a lymph node, the lymph node should be removed surgically; otherwise, cancer can spread to other part of the body through lymphatic system. This procedure is called as sentinel node biopsy. In the more radical cases, several lymph nodes should be removed in the armpit by an operation called axillary lymph node dissection (Nordqvist, 2016).

1.2.2 Radiotherapy

In radiation therapy, high energy rays like X-rays or particles are used to destroy cancer cells. The radiation could come from an external machine outside the body, called external beam radiation. On the other hand, in the internal radiation type a radioactive source could be placed inside the body for a short time. One type or combination of them could be used for treatment which depends on type or stage of the cancer. The patients could be needed radiation therapy after some types of surgery if cancer cells spread to other parts of the body (Sedlmayer *et al*., 2013).

1.2.3 Hormone Therapy

Approximately 70% of the breast cancers are sensitive to estrogen or progesterone hormone (ER^+ or PR^+) which means that cancer cells have receptors on the surface and hormones (estrogen or progesterone) bind to them, leading the activation of genes that are responsible for cellular proliferation. Therefore, if the level of hormone decreases or hormone-receptor binding is prevented in hormone sensitive cancer cells, the treatment would be successful. For this purpose, several drugs are produced; Toremifene (Fareston) and Tamoxifen prevent estrogen binding while Fulvestrant decreases estrogen receptor level (Chlebowski & Anderson, 2012).

1.2.4 Chemotherapy

Chemotherapy, usually refers to the use of medicines or drugs to treat cancer. This therapy type could be applied before/after the surgery or as main treatment. In adjuvant therapy, the anti-cancer drugs could be given after the surgery to remove all cancer cells which spread to other parts of the body or could not be seen in imaging tests. Conversely, chemotherapy could be applied before the surgery to shrink the tumor that is too big for removal by surgery (Kuehn *et al.*, 2013).

However, chemotherapy acts not only on the cancer cells, but also actively dividing healthy cells such as the cells of skin, hair, nails, mouth, digestive tract and reproductive system (Botchkarev & Sharov, 2016). Thus, the chemotherapy has massive side effects as shown in Figure 1.6.

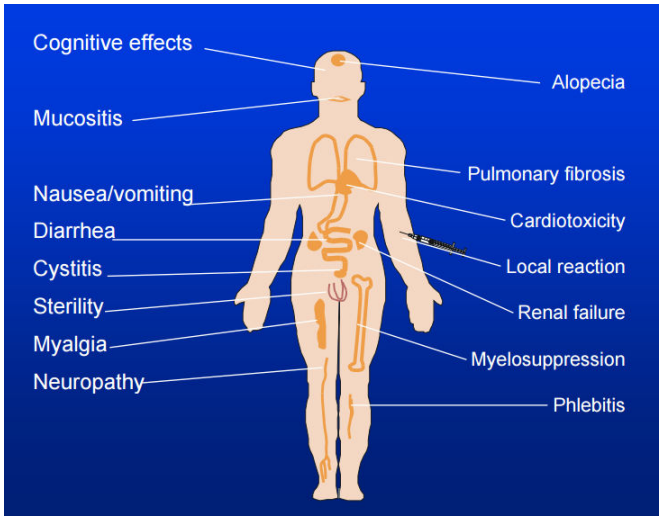

Figure 1.6 Side effects of chemotherapy (Page & Takimoto, 2005)

1.2.4.1 Types of Chemotherapy Drugs

Chemotherapy drugs can be classified in terms of chemical structure or interaction with another drug. If the action mechanism of the drug is known, the side effects could be predicted, so that treatment strategy (type and dose of drug) could be planned easily. Chemotherapeutic drugs can be classified according to their action mechanisms (Meschino, 2010).

a) **Alkylating agents** damage to DNA directly to prevent cell proliferation. The abnormal base pairing or DNA strand breaks are formed, so tumor development is prevented in most of the cancer types including leukemia, lymphoma, multiple myeloma and sarcoma, lung, breast, and ovary cancers. Examples of the alkylating agents are temozolomide and carmustine.
b) **Antimetabolites** interfere with DNA and RNA growth by acting as purines or pyrimidines; thus, they prevent tumor cells' division. They are commonly used to treat leukemia, breast, ovary, and the intestinal tract cancers. Gemcitabine, 5-fluorouracil and 6-mercaptopurine are classified in this group.
c) **Topoisomerase inhibitors** interfere with topoisomerase enzymes which separate the DNA strands. Consequently, DNA could not be copied S phase of the cell cycle. This group of drug is used in treatment of certain leukemias, lung, ovarian and gastrointestinal cancers. Topotecan and irinotecan inhibit Topoisomerase I enzyme whereas etoposide and teniposide inhibit Topoisomerase II enzyme.
d) **Anthracyclines** interfere with enzymes involved in DNA replication. They form complexes with DNA by intercalating between base pairs of the DNA strand, so DNA synthesis and function are inhibited in cancer cells. Doxorubicin, daunorubicin, idarubicin, and epirubicin belong to anthracycline group.

1.2.4.1.1 Doxorubicin

Doxorubicin, also known as doxorubicin hydrochloride, is used to treat several types of cancers including breast, ovarian, bladder, lung, thyroid, stomach cancers, neuroblastoma, lymphoma and some types of acute leukemias. The commercial name of this drug is Adriamycin®. It could be given intravenously with a maximum dose of 60-90 mg/m^2 at 21-day intervals. Furthermore, the terminal half-life of doxorubicin is 20-48 hours (Not, 2016). Doxorubicin is not available as a tablet, it can only be administered intravenously (Cancer Treatment Centers of America, 2015). However, it has several life treating side effects such as heart failure, bone marrow suppression and risk for development of other type of cancer such as acute myelogenous leukemia. Hence, the dose of drug and duration of therapy is highly important (Not, 2016).

Doxorubicin, anti-tumor antibiotic, binds directly to DNA by intercalating between base pairs on the DNA helix. It also inhibits topoisomerase II, i.e. enzyme cutting both of DNA strands to open DNA strands and supercoils by using ATP, leading to inhibition of DNA repair and replication. Hence, DNA (and RNA) synthesis is inhibited, so new cells could not be produced. Despite that the drug is maximally cytotoxic in S phase, it is not cell cycle-specific (Thorn *et al.*, 2012).

Doxorubicin could be also given in combination with other anti-cancer drugs. It could be used to treat advanced-stage breast cancer, before surgery to shrink the large breast cancer tumors or after the surgery to prevent breast cancer relapse (Veronese *et al.*, 2005). The chemical structure of doxorubicin is showed in Figure 1.7. Doxorubicin has a lipophilic anthracycline ring. On the other hand, there are many hydroxyl groups and amino sugars at the saturated end of the ring, so the hydrophilic center is formed (Xu, Chen, Ma, Wang, & Jing, 2008).

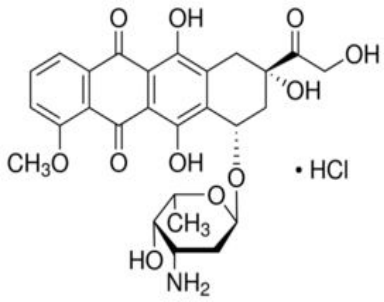

Figure 1.7 Chemical structure of doxorubicin (hydrochloride) (Sigma Aldrich Datasheet, 2015)

1.2.4.2 Multidrug Resistance

Multidrug resistance (MDR) is a phenomenon where cancer cells have a cross-resistant phenotype against structurally or functionally unrelated chemotherapeutics (Pan, Liu, He, Wang, & Shi, 2013). MDR might be intrinsic in which cancer cells have innate (pre-existent) resistance against the drug. In contrast, in acquired MDR, cancer cells develop resistance during chemotherapy or recursion of the disease may be observed after successful chemotherapy (Saraswathy & Gong, 2013). There are different types of factors leading to multidrug resistance in cancer cells as shown in Figure 1.8.

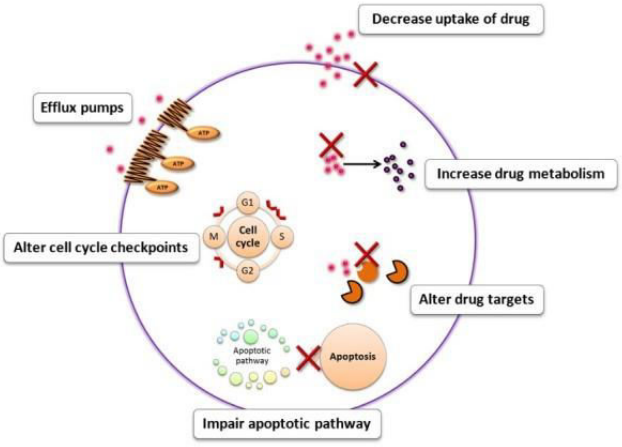

Figure 1.8 Contributing factors of MDR (Saraswathy & Gong, 2013)

MDR occurs as the cancer cells loose sensitivity to anti-cancer drugs; hence, higher amounts of drugs are needed for treatment. There are different strategies for overcoming MDR such as using MDR modulators for re-sensitization and inhibition of the pump that are functional in drug influx and efflux respectively, RNA interference (RNAi) therapy and using multifunctional nanocarriers loaded with chemotherapeutic drug and MDR inhibitor (Saraswathy & Gong, 2013).

P-gp is a transmembrane protein functional in transport of the intracellular drug out of the cell and ATP is necessary for the drug efflux process. Thus, P-gp is a key structure of MDR phenotype for most of the drug resistant cancer cells. If the pump is inhibited by preventing its efflux function or by using compounds competing with anti-cancer drugs as substrate of P-gp, MDR could be overcome (Cuperus, Claudel, Gautherot, Halilbasic, & Trauner, 2014).

1.2.5 Targeted Therapy

Targeted therapy is a type of cancer treatment in which drugs or other substances are used to more precisely identify and attack cancer cells. In conventional chemotherapy, drugs usually kill rapidly dividing cells by interfering with cell division whereas in targeted therapy, the drugs are given in a way to kill only cancer cells. The main purpose of targeted therapy is to fight cancer cells with more precision and potentially fewer side effects (American Cancer Society, 2013).

1.2.5.1 Principles of Drug Targeting

Nanocarriers are the promising transporters to deliver chemotherapeutic drugs to tumor site by active, passive and triggered targeting (Figure 1.9). In passive tissue targeting, leaky tumor vasculature and dysfunctional lymphatic drainage system, which is called EPR effect, is used; hence, this allows the release of anti-cancer drug at the tumor site. On the other hand; in active cellular targeting, the surface of nanocarriers carrying chemotherapy drugs are functionalized with ligands or antibodies that provide selective

recognition of receptors or antigens overexpressed in cancer cells. In triggered drug targeting, external stimulus is used to trigger the nanocarriers for release of the content. For this purpose heat, light, ultrasound and magnetic field can be used (Lammers *et al* , 2012).

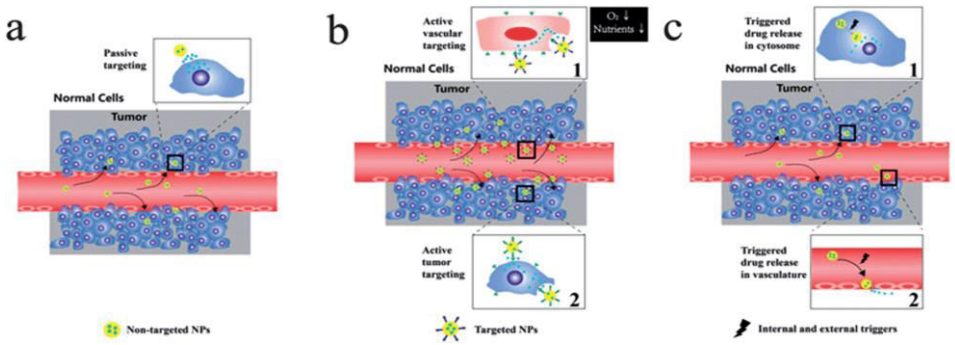

Figure 1.9 (a) Passive , (b) active and (c) triggered targeting (Lei Zhang, Li, & Yu, 2014)

1.2.5.2 Nanocarriers for Targeted Therapy

Different types of nanocarriers could be used for targeted drug delivery as shown in Figure 1.10.

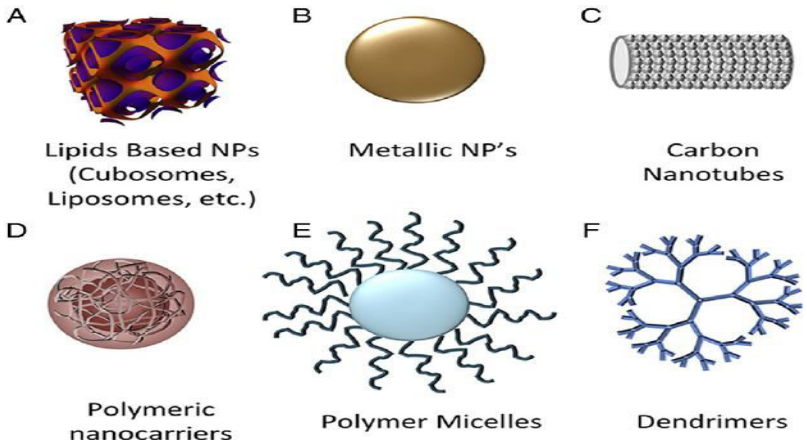

Figure 1.10 Nanocarrier types (Sagnella, McCarroll, & Kavallaris, 2014)

When the nanocarriers reach tumor site, they can release the drug content next to cancerous cells or they can bind to membrane of the cancer cells and release the drug in sustained way. Furthermore, they can be internalized by the cancer cells, so the content is released in the cell. The advantage of the nanocarriers is not only to deliver anti-cancer drugs to tumors by targeting, but also to protect the chemotherapeutic drugs from degradation, increase the half-life of the drugs, reduce renal clearance and increase the payload and solubility of the drugs (Pérez-herrero & Fernández-medarde, 2015)**.**

1.3 Magnetic Nanoparticles (MNPs)

Magnetic nanoparticles have been important in nanoscale biomedicine because of their unique physical and chemical properties. As it is understood from their names, they are nanoscale sized and magnetic, so that they could be manipulated by external magnetic field stimulation (Zhao, Zhang, & Feng, 2012). MNPs can be composed of magnetic elements, such as iron, cobalt, nickel and their oxides like maghemite, magnetite, cobalt ferrite.

Despite many pure phases of iron oxide are available in nature, the most popular MNPs are the nanoscale zero-valent iron, Fe_3O_4 and γ-Fe_2O_3. However, they have different physicochemical properties owing to difference in their iron oxidation states. The mostly studied one is magnetite (Fe_3O_4) that is a ferromagnetic black colored iron oxide of Fe(II) and Fe(III). The reason of the magnetite being the preferred type is that the Fe^{2+} state is available with the potential of acting as an electron donor (Mody *et al.*, 2013).

1.3.1 Types of Magnetization

Magnetism is the force of attraction or repulsion of a magnetic material owing to the arrangement of its atoms, particularly electrons. The substances that alter the value of magnetic field where they are placed are called magnetic materials. The materials could be classified according to their magnetic states (Figure 1.11) (Sirdeshmukh *et al.*, 2014).

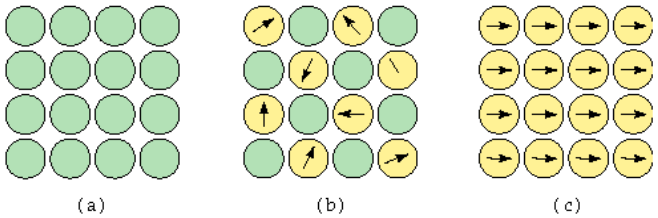

Figure 1.11 (a) diamagnetic state, (b) paramagnetic state and (c) ferromagnetic state (Akbarzadeh, Samiei, & Davaran, 2012)

The **diamagnetic** materials do not have a permanent dipole moment in the absence of an external magnetic field because all the orbital shells are filled and there is no unpaired electron. However, when the magnetic filled is applied, they produce a magnetic field in the opposite direction, so they are repelled by the applied magnetic field.

The **paramagnetic** materials produce randomly aligned magnetic moments due to unpaired electrons in partially filled orbital; hence, the net magnetization is zero in the absence of magnetic field. When an external magnetic field is applied, the magnetic moments align to produce a small net magnetization.

Another type of magnetic material is ferromagnetic one. **Ferromagnetic** materials have permanent aligned dipole moments, so they retain their magnetization even without any magnetic field application. In the **ferrimagnetic** materials, there is a weaker permanent dipole moment in the absence of magnetic field. Also, they have unequal in magnitude and antiparallel magnetic dipoles. Conversely, **anti-ferromagnetic** materials have equal and antiparallel dipole moments; thus, they cancel each other (Mohammed, Gomaa, Ragab, & Zhu, 2016).

The last type is **superparamagnetic** materials. They are small nano-sized ferromagnetic or ferrimagnetic particles. The size could be from a few nanometers to a couple of tenth of nanometers which depends on material. Moreover, superparamagnetic materials are single domain particles due to small size, so the total magnetic moment in the nanoparticle is considered as one giant moment which is composed of all the individual

magnetic moments of the atoms in nanoparticle. These nanoparticles have zero coercivity and no hysteresis loop; hence, they are like paramagnetic materials. In contrast, they are like ferromagnetic materials because of having high magnetic saturation values.

Thanks to these properties, superparamagnetic nanoparticles are commonly used targeted delivery applications. They could be targeted easily by using external magnetic field as they are magnetized when external magnetic field is applied; however, they do not show any magnetization when the magnetic field is removed. Thus, they do not agglomerate in the absence of external magnetic field. Therefore, the emboli formation in blood capillaries is prevented (Bini, Marques, Santos, Chaker, & Jafelicci, 2012).

1.3.2 Biomedical Applications of Magnetic Nanoparticles

Magnetic nanoparticles have several advantages like easy surface modification, attachment of biocompatible polymers and molecules such as antibodies, ligands, and proteins onto their surface. As the most important property, they could be manipulated by using external magnetic field. Hence, they could be used in several types of biomedical applications (Figure 1.12) such as magnetic resonance imaging, cancer hyperthermia, cell separation and drug delivery.

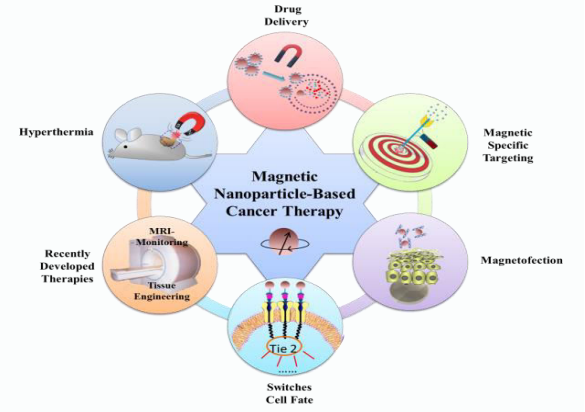

Figure 1.12 Biomedical applications of magnetic nanoparticles (Yu, Huang, Yousaf, Hou, & Gao, 2013)

1.3.3 Magnetic Nanoparticles for Drug Delivery in Cancer Therapy

In the MNP based drug delivery systems, an inorganic nanoparticle core is produced and then biocompatible surface coating is performed. Therefore, stabilization is provided under physiological conditions. The therapeutic drugs are specifically targeted to tumor site. Hence, the deleterious side effects associated with nonspecific uptake of the anti-cancer drugs by healthy cells are avoided. Moreover, the favorable biocompatibility and biodegradability of the MNPs have provided the widespread use in biomedical applications. The cytotoxic effect of MNPs were obtained when 400 mg/kg nanoparticle were given to rat; however, that amount was tolerable in human body (Arias, Gallardo, Gómez-Lopera, Plaza, & Delgado, 2001). Lower concentration was sufficient to deliver the drug to disease site (Tansik, Yakar, & Gündüz, 2014). The iron in the MNPs could be added to iron stores of the body and incorporated by erythrocytes as hemoglobin. Consequently, they could be used safely also *in vivo* studies (Sun, Lee, & Zhang, 2008).

1.3.4 The Principle of Magnetically Targeted Drug Delivery

Firstly, cytotoxic drug is attached to magnetic carriers which are intravenously injected to body in a colloidal suspension form. Afterwards, therapeutic agent loaded magnetic carriers are attracted to specific disease site by using external magnetic field. Finally, the drugs are released in the targeted site, but the duration of release can change depending on the type of the carrier. The process of drug delivery by using magnetic nanoparticles is shown in Figure 1.13.

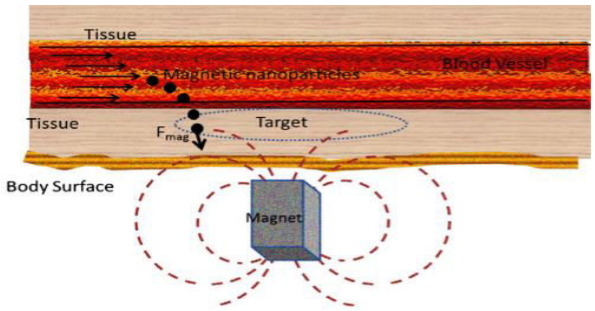

Figure 1.13 Drug delivery process by using MNPs (Lakshmanan *et al.*, 2014)

1.3.5 The Synthesis Methods for MNP

There are different types of synthesis methods for production of magnetic nanoparticles, such as co-precipitation, thermal decomposition, micro-emulsion and hydrothermal method. These methods have both advantages and drawbacks as shown in Table 1.1. In most studies, the co-precipitation technique is preferred as it is very simple and the needed chemicals are cheaper than others. Moreover, the size of the synthesized nanoparticles is almost uniform. Despite of these drawbacks, it is still used commonly since the production yield is high in this method. Thus, high number of uniform nanoparticles could be produced by using this simple method in a short time.

Table 1.1 Comparison of different methods for MNP synthesis (Lakshmanan *et al.*, 2014)

Method	Synthesis complexity	Synthesis Time	Solvent	Size distribution	Morphology	Production
Co-precipitation	Very Simple. ~room temperature (20 – 90°C).	Minutes	Water	Good	Not good	High
Thermal decomposition	Complex. Inert Atmosphere (100-320°C).	Hours	Organic	Very good	Very good	High
Micro-emulsion	Complex. Inert Atmosphere (20-50°C).	Hours	Organic	Good	Good	Low
Hydrothermal	Simple. High pressure. ~220°C	Hours/days	Water/ ethanol	Very good	Very good	Medium

1.3.5.1 The Co-precipitation Method

Iron oxide nanoparticles, Fe_3O_4 or γ-Fe_2O_3, could be synthesized with co-precipitation method easily. For this purpose, the salts of Fe^{2+} and Fe^{3+} (generally chloride salts) are added in 1:2 molar ratios are co-precipitated in deionized water at alkaline pH, so Fe_3O_4 is produced. The reaction for the magnetite (Fe_3O_4) formation is showed in Equation 1.1.

$$Fe^{2+} + 2\ Fe^{3+} + 8\ OH^- \longrightarrow Fe_3O_4 + 4\ H_2O \qquad (1.1)$$

The reaction should be performed under non-oxidizing environment. Therefore, nitrogen should be provided to eliminate oxygen. Otherwise, in the presence of oxygen, magnetite (Fe_3O_4) might be oxidized to maghemite (γFe_2O_3). At the end of MNP production process, black precipitation is formed and the color of the solution is changed from the yellow to black. This method is very simple , but there are some crucial points in the procedure; the types and molar ratio of the salts, the pH of the reaction medium and ionic strength of the water affect the size , shape and content of the magnetic nanoparticles (Si, 2015).

1.3.5.2 Surface Modifications of MNPs

It is important that MNPs should be stable in cell culture media or in the solutions containing high amount of proteins and salts to be applicable in biomedicine. Hence, their surfaces should be coated for stabilization and functionalization. The MNPs having hydrophobic or hydrophilic cores could be synthesized by using different methods. However, their interactions with the surrounding media is related with the molecules on the magnetic surface (Colombo *et al.*, 2012) .

The MNPs are not attracted magnetically by each other in the absence of magnetic field because of superparamagnetic properties. However, they still have a strong tendency to agglomerate owing to their high surface energy. Although, MNPs have colloidal electrostatic stabilities due to repulsion between their surface charges, they aggregate in biological solutions since the salts or other electrolytes in the solution may neutralize these charges. When the MNPs are injected intravenously, their surfaces are exposed to opsonization which is the first step of clearance by the reticuloendothelial system (RES). Therefore, their surfaces should be modified to avoid from reticuloendothelial system and to maintain longer plasma half-life. As a result, agglomeration and opsonization could be prevented by surface coating with surfactants like oleic acid (Yallapu, Foy, Jain, & Labhasetwar, 2011). The structure of oleic acid is seen in Figure 1.14.

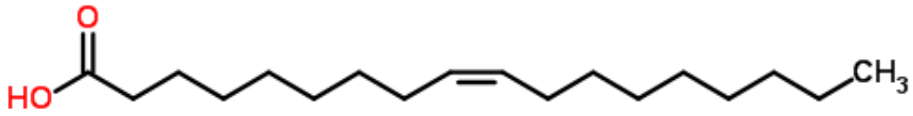

Figure 1.14 The structure of oleic acid. Retrieved from http://www.chemspider.com/Chemical-Structure.393217.htmL

Besides to oleic acid, the nanoparticle surface could be modified by polymers such as poly(lactic-co-glycolic acid) (PLGA), poly(ethylene glycol) (PEG), poly(vinyl alcohol) (PVA) and poly(amidoamine) (PAMAM) dendrimer. The additional modification gives the nanoparticles biodegradability feature. Thus, the nanoparticles could release the drugs at a determined rate by polymer degradation. Moreover, their colloidal stabilities against aggregation were improved by reducing the inter particle forces with coating process (Issa, Obaidat, Albiss, & Haik, 2013).

1.3.5.2.1 Poly(dl-lactic-co-glycolic acid) (PLGA)

Poly(lactic-co-glycolic acid) (PLGA) is a polymer preferred in biomedical applications due to their biocompatible and biodegradable property. When they are degraded in the body by hydrolysis of ester linkages, two metabolites are produced; lactic acid and glycolic acid. These monomers have minimum systemic toxicity since they can be metabolized via Krebs cycle in the body; thus, they are removed from the body as carbon dioxide and water. Moreover, glycolic acid also can be excreted unchanged in kidney. Consequently, US Food and Drug Administration (FDA) approved the PLGA use in humans for drug delivery. PLGA polymers are not only commercially available, but also could be synthesized from their monomers. Their molecular weights and monomer ratios may be different depending on the composition. The PLGA polymers are named according to their monomer ratios like PLGA 50:50 meaning that 50% of the polymer is lactic acid and 50% is glycolic acid (McCall & Sirianni, 2013). The

chemical structure of the PLGA is given in Figure 1.15 where x and y show the unit number of the lactic acid and glycolic acid, respectively.

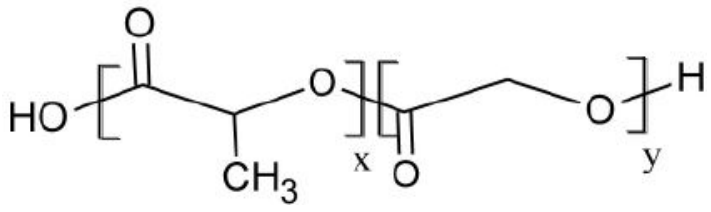

Figure 1.15 Chemical structure of PLGA (Shabir, Alhusban, Perrie, & Mohammed, 2011)

PLGA nanoparticles are internalized by cells through clathrin-mediated endocytosis and partly fluid phase pinocytosis. These nanoparticles escape the endo-lysosomes and enter the cytoplasm within short time of incubation. The interactions of the nanoparticles with the membrane of the vesicles are facilitated, so the membrane is destabilized transiently and locally. As a result, nanoparticles could escape into cytosol (Danhier *et al.*, 2012). This internalization process is schemed in Figure 1.16. Moreover, PLGA provides the rate determined drug release since drug is released from the nanoparticle through polymer degradation (Chiang *et al.*, 2012).

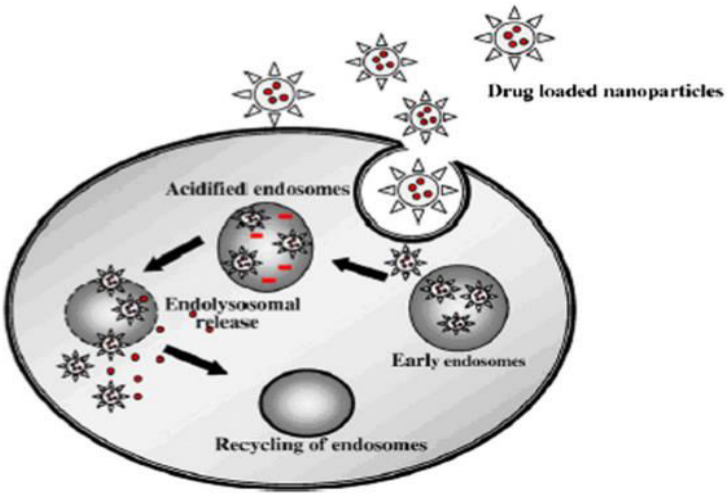

Figure 1.16 Internalization of PLGA nanoparticles by a cell (Danhier *et al.*, 2012)

Degradation of PLGA nanoparticle results in delayed inflammatory responses in the treatment site since slow degrading polymers do not lead to as intense response as fast degrading polymers (Tamariz & Rios-ramírez, 2013). Consequently, coating of magnetic nanoparticles with PLGA could be a reasonable strategy for targeted drug delivery.

There are several methods for production of PLGA-based nanoparticles, including nanoprecipitation, oil in water emulsion, spontaneous emulsification- solvent diffusion and spraying method (Alimohammadi & Joo, 2014).

1.3.5.2.1.1 Nanoprecipitation Method

The nanoprecipitation method is a simple technique for production of PLGA nanoparticles. Nanoprecipitation method does not necessitate high temperatures, extended stirring or sonication and oily aqueous phase. Since these conditions might damage polymer or drug structure, nanoprecipitation method is advantageous. Briefly, two types of miscible liquids are needed (Figure 1.17). The first one is organic solution, i.e. solvent, in which PLGA polymer and drug are dissolved, but they should not be dissolved in the second system containing a stabilizer. The second aqueous solution is called non-solvent. The solvent containing PLGA and drug is added to the non-solvent, so nanoprecipitation occurs by a rapid desolvation of PLGA. In that time, the solvent is diffused into the dispersing medium, so polymer precipitated where drug is entrapped immediately. Generally, acetone is used as solvent whereas the non-solvent is water. Furthermore, this method is applied for lipophilic drug loaded nanoparticle synthesis owing to miscibility of the solvent with the aqueous phase, but it is not suitable to encapsulate water-soluble drugs (Yadav & Sawant, 2010).

The stabilizer in the non-solvent could be used, although it is not necessary. In PLGA nanoparticle synthesis, several types of stabilizers can be used: PVA and TPGS are most preferred ones (Lai *et al.*, 2014). In addition to being stabilizer, TPGS could be a component of the synthesized nanoparticle; therefore, TPGS should be added to solvent

with PLGA. By this way, TPGS is also delivered to target site and released by nanoparticle degradation (Zeng *et al.*, 2013).

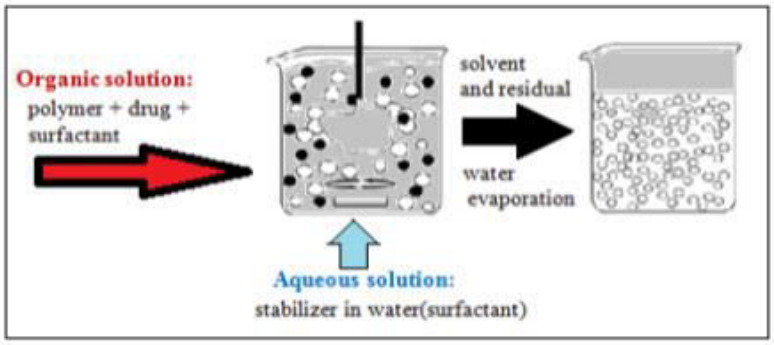

Figure 1.17 Nanoprecipitation method for nanoparticle synthesis (Bhatt & Goswami, 2013)

1.3.5.2.2 D-alpha-tocopheryl Polyethylene Glycol 1000 Succinate (TPGS or Vitamin E TPGS)

D-alpha-tocopheryl polyethylene glycol 1000 succinate (TPGS or vitamin E TPGS) is a water-soluble derivative of the natural vitamin E. It is produced by esterification of vitamin E succinate with polyethylene glycol (PEG). TPGS has non-ionic and amphiphilic structure which is composed of lipophilic alkyl tail and hydrophilic polar head portion. The chemical structure of the TPGS is shown in Figure 1.18.

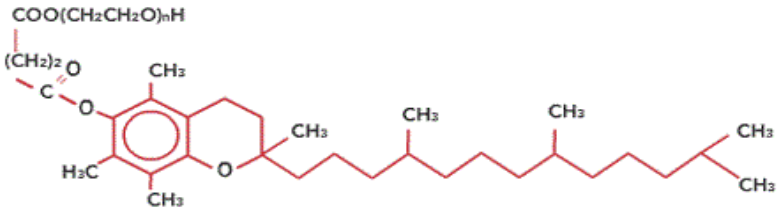

Figure 1.18 Chemical structure of TPGS. Retrieved from http://antareshealthproducts.com/vitamin-e-tpgs/tpgs-properties/

In recent years, TPGS has been used for cancer treatment to invert multiple drug resistance (MDR) in cancer cells. MDR reduces the drug efficacy of the many anti-cancer agents and one of the most important mechanisms in MDR is the efflux of the drugs from cells by P-glycoprotein pump (P-gp) as explained in section 1.2.4.2 (Z. Zhang & Feng, 2006).

In the previous studies, it has been reported that TPGS can inhibit P-gp pump by preventing the ATPase activity of the pump. Additionally, it has long-standing safety record in biomedical applications. In addition to these, TPGS does not interact with other drugs, so it can be used in the drug delivery studies to overcome MDR (Y. Liu, Huang, & Liu, 2010). Thus, both anti-cancer drug and TPGS can be delivered to disease site to treat the cancer and to overcome MDR.

Besides these advantages of TPGS, it increases the stability and blood circulation time of the nanoparticles; hence, it enhances bioavailability. It is also an excellent emulsifier and solubilizer of hydrophobic drugs, thanks to its bulky structure and large surface area (Sonali *et al*., 2015).

The last but not the least important property of TPGS is that it has been approved by FDA for using as a pharmaceutic adjuvant (Guo, Luo, Tan, Otieno, & Zhang, 2013).

1.4 Aim of the Study

The main aim of the study is to design a potential targeted delivery system for the co-delivery of doxorubicin and vitamin E TPGS breast cancer cells by using magnetic PLGA nanoparticles. The objectives of the current study are listed below:

- To synthesize Fe_3O_4 magnetic nanoparticles (MNPs) by co-precipitation method
- To coat the surface of MNPs with oleic acid (OA)
- To produce PLGA coated magnetic nanoparticles containing TPGS
- To characterize the synthesized nanoparticles in terms of physical and chemical properties

- To determine the efficiency of doxorubicin loading on nanoparticles
- To show the drug release profile of drug loaded nanoparticles (Dox-PLGA-TPGS-MNP)
- To visualize the nanoparticle internalization in drug-sensitive (MCF-7) and drug-resistant (MCF-7/Dox) cells
- To show the targetable ability of PLGA-TPGS-MNP
- To study the cytotoxic effects of the Dox-PLGA-TPGS-MNPs on MCF-7 and MCF-7/Dox cells
- To determine the effect of TPGS on drug accumulation in MCF-7/Dox cells

CHAPTER 2

MATERIALS AND METHODS

2.1 MATERIALS

2.1.1 Materials for Nanoparticle Synthesis and Drug Loading Studies

Iron(II) chloride tetrahydrate ($FeCl_2.4H_2O$), iron(III) chloride hexahydrate ($FeCl_3.6H_2O$), poly(dl-lactide-co-glycolide) (PLGA; lactite: glycolide MW 40000:75000), D-α-Tocopherol polyethylene glycol 1000 succinate (TPGS), triethylamine and acetone were purchased from Sigma-Aldrich (U.S.A). Oleic acid was purchased from AppliChem.

Dimethylsulfoxide(DMSO), acetic acid (CH_3COOH) and ammonium hydroxide solution (32% of ammonia, NH_4OH) were obtained from Merck (Germany). Nitrogen gas was provided from Asya Gaz (Turkey). Doxorubicin HCl (579.98 g/mole) was purchased as Adriamycin.

2.1.2 Materials for Cell Culture Studies

MCF-7 monolayer type human epithelial breast adenocarcinoma cell line was provided by SAP Institute (Ankara-Turkey). 1000 nM doxorubicin-resistant MCF-7 cells (MCF-7/Dox) was previously developed in our laboratory (Kars *et al*. 2006).

Phosphate buffered saline(PBS), 0.25% Trypsin-EDTA solution, gentamycin sulphate, 0.5% trypan blue and XTT cell proliferation kit were obtained from Biological Industries, Israel.

RPMI 1640 medium ((1x), 2.0 g/l $NaHCO_3$, stable glutamine) was purchased from Lonza, Switzerland and fetal bovine serum (FBS) was from Biochrom, Germany. Prussian blue staining was provided from Sigma- Aldrich.

2.2 METHODS

2.2.1 Synthesis of Magnetic Nanoparticles

There are different methods for preparation of magnetic nanoparticles used in recent studies; co-precipitation, thermal decomposition, hydrothermal synthesis, microemulsion and sonochemical synthesis (Wu, He, & Jiang, 2008). In this study, Fe_3O_4 magnetic nanoparticles (MNPs) were prepared by using the co-precipitation method (Rouhollah *et al.*, 2013). The synthesis was performed in five-necked round bottom flask as in Figure 2.1. $FeCl_2.4\ H_2O$ and $FeCl_3.6H_2O$ salts (molar ratio of Fe(II): Fe(III) = 1:2) were vigorously mixed and dissolved in 150 ml of deionized water (diH_2O). The mixture was heated to 90°C and mechanically stirred (Heildolf RZR 2021, Germany) for 1 hour under nitrogen gas. The N_2, which is an inert gas, was used to provide inert atmosphere during reaction. Otherwise, magnetite may be converted to maghemite because of oxygen in the environment (Khosroshahi & Ghazanfari, 2010). After that, 25 ml of ammonium hydroxide solution (32%, v/v) was added to mixture dropwise under continuous stirring by using a pump. At the end of ammonium addition, almost 2 hours later, black magnetite precipitates were observed. The precipitated Fe_3O_4 was washed with distilled water and ethanol several times, then isolated by using a magnet. Finally, one part of the isolated magnetic nanoparticles were air dried for oleic acid coating and the other part was stored in ethanol (Tansik *et al.*, 2014) .

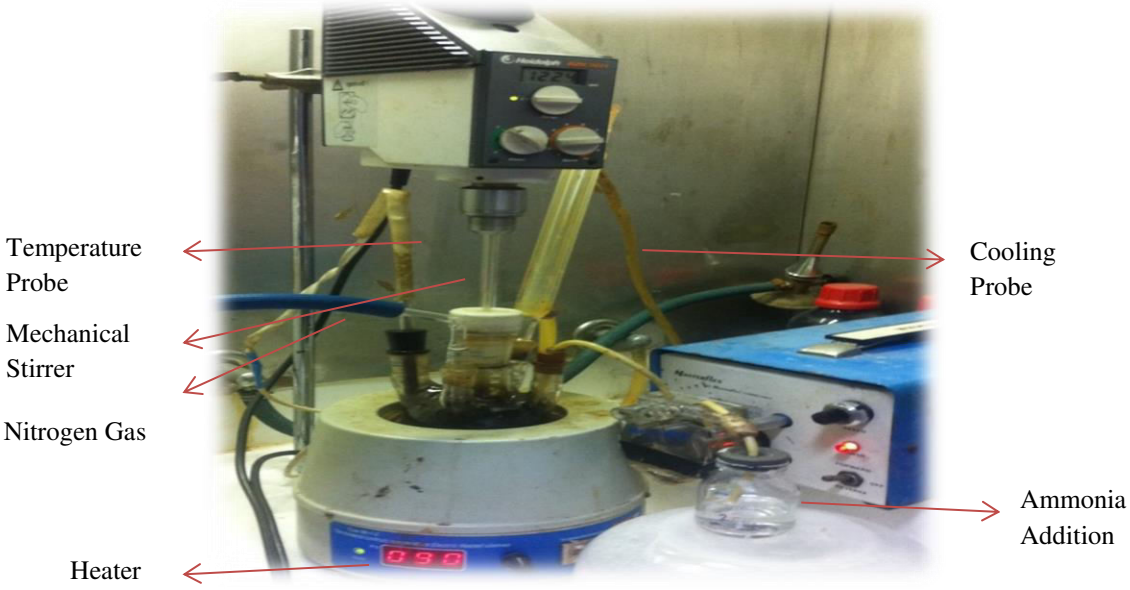

Figure 2.1 Synthesis of MNP by co-precipitation method

2.2.2 Coating of Magnetic Nanoparticles with Oleic Acid

10 ml of oleic acid was added to certain amount of air dried MNPs and vigorously stirred for 2 h at room temperature. Then, oleic acid was discharged and particles were washed with 20-25 ml acetone three times to remove excess oleic acid. After air-drying, OA-MNPs could be used for further studies (Okassa *et al.*, 2007).

2.2.3 Synthesis of Polymeric Magnetic Nanoparticles Containing TPGS

Drug free polymeric nanoparticles NPT20 (PLGA-TPGS-MNPs containing 20% of TPGS) were synthesized by modified nanoprecipitation method (Zhu *et al.*, 2014):
Firstly, the organic phase was prepared; 20 mg of TPGS and 80 mg of PLGA were dissolved in 8 ml of acetone by vortex and sonication. (For synthesis of NPT0, not containing TPGS in core, 100% PLGA used). On the other side, 10 mg of OA-MNPs were dispersed in 2 ml of acetone by sonication for 5 minutes. The mixtures should be placed in ice during sonication to prevent heating of solution. OA-MNP in acetone was

added to organic phase and mixed by vortex. Afterwards, the aqueous phase (0.03% TPGS) should be prepared; 30 mg of TPGS was dissolved in 100 ml of distilled water by vortex. After that, the dissolved mixture containing TPGS, PLGA, OA-MNP was added to TPGS solution (0.03% TPGS) dropwise under mechanical stirring to form a homogenous solution. Finally, the solvent (acetone) was evaporated by uncovered stirring overnight. The nanoparticles were separated by a magnetic decantation and stored at 4°C**.**

2.2.4 Conversion of Water Soluble Dox-HCl to Water Insoluble Dox

Doxorubicin hydrochloride, the hydrochloride salt of doxorubicin, is water soluble, but it is not dissolved in acetone. However, nanoprecipitation method utilizes acetone as the solvent. Accordingly, it should be converted to water insoluble form so that in nanoprecipitation method, lipophilic drug encapsulation can occur efficiently. For this purpose, Dox-HCl was stirred with triethylamine (TEA) in acetone for 24 hours. Afterwards, acetone was evaporated until water insoluble doxorubicin which could be used in drug loaded nanoparticle synthesis was obtained (Kumar, Kulkarni, Nagesha, & Sridhar, 2012). After this point, water-insoluble doxorubicin is referred as doxorubicin, shortly.

2.2.5 Synthesis of Doxorubicin Loaded TPGS Containing Polymeric Magnetic Nanoparticles

The same procedure was performed to prepare doxorubicin loaded magnetic polymeric nanoparticles as explained in section 2.2.3. Different from that, 2 mg of Dox was dissolved in acetone and mixed with OA-MNP solution, and then added into the organic phase. Moreover, the evaporation process was performed in dark due to the light sensitive nature of doxorubicin. Finally, the synthesized nanoparticles were purified by magnetic decantation and stored at 4°C and dark. Nanoprecipitation method for Dox-PLGA-TPGS-MNP synthesis is shown in Figure 2.2.

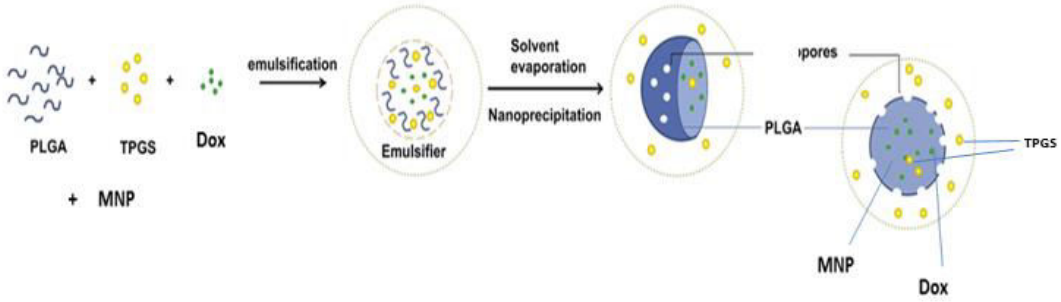

Figure 2.2 Synthesis of Dox-PLGA-TPGS-MNP by nanoprecipitation method (edited scheme) (Zhu *et al*., 2014)

2.2.6 Drug Loading

The amount of doxorubicin loaded into magnetic TPGS-PLGA NP and entrapment efficiency (EE%) were determined by UV spectrophotometer (Multiskan GO, Thermo Scientific). For this purpose, different amounts of doxorubicin were added to organic phase during nanoparticle synthesis procedure. At the end of process, nanoparticles were separated by magnetic decantation and absorbance of the supernatant was measured at 480 nm by UV spectrophotometer. Dox NPT0 (Dox loaded nanoparticle without TPGS in core) was also synthesized by nanoprecipitation method as explained in section 2.2.3 in order to determine the effect of TPGS on drug loading. Finally, the amount of doxorubicin was determined by using doxorubicin calibration curve. The drug content of the nanoparticle could be determined by using the equations, below:

$$\text{EE}(\%) = \frac{(amount\ of\ drug\ added) - (amount\ of\ drug\ in\ the\ supernatant)}{(amount\ of\ drug\ added\ during\ synthesis)} \text{x}100 \qquad (2.1)$$

$$\text{Loading content} = \frac{(amount\ of\ drug\ added) - (amount\ of\ drug\ in\ the\ supernatant)}{amount\ of\ synthesized\ NPs} \qquad (2.2)$$

Loading efficiency (%) = $\frac{(experimental\ amount\ of\ drug\ loaded\ \ in\ 1\ mg\ NP)}{(theoritical\ amount\ of\ \ drug\ loaded\ \ in\ 1\ mg\ NP)}$ x 100 (2.3)

2.2.7 Drug Release

To determine drug release profile of drug loaded nanoparticles, sample and separate method was used (Tansık *et al.*, 2014) . Briefly, 1 mg of Dox-PLGA-TPGA-MNP was placed into Eppendorf tube containing release media (1 ml of PBS, pH 7.4). At 3 h intervals, nanoparticles are separated by using Nd–Fe–B magnet, and then fresh release media was added to tubes. The drug concentrations in removed medium were determined by spectrophotometric measurements at 480 nm. Empty nanoparticles were used as blank. The standard curve was used to calculate the amount of released drug. The procedure was performed in triplicates and at specified time intervals for 35 days. To show the effect of TPGS on drug release rate, Dox NPT0 was synthesized and the same steps were performed.

2.2.8 Characterization of Nanoparticles

Fourier transform infrared spectroscopy (FTIR) (FTIR Nicolet 6700 FTIR Spectrometer), zeta-potential (MALVERN Nano ZS90), scanning electron microscopy (SEM) (QUANTA 400F Field Emission Scanning Electron Microscope), transmission electron microscopy (TEM) (FEI Tecnai G2 Spirit BioTwin) X-ray photoelectron spectroscopy (XPS) (PHI 5000 Versa Probe), and vibrating sample magnetometer (VSM) (EV/9, ADE Magnetics), dynamic light scattering (DLS) (Malvern ALV/CGS-3), UV spectrophotometer (Shimadzu, UV-1208) and thermal gravimetric analysis (TGA) were performed for characterization of drug free and drug loaded nanoparticles.

2.2.8.1 Fourier Transform Infrared (FTIR) Spectroscopy

The purity and chemical structure of the synthesized nanoparticles were determined by FTIR spectroscopy (Thermo Scientific Nicolet 6700 FT-IR Spectrometer) after lyophilization by KBr method.

2.2.8.2 Zeta-Potential Analysis

The surface charges of the nanoparticles were measured by zeta-potential instrument (Nano-ZS, MALVERN Nano ZS90) at 25˚C. Before analysis, samples were dispersed in water or DCM depending on the polarity. Moreover, zeta potential measurement gives information about the stability of the nanoparticles; the nanoparticles having greater than +25 mV or less than -25 mV are considered as physically stable (Nanocomposix, 2012).

2.2.8.3 Scanning Electron Microscopy (SEM)

Scanning electron microscope (SEM) was used to inform about the morphology of nanoparticles. The instrument (QUANTA 400F Field Emission Scanning Electron Microscope) scans the surface of nanoparticles with a focused beam of electrons interacting with atoms of the nanoparticles, so signals are formed and the surface topography is determined.

2.2.8.4 Transmission Electron Microscopy (TEM)

Transmission electron microscope (TEM) was used to determine shape and size of MNPs and OA-MNPs. FEI Tecnai G2 Spirit BioTwin microscope was utilized in analysis; the beam of electrons is transmitted through the sample, so the images are formed owing to electron interactions.

2.2.8.5 Vibrating Sample Magnetometer (VSM)

Vibrating sample magnetometer (VSM) (EV/9, ADE Magnetics) was used to determine magnetization properties of synthesized OA-MNPs at room and body temperature (10-6 emu sensitivity and 22 kOe maximum magnetic field).

2.2.8.6 Dynamic Light Scattering (DLS) Analysis

Hydrodynamic sizes of nanoparticles were determined by dynamic light scattering (DLS) analysis (Malvern ALV/CGS-3). For analysis, samples were dispersed in proper solutions and sonicated.

2.2.8.7 UV Spectrophotometer Analysis

UV spectrophotometer (Shimadzu, UV-1208) was used in drug loading and drug release studies. The amount of drug in supernatant was determined by measuring the absorbance values at 480 nm.

2.2.8.8 Thermal Gravimetric Analysis (TGA)

Thermal gravimetric analysis was performed to confirm the presence of TPGS in total nanoparticle formation and to determine the chemical content of polymeric magnetic nanoparticles. Free TPGS was used as control. The samples were loaded to instrument and heated from 40°C to 600°C with a rate of 10°C/min. The thermograms represented the weight loss profiles of samples.

2.2.8.9 X-ray Photoelectron Spectroscopy (XPS)

X-ray photoelectron spectroscopy (XPS) is a surface analysis technique; thus, it is used to determine the elemental composition of nanoparticle surface. The modifications on the oleic acid coated nanoparticles were identified by XPS spectrophotometer (PHI 5000 VersaProbe).

2.2.8.10 Hydrophobicity and Magnetic Sensitivity Test

Dispersion abilities of oleic acid coated magnetic nanoparticles in hydrophilic and hydrophobic environment were observed by hydrophobicity test. On the other hand, their behaviors in the presence or absence of magnetic field were determined.

2.2.9 Cell Culture Studies

2.2.9.1 Cell Lines and Culture Conditions

In this study, two types of cells were used: Parental MCF-7 cells, a human breast carcinoma cell line and doxorubicin resistant MCF -7 cells (MCF-7/Dox) which were developed by the previous members of our laboratory (Kars, 2006). Both cell lines were cultivated in RPMI 1640 medium (10% (v/v) fetal bovine serum (FBS) and 1% (v/v) gentamycin as supplementary) at 37°C in 5% CO_2 incubator (Heraeus, Hanau, Germany). These cell lines should attach the surface as monolayer to continue proliferating, so 25 or 75 cm^2 polystyrene tissue culture flasks were used.

For cell based experiments, doxorubicin resistant MCF-7 cells (MDF-7/Dox) were developed from parental MCF-7 cell line by our previous lab members (Kars *et al.*, 2006). For this purpose, the drug is given to cells by gradually increasing concentration so that cells are not killed. Until the cells are not affected from the drug addition it is continued, so the cells are resistant to highest concentration of drug so that to be alive. The cells are resistant to 1000 nM doxorubicin.

2.2.9.2 Cell Passaging

MCF-7 cells are adherent, so they propagate as a monolayer by attaching the surface of flask (Greiner Bio-One Germany). When the surface area of the flask (80% of the surface) is covered by cells, i.e. cells are confluent, the proliferation is halted. If this stage is too long, cells will die because of nutrient deficiency and waste product

accumulation. Thus, cells should be passaged in proper time intervals by transforming some portion of the cells to a new cell culture flask under sterile conditions in Bioair Laminar Flow (Euroclone, Pavia, Italy). For this purpose, old medium is removed and the surface of the flask washed with 5 ml of PBS to remove residual medium containing serum. It is a critical step since serum inhibits the trypsin enzyme used for detachment of cells from the surface. After washing, 1-2 ml of trypsin-EDTA solution (Biological Industries, Israel) is added to flask and then flask is bobbed slowly such that trypsin covers the surface. The flask is placed into the incubator for 5 minutes such that trypsin acts optimally at 37°C. EDTA chelates remaining calcium ions after PBS treatment. These calcium ions are necessary for integrin protein that helps cell to cell interaction. As there is no calcium, cell to cell adhesion does not take place (K. Liu, Markakis, & Smith, 1990). After the detachment of cells are observed under microscope, 3 ml of fresh medium is added to flask. The cell suspension is homogenized by pipetting and 1 ml suspension is remained in flask while another portion is removed. Finally, the volume is completed to 12 ml with fresh medium and flask is placed into incubator. 2 days later cell confluence is controlled and cells are passaged if necessary. In drug resistant cells, 500 mM doxorubicin with a final concentration of 1 µM is added in each passaging for continuity of resistance.

2.2.9.3 Cell Freezing

Cells could be stored by freezing for long periods and 80% confluence should be preferred for freezing. The cells on the flask were trypsinized, to detached from the surface and then resuspended in a falcon tube containing 5 ml of medium. The cell solution was centrifuged at 1000 rpm for 5 minutes and the supernatant is removed. After that, 5 ml of PBS was added to cell pellet and again centrifuged at the same speed and duration (optional washing step). Finally, supernatant was discarded and 1 ml of cold freezing medium was added to cells. The freezing medium was composed of 90% (v/v) heat inactivated FBS and 10% (v/v) DMSO. The cells in freezing medium was taken into a cryovial and then placed into -20 °C for 2-3 hours and then -80 °C for

overnight incubation. To store for longer periods, the cryovials were transferred into liquid nitrogen container.

2.2.9.4 Cell Thawing

The frozen cells were taken from the nitrogen container and placed into to water bath (37 °C) for thawing. This process should be done immediately since frozen cells were in DMSO which is toxic for cells at the temperatures higher than +4°C. The cells in freezing medium were transferred to a falcon tube and centrifuged at 1000 rpm for 5 minutes, so the supernatant was discarded. The cells in pellet were resuspended in fresh medium and transferred into cell culture flask. Cells were incubated in the certain conditions (37°C, 5% CO_2).

2.2.9.5 Viable Cell Counting

The number of cells used in experiments are important for most of the studies such as cytotoxicity and internalization. The most common technique for counting cells is trypan blue dye exclusion method. It differentiates the viable and dead cells; the dead cells are stained blue while the viable ones are unstained. Viable cells have intact membrane; thus, trypan blue could not penetrate through cell membrane whereas dead cells have nonfunctional and disrupted cell membrane, thus cells take the dye and are seen blue. Briefly, the cells were detached from the surface by using trypsin and resuspended in fresh medium. Afterwards, certain amount of cell suspension was taken and mixed with trypan blue in an Eppendorf tube (cell suspension : dye = 9 : 1). The cells in solution were counted by using Hemocytometer (Neubauer, Bright-line, Hausser Scientic, USA) phase contrast microscopy (Olympus, USA). 10 µl of trypan blue-cell mixture was loaded to hemocytometer by pipette and visualized under microscope. The hemocytometer used in this study has 16 large squares; each of which contains 16 small square having 0.00025 mm^3 volume (total 256 small squares). The number of unstained

cells were counted under microscope, and total number of cells in 1 ml of cell suspension was calculated by the formula below:

$$\text{Cell number / ml} = \frac{\text{cell number in 16 large squares}}{256} \text{ x 4 x } 10^6 \quad (2.4)$$

2.2.9.6 Prussian Blue Staining for Detection of Nanoparticle Internalization

At the beginning, 2×10^5 cells were seeded to each well of 6-well plate and the volume were completed to 2 ml with medium. The cells were incubated at 37°C for 24 hours. Then, old medium was removed and the cells were washed with PBS. Nanoparticles were sterilized by washing medium and 2 ml of fresh media containing the same concentration of NPT20 and NPT0 were added to wells, so that the cells were incubated for 5 hours in the incubator (37°C). At the end of this time, medium is discarded, the cells were fixed with methanol at -20°C for 10 min and stained by the Prussian blue method at dark and room temperature: The equal volumes of potassium ferrocyanide and hydrochloride acid solutions were mixed and 1 ml of the mixture was added to each well. Cells were incubated for 10 minutes. Later, the dye was removed and the wells were washed with PBS. The second dye containing pararosaniline and PBS (1:50 w/w) was added to each well and waited for 5 minutes. Again, washing step was performed. Finally, the cells which internalize the nanoparticles could be observed under light microscope.

2.2.9.7 Magnetic Targeting of NPT20 with an External Field

In order to show magnetic properties of NPT20, 1×10^4 of MCF-7 cells were seeded in three well canal-connected slide (Parsian *et al*., 2016). The cells were incubated at 37°C for 24 hours to be attached on slide. Then, medium was removed and a magnet was placed under the middle well of slide. Then, a fresh medium containing 0.2 mg/ml NPT20 is given to cells and the behavior of the nanoparticles in the presence and

absence of magnetic field was observed. Finally, the cells were incubated for 5 hours and then imaged under light microscope (Only middle well was exposed to magnetic field while two others were not.)

2.2.9.8 Determination of Drug Accumulation

To show the effect of TPGS on drug accumulation, $2x10^5$ MCF-7/Dox cells/well were seeded on six-well plate and incubated overnight 37°C. Medium was removed and fresh medium containing 20 µg/ml NPT20 or NPT0, 200 µg/ml NPT20 was added. 5 µg/ml TPGS was added to one well as positive control and only fresh medium was added to another well as negative control. The cells were incubated for 3 h and then 5µM doxorubicin was added to each well and incubated for additional 1 h. Afterwards, medium was removed, cells were washed with PBS and fixed by cold methanol. Finally, the cells were observed under florescence (FLoid) microscope by using red filter.

2.2.9.9 XTT Cell Proliferation Assay

XTT Cell Proliferation Assay Kit (Biological Industries, Israel) was used to determine cell proliferation profile and the cytotoxicity of the drug or NPs. This assay depends on the reduction of the XTT reagent (a tetrazolium salt) by the mitochondrial enzyme activity of the living cells. At the end of the reaction, XTT is reduced to water soluble formazan which is an orange colored compound and its intensity could be measured with spectrophotometry. Thus, the measured absorbance value is proportional with the living cell number (Figure G.3).

Briefly, MCF-7 and MCF-7/Dox cells were trypsinized and detached from the flask. After the dilution of cells with medium, 1×10^4 cells were seeded to each well on 96-well plate except first column since it was used as medium control. The cell attachment was allowed by incubating them at 37°C for 24 hours. After that, the old medium was removed to discard the unattached dead cells. 100 µl of medium was added to first and

second column which are medium control (MC) and cell control (CC) columns, respectively. Into the other columns from 4 to 12, 50 µl of medium was added. The third column, which is called high drug dose column (HDD), contained 150 µl of medium with the maximum concentration of drug or NPs. The concentrated drug or NP were serially diluted by taking 100 µl portion from the third column and passing it to the next column. Afterwards, all volumes of columns from 3 to 12 were completed to 100 µl by adding 50 µl of medium. Cells were incubated for 72 hours at the same incubation conditions. After that, 50 µl of XTT and activator reagent mixture was added to each well, and cells incubated for 4 hours at 37°C, and dark. Finally, the absorbance of formazan was measured at 492 nm and background absorbance was measured at 600 nm with Anthos 2010 96-well plate reader (Biochrom, Germany).

After measurements, the inhibitory concentration 50 (IC_{50}) of the drug or nanoparticles were determined by plotting the curve for cell proliferation percentage versus concentration. IC_{50} value is the concentration of the agent killing 50% of the cell population.

The proliferation rate of cell control group was accepted as 100% and that of other groups was calculated relative to cell control.

This assay was performed for both sensitive and drug resistant cell lines. Consequently, the resistance index (R) which is the ratio of IC_{50} of resistant cells to sensitive ones was also determined.

2.2.9.10 Stability of Dox NPT20s

To determine the stability of nanoparticles and compare the freshly synthesized and long-term stored nanoparticles in terms of cytotoxic effects, Dox NPT20s were stored at 4°C and dark conditions for 5 weeks. Then, XTT cell proliferation assay was performed as explained above.

CHAPTER 3

RESULTS & DISCUSSION

3.1 Synthesis and Characterization of Magnetic Nanoparticles

In the current study, magnetic iron oxide nanoparticles were synthesized by co-precipitation method which is preferred because of its ease to perform and yield of uniform small sized particles. Afterwards, the surface of the magnetic nanoparticles was coated with oleic acid to prevent agglomeration and to make them compatible with polymer coating and drug loading.

The synthesized nanoparticles were characterized in terms of chemical content, surface charge, magnetic property, size and shape by using FTIR, zeta potential, VSM, XPS and TEM analyses.

3.1.1 Hydrophobicity and Magnetic Sensitivity Test

The synthesized MNPs were dispersed in water due to their hydrophilic properties (Figure 3.1 a). However, after their surfaces were coated with oleic acid, they gained hydrophobic property, so they were dispersed in DCM which is hydrophobic (Figure 3.2 b). In addition to these, OA-MNPs were in the DCM part of the water/DCM mixture where two separate phases were formed. Thus, it could be seen that the synthesized MNPs were coated with oleic acid successfully.

a) b)

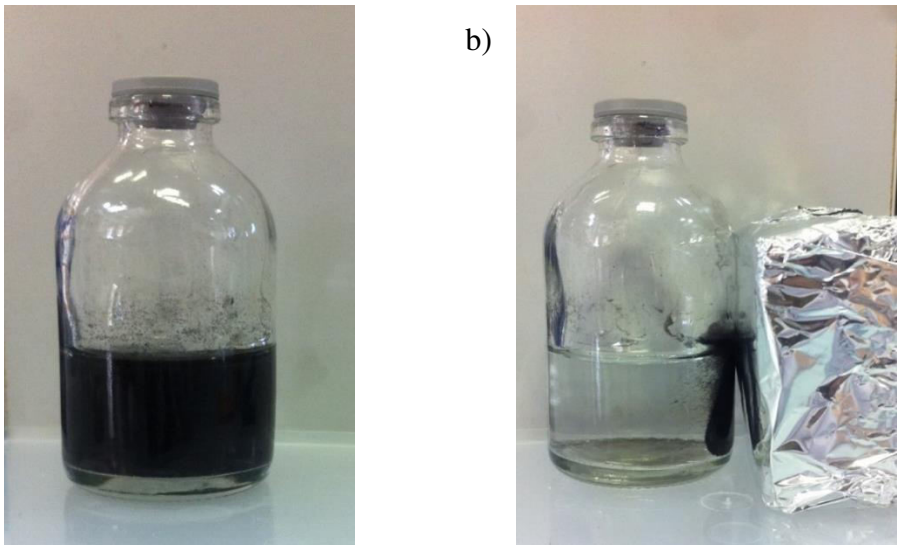

Figure 3.1 MNP in water (a) in the absence and (b) presence of magnet

a) b)

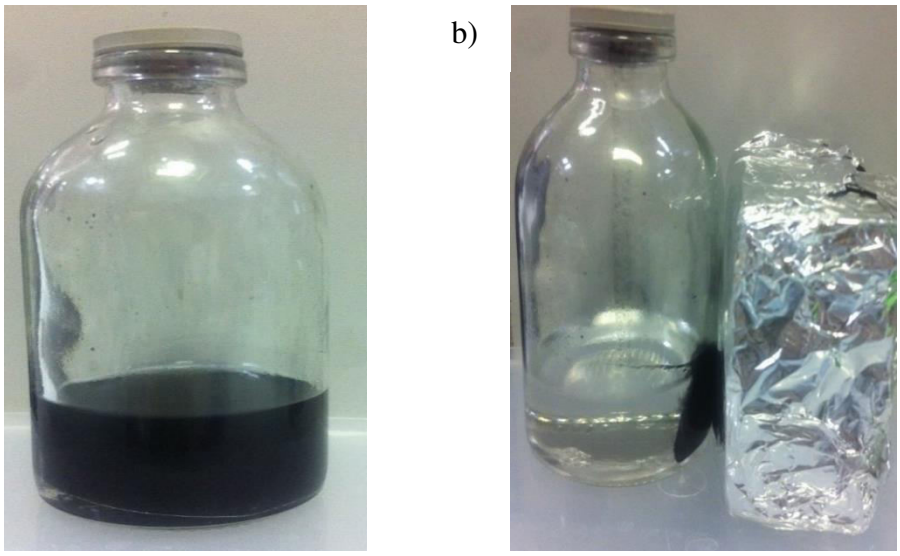

Figure 3.2 OA-MNP in DCM (a) in the absence and (b) presence of magnet

On the other side, to test magnetic sensitivity of MNP and OA-MNP, an external magnetic field was applied to them by using a Nd-Fe-B magnet. When the magnetic field is applied (Figure 3.1 b, 3.2 b and 3.3 b), both types of nanoparticles were attracted by the magnet, so the solutions became transparent. Hence, it could be said that not only

the synthesized MNPs had magnetic property, but also their oleic acid coated forms had. When the magnet was removed, the MNPs dispersed in water whereas OA-MNPs did in DCM again due to their superparamagnetic properties (Figure 3.1 a and 3.2 a).

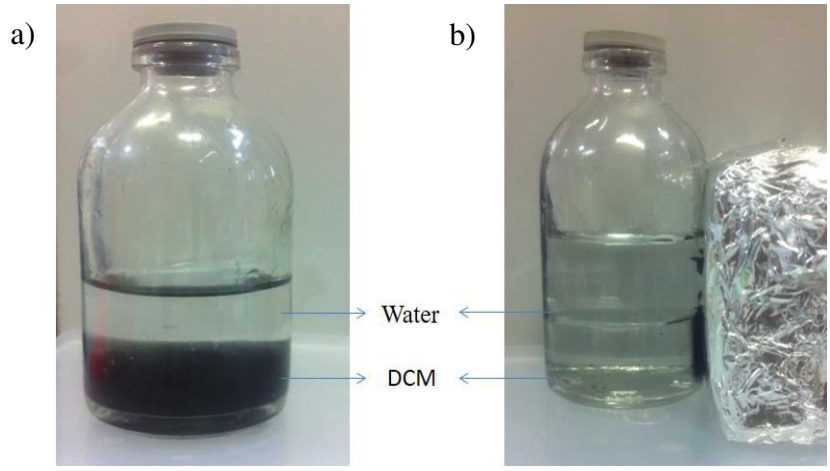

Figure 3.3 OA-MNP in water / DCM mixture (a) in the absence and (b) presence of magnet

3.1.2 Transmission Electron Microscopy (TEM)

The size and morphologies of the synthesized MNPs and OA-MNPs were analyzed by transmission electron microscope (TEM) imaging (Figure 3.4 and Figure 3.5). As shown in Figure 3.4 spherical MNPs were agglomerated in water and their sizes were between 8 and 11 nm.

Smaller nanoparticles have higher surface area to volume ratio. The nanoparticles with high surface area to volume ratio have higher tendency for agglomeration. Coating of surface provides more resistance to agglomeration and avoidance of biological clearance and more successful targeting (Issa *et al.*, 2013).

In this study, MNPs were coated with oleic acid to prevent agglomeration; hence, OA-MNPs were uniformly dispersed in ethanol compared to uncoated MNPs (Figure 3.5). Besides, OA-MNPs were spherical in shape and their size ranges between 8 and 16 nm.

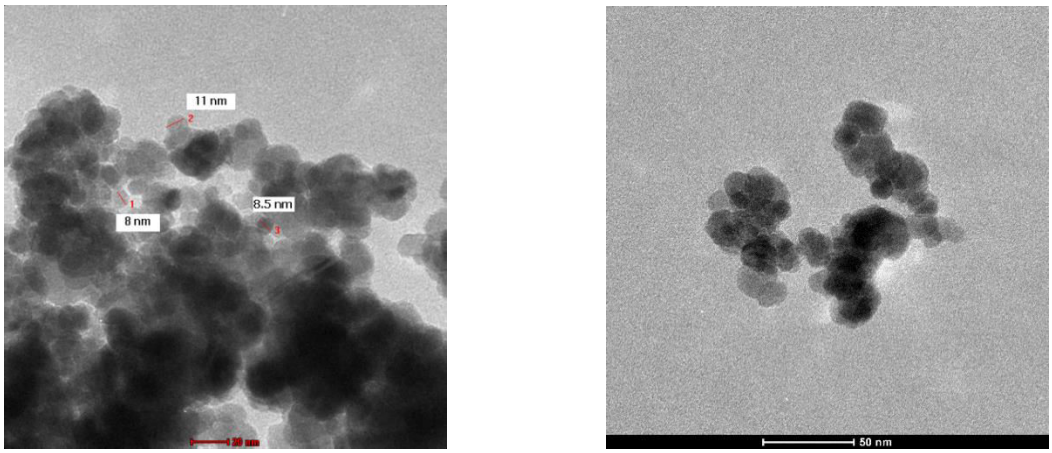

Figure 3.4 TEM images of the MNP in water

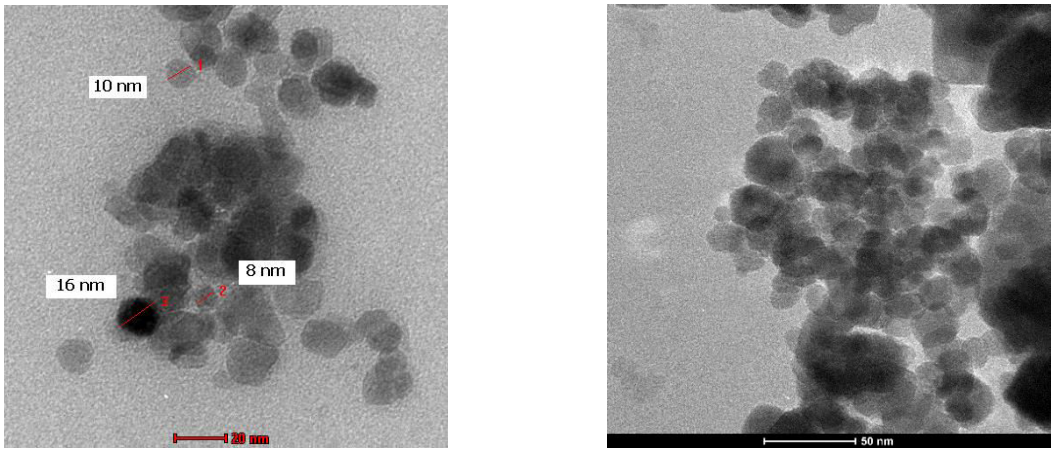

Figure 3.5 TEM images of the OA-MNP in ethanol

Magnetic sensitivity test and TEM imaging results confirmed that MNPs and OA-MNPs were superparamagnetic as explained in section 1.3.1 since both were small sized (8-16 nm) and attracted by external magnetic field whereas no magnetism was observed in the absence of the field.

3. 1.3 Fourier Transform Infrared Spectroscopy (FTIR)

Fourier transform infrared spectroscopy (FTIR) analysis was done for MNP and OA-MNP to show oleic acid coating. The spectrum is shown in Figure 3.6. In FTIR spectrum of MNP, there was a band at 573 cm^{-1} which belonged to vibrations of the Fe-O bonds of magnetite. The band shifted to 565 cm^{-1} in OA-MNP. The bands at 1424,1525, 2850 and 2926 cm^{-1} were present in OA-MNP but not in MNP. Two sharp bands at 1424 and 1525 cm^{-1} corresponded to symmetric COO^- (Vs (COO^-)) and asymmetric COO^- (Vas (COO^-)) respectively. These bands came from oleate ion immobilized on the surface of coated nanoparticles; thus, oleic acid adsorption was confirmed. Two other bands at 2926 cm^{-1} belonged to symmetric CH_2 stretching while 2850 cm^{-1} showed asymmetric CH_2 stretching in oleic acid (Mahdavi *et al*., 2013).

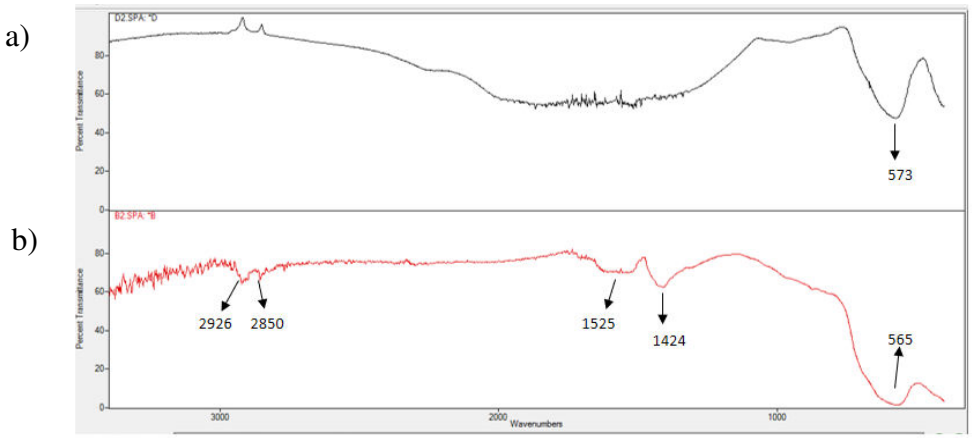

Figure 3.6 FTIR spectra for (a) MNP and (b) OA-MNP

Mahdavi *et al*. mentioned that the interaction between the carboxylate head of oleic acid and metal atom was categorized in three groups; unidentate, chelating bidentate and bridging complex. The interaction type could be identified by using wavenumber separation, λ, between the Vas (COO^-) and Vs (COO^-) bands. If λ is between 200 and 320, it shows monodentate bond interaction. Bridging complex is seen between 140 and 190 cm^{-1} wavelengths and chelating bidendate is seen when λ is smaller than 110 cm^{-1}

(Mahdavi *et al*., 2013). λ is calculated by subtracting Vs from Vas. In our case, λ = Vas – Vs = 101, so it could be said that the interaction between oleic acid and iron was chelating bidentate in which one metal ion binds with two carboxylate oxygen atoms. The interaction is shown in Figure 3.7.

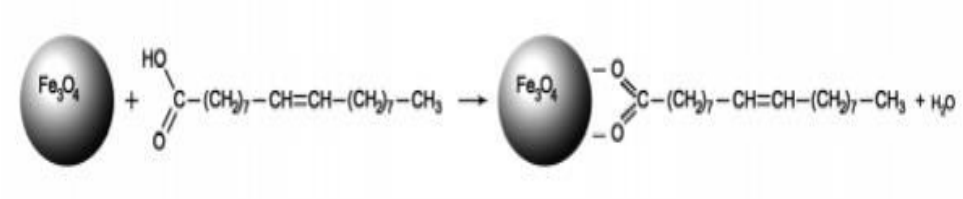

Figure 3.7 Chelating bidentate interaction between the COO^- group of oleic acid and the iron atom (Mahdavi *et al*., 2013)

3.1.4 Vibrating Sample Magnetometer (VSM)

Magnetic hysteresis curve for OA-MNP was obtained at room (25°C) and body (37°C) temperatures by vibrating sample magnetometer where the applied magnetic field was changed, so the magnetization property of the coated MNP could be observed. In the VSM analysis of OA-MNP, which is shown in Figure 3.8, remanence (the remained magnetization after the magnetic field is removed) and coercivity (the magnetic field required to wipe off residual magnetism after the material saturated) were not present (Lee & Hyeon, 2012). Thus, it was confirmed that OA-MNP were superparamagnetic as explained in section 1.3.1 due to having small size (8-16 nm) and this type of hysteresis curve (Schrefl, Hrkac, Suess, Scholz, & Fidler, 2003). It could be seen that the curves for magnetization and demagnetization were overlapped; therefore, they appeared as one curve. Moreover, the saturated magnetization (MS) of the OA-MNPs was 61 emu/g at 25 °C and 37 °C which is consistent with the other studies in literature. In fact, Lin *et al* reported that the saturation value for 4.8 nm sized magnetic nanoparticles is 58 emu/g at room temperature. The difference between these values could be owing to difference in size of the nanoparticles because the size affects the magnetic saturation so that larger

particles of magnetite show greater magnetization (Lin & Scott, 2012). Other than the size, the magnetic property of chemical used for coating is affected on MS value. The MS value decreased after coating of MNP with oleic acid which was previously determined in our laboratory (Tansik *et al.*, 2014). It might be because of diamagnetic property of oleic acid, but OA-MNPs were superparamagnetic even if they were coated.

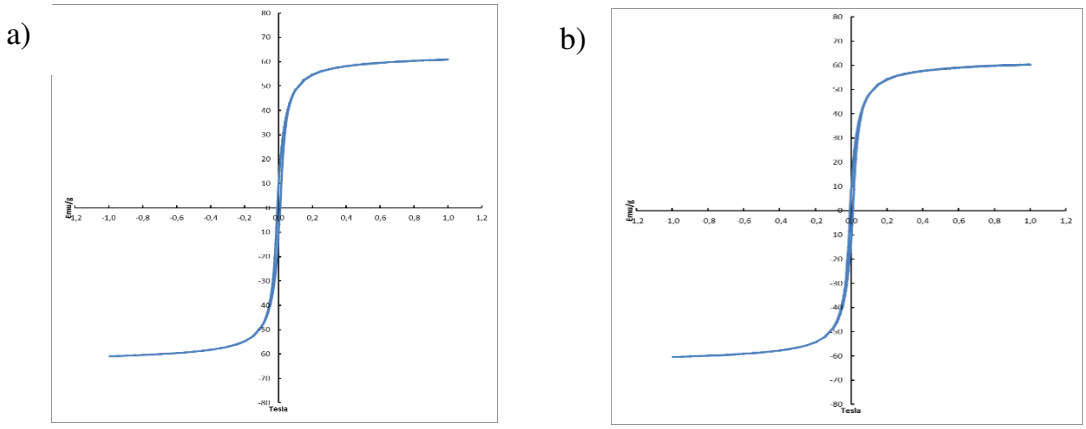

Figure 3.8 VSM analysis of OA-MNP MNP at (a) 25°C and at (b) 37°C

3.1.5 X-ray Photoelectron Spectroscopy (XPS)

X-ray photoelectron spectroscopy (XPS) analysis was employed to identify the surfaces of the synthesized nanoparticles because it is a quantitative elemental analysis technique for the surfaces of materials. Figure 3.9 and 3.10 show the XPS spectra of the MNP and OA- MNP, respectively. The peak at 710.8 eV is the characteristic of Fe2p3/2 core level electron whereas 724.1 eV is of Fe2p1/2 ; thus, they are due to oxidation state of Fe in Fe_3O_4 (Cruz *et al.*,2016). The peaks at 710.6 and 710.7 eV were obtained in both MNP (Figure 3.9) and OA-MNP (Figure 3.10). On the other hand, when the C1s core is considered, the photoelectron peak at 284.6 eV shows the carbon atom in aliphatic chain (C-C / C-H) while the peak at 288.0 eV shows carboxylate (COO^-). Moreover, C1s peak at 290 eV corresponds to carboxylic carbon (COOH) of the free acid (Ling *et al.*, 2006). In the XPS spectra for the OA-MNP, there were peaks at 284.2 and 288.1 eV and no peak at 290 eV. Thus, it could be said that there is no free acid on the surface of OA-

MNP, oleic acid and iron bind to each other with a bond through oxygen atom of carboxylic acid and iron subunit.

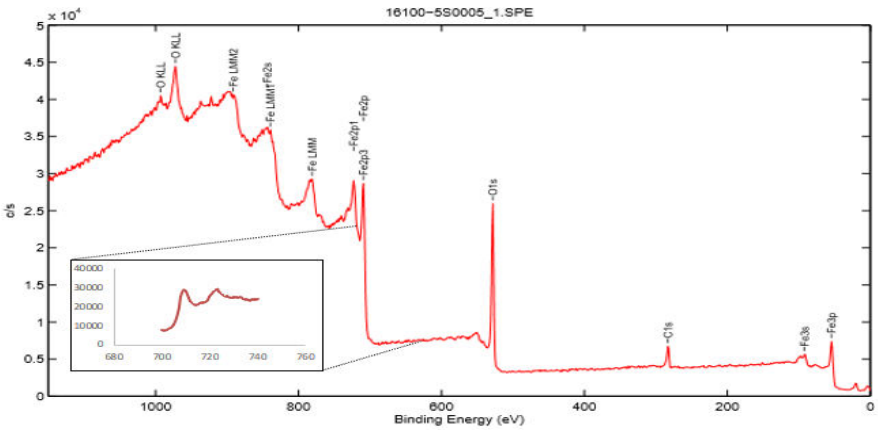

Figure 3.9 X-ray photoelectron spectra of the synthesized MNPs (Fe2p spectrum was expanded.)

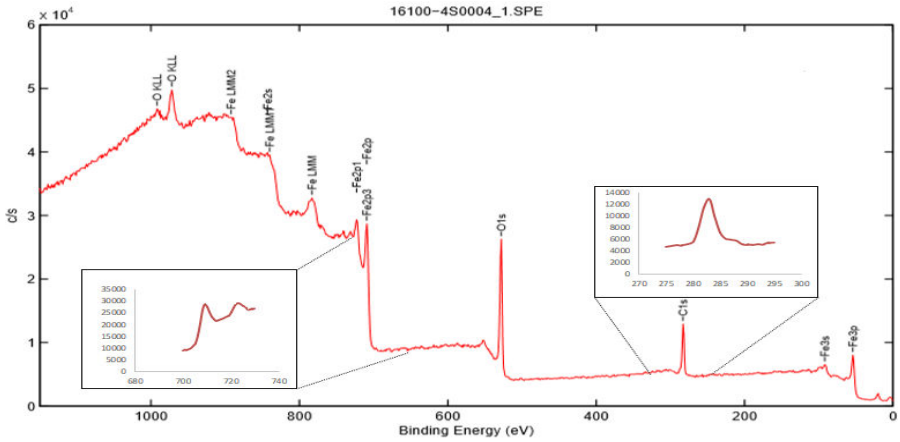

Figure 3.10 X-ray photoelectron spectra of OA-MNPs (Fe2p and C1s spectra were expanded.)

3.1.6 Zeta Potential Analysis

Zeta potential of the nanoparticles is the measurement of the surface charges in a solution. The charged particles attract the opposite charged ions; thus, a double layer of ions is formed. This layer travels with the nanoparticle in the solution. Accordingly, a

potential which is produced between the layers is called zeta potential. The value of this potential is important for applications in biomedicine because it gives information about the colloidal stabilities of nanoparticles. The particles having the values greater than +25 mV or less than -25 mV are considered as stable (Estoration & Awai, 2009 ; Nanocomposix, 2012).

The zeta potential of the MNPs and OA-MNPs were measured by using zetasizer. The value was -18.9 mV for MNP whereas -34.7 mV for OA-MNP (Figure 3.11). The OA-MNP had more negative charge due to hydroxyl groups coming from oleic acid. Thus, by looking this result it could be seen that the surface of synthesized MNPs were coated with oleic acid successfully. At this stage of the study, the stabilities of these nanoparticles were not so critical because they will be coated with polymers, loaded with drugs, so their final zeta potentials were important for *in vitro* or *in vivo* applications. Zeta potential analysis indicated that OA-MNPs were more stable than MNPs.

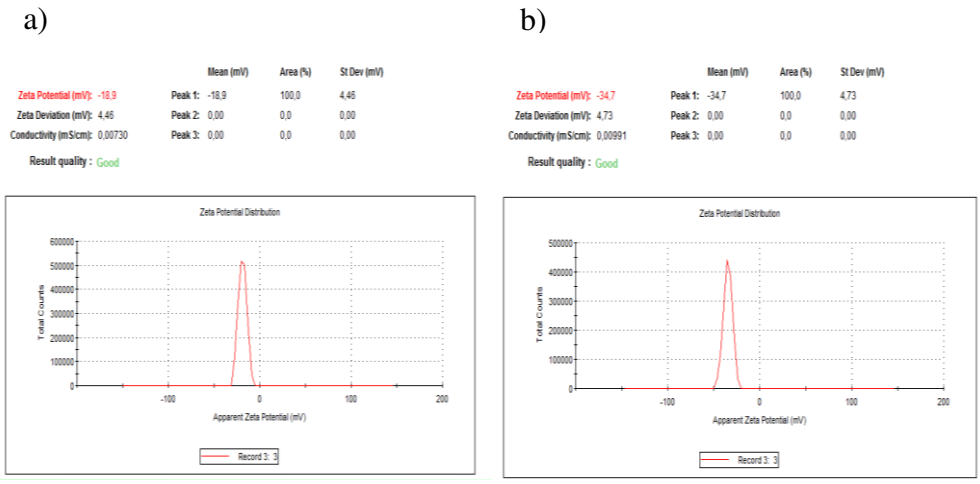

Figure 3.11 Zeta potential of (a) MNP and (b) OA-MNP

3.2 Synthesis and Characterization of Magnetic Polymeric Nanoparticles

The surface of the MNPs was modified with oleic acid, then they were coated with PLGA and TPGS by nanoprecipitation method.

The synthesized nanoparticles were characterized with respect to size, morphology, surface charge and chemical content by DLS, SEM, zeta potential, FTIR and TGA techniques, respectively.

3.2.1 Fourier Transformed Infrared Spectroscopy

The chemical contents of the PLGA nanoparticle containing TPGS (PLGA-TPGS NP) and its magnetic form (PLGA-TPGS-MNP) were determined by FTIR spectroscopy as in Figure 3.12.

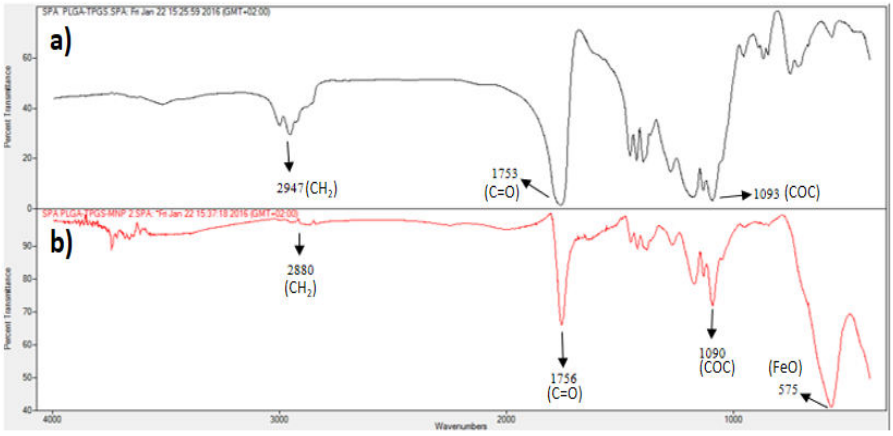

Figure 3.12 FTIR spectrum of (a) PLGA-TPGS NP and (b) PLGA-TPGS-MNP

The bands at 1090 cm^{-1} and 1093 cm^{-1}, characteristic ester bond of PLGA and TPGS chains, were observed in PLGA-TPGS-MNP and PLGA-TPGS NPs, respectively. Moreover, the peaks for C=O stretch of PLGA and TPGS were present in both nanoparticles, but the peak was obtained at 1756 cm^{-1} for PLGA-TPGS-MNP whereas it shifted to 1753 cm^{-1} in the other. There were peaks around 3000 cm^{-1} belonging to CH_2

stretching came from oleic acid coated MNP and/or PLGA (Ma *et al.*, 2010). On the other hand, in the PLGA-TPGS-MNP, the band at 575 cm^{-1} because belonged to magnetite , but it absent in PLGA-TPGS NP (Rawat *et al.*, 2015).Therefore, these FTIR results suggested that the MNPs successfully incorporated to TPGS and PLGA polymer.

3.2.2 Zeta Potential Analysis

The zeta potential, surface charge, of PLGA nanoparticle which did not contain TPGS as matrix material was measured as -40.5 mV whereas the potential for PLGA nanoparticle containing 20% TPGS, called PLGA- TPGS NP, was -19.9 mV. When TPGS was used as an additional material to PLGA , there was a decrease in absolute value of zeta potential because TPGS, as a neutral compound, shielded a portion of the negative charge on the PLGA nanoparticle surface (Zhu *et al.*, 2014a).

On the other side, the zeta potential value for the TPGS-PLGA-MNP was slightly more negative, -23.1 mV, than the TPGS-PLGA NP. Hence, it could be concluded that magnetic nanoparticles were more stable than nonmagnetic polymeric nanoparticles. The zeta potential analyses are shown in Figure 3.13.

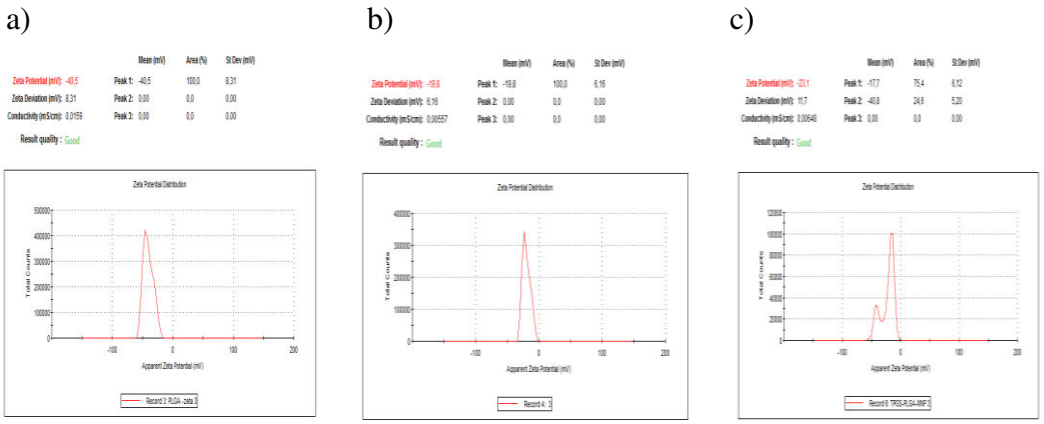

Figure 3.13 Zeta potential of (a) PLGA NP, (b) PLGA-TPGS NP and (c) PLGA-TPGS-MNP

3.2.3 Dynamic Light Scattering (DLS) Analysis

The size of NPT20 was determined by measuring the random changes in the intensity of light scattered from the solution containing nanoparticles in the solvent. The diameters changed from 120 to 130 nm. However, the size of majority of the particles was determined as 125 nm as shown in Figure 3.14.

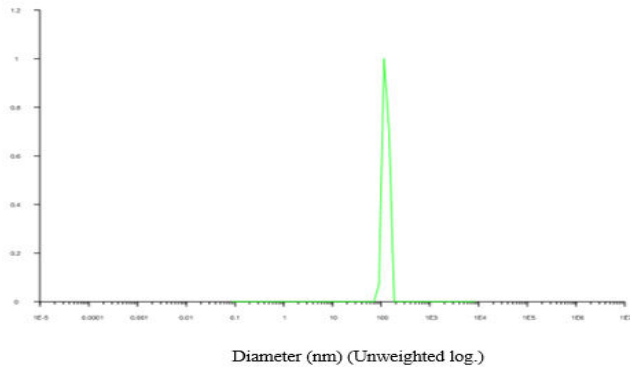

Figure 3.14 Hydrodynamic size distribution of PLGA-TPGS-MNP (NPT20)

3.2.4 Thermal Gravimetric Analysis (TGA)

Thermal gravimetric analysis was performed to show the existence of TPGS in the nanoparticles and to investigate the thermal profile of the TPGS in PLGA-TPGS NP and PLGA-TPGS-MNP (NPT20). Free TPGS was used for control as shown in Figure 3.15. The thermogram of PLGA-TPGS NP shows the thermal loss of nanoparticles in Figure 3.16.

In the thermogram for control sample, TPGS, there was one phase with 99.48% weight loss. It is known that the combustion temperature for TPGS is between 350 and 500°C (Zhu *et al.*, 2014b). Consequently, almost all TPGS was lost in that temperature range.

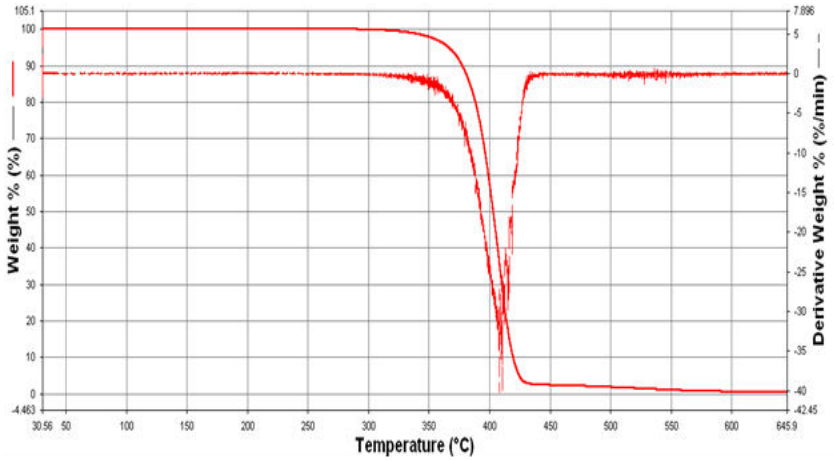

Figure 3.15 Thermal gravimetric analysis of TPGS

In the thermogram for PLGA- TPGS NP, there were two phases for PLGA combustion between 220 and 350°C and for TPGS between 350 and 500°C as shown in Figure 3.16. Analysis showed that 80% of the total weight was PLGA whereas 20% was TPGS. This was expected because during the nanoparticle synthesis the components were added with the 4:1 weight ratio. Thus, in this study, the magnetic nanoparticles containing 20% TPGS were called NPT20. Moreover, it was proved that TPGS was a remnant in the nanoparticle.

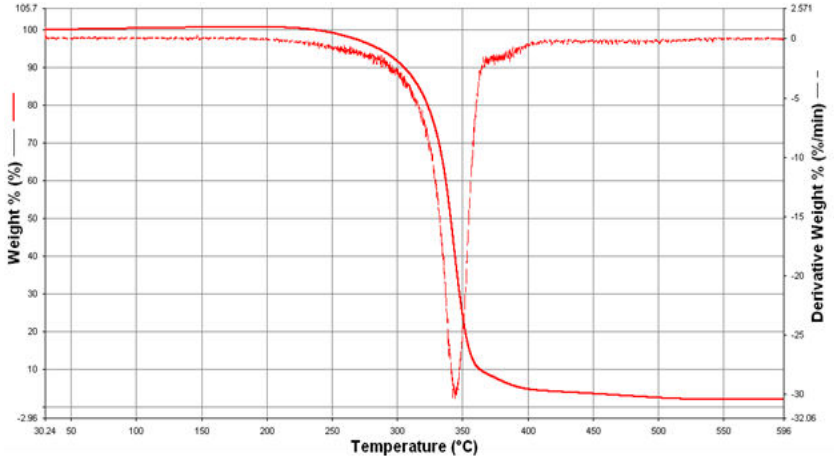

Figure 3.16 Thermogram for the weight loss of PLGA-TPGS NP

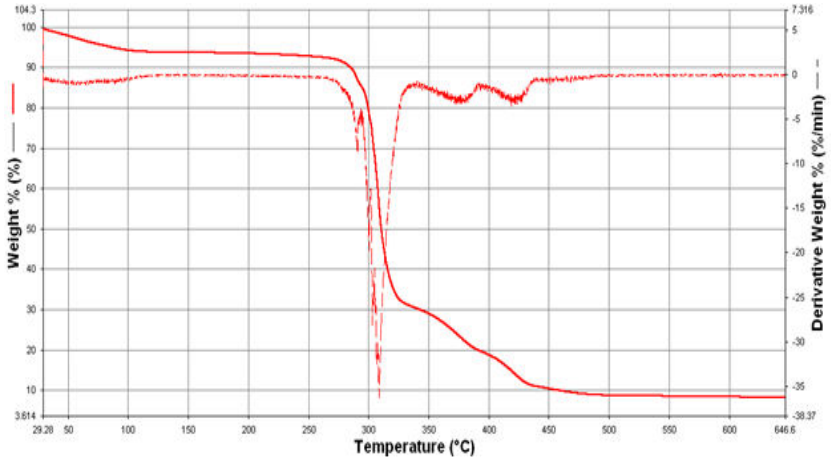

Figure 3.17 Thermogram for weight loss of PLGA-TPGS-MNP (NPT20)

On the other hand, in the thermogram for NPT20 there were three weight loss phases as shown in Figure 3.17. At the temperatures between 20 and 140°C water evaporation, between 220 and 350°C PLGA combustion and between 350 and 500°C TPGS combustion occurred. Moreover, OA combustion was between 140 and 600°C and the residue (8.58 %) was due to MNP encapsulated in PLGA-TPGS-MNP (NPT20).

3.2.5 Scanning Electron Microscopy

The morphology of the synthesized PLGA-TPGS-MNP (NPT20) was visualized under scanning electron microscope, so SEM images of the nanoparticles are shown in Figure 3.18. As it could be seen the synthesized nanoparticles were spherical shaped.

a)

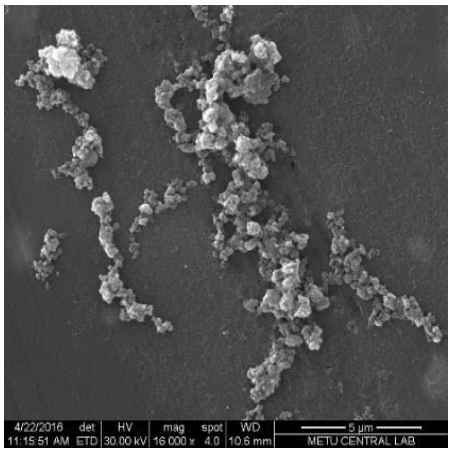

b)

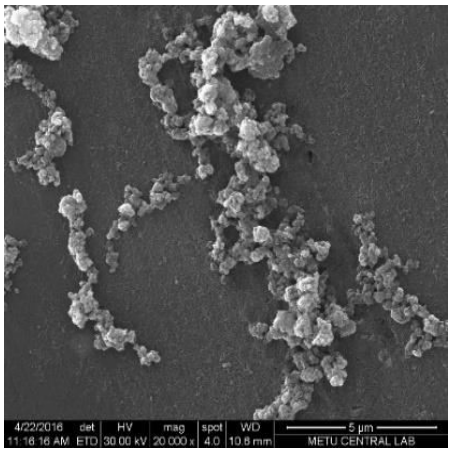

c)

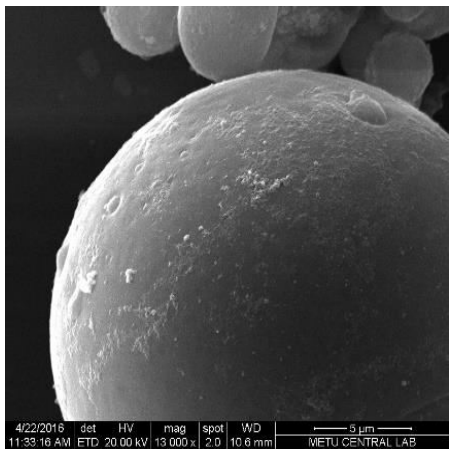

Figure 3.18 SEM image of (a), (b) NPT20 and (c) MPT20

It is known that TPGS is a pore forming agent because it is soluble in both water and organic solvent. Therefore, it could leach away from aqueous phase during nanoparticle synthesis procedure (Zhu *et al*., 2014b). Hence, the porous structure is formed on the surface of nanoparticles. The porous structure on the nanoparticles could not be observed due to inadequate magnification. Hence, microparticles (MPT20) were produced as shown in Figure 3.18 c. However, a perfect visualization of the surface could not be provided by SEM because of resolution limitation.

3.3 Synthesis and Characterization of Drug Loaded Magnetic Polymeric Nanoparticles

3.3.1 UV-Vis Absorption Spectroscopy

UV-Vis absorption spectroscopy was used to confirm encapsulation of doxorubicin in Dox NPs. For this purpose, measurements were performed between 400 and 600 nm wavelengths.

Doxorubicin was dissolved in DCM and used as control. On the other hand, Dox NPT20 and NPT20 were dissolved in DCM and the absorbance of these samples was measured. As shown in Figure 3.19, free doxorubicin and Dox NPT20 gave a peak at 479 nm while NPT20 did not, which indicated the presence of doxorubicin in the Dox NPT20 since excitation wavelength of doxorubicin is 480 nm (Dost, 2014).

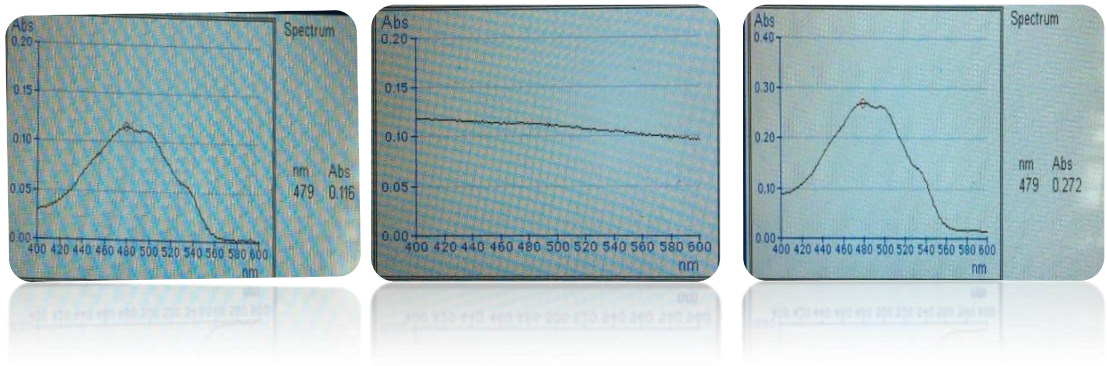

Figure 3.19 UV-Vis absorption spectra of Dox NPT20, NPT20 and free doxorubicin dissolved in DCM, respectively

3.3.2 Fourier Transform Infrared Spectroscopy (FTIR)

Fourier transform infrared spectroscopy (FTIR) analysis was performed for free doxorubicin and Dox NPT20. The FTIR spectra is shown in Figure 3.20 where the peaks for the specific bonds belonging doxorubicin were cited; 1073 cm^{-1} (C-O), 1448 cm^{-1} (C-C), 1610 cm^{-1} (N-H), 1726 cm^{-1} (C-O) and 2881 cm^{-1} (C-H) (Nguyen *et al.*, 2015). These peak values were also present in Dox NPT20 with slight shifting; 1096 cm^{-1} (C-O), 1451 cm^{-1} (C-C), 1604 cm^{-1} (N-H), 1753 cm^{-1} (C-O) and 2884 cm^{-1} (C-H). Thus, the encapsulation of doxorubicin in the Dox NPT20 was confirmed with FTIR analysis.

a)

b)

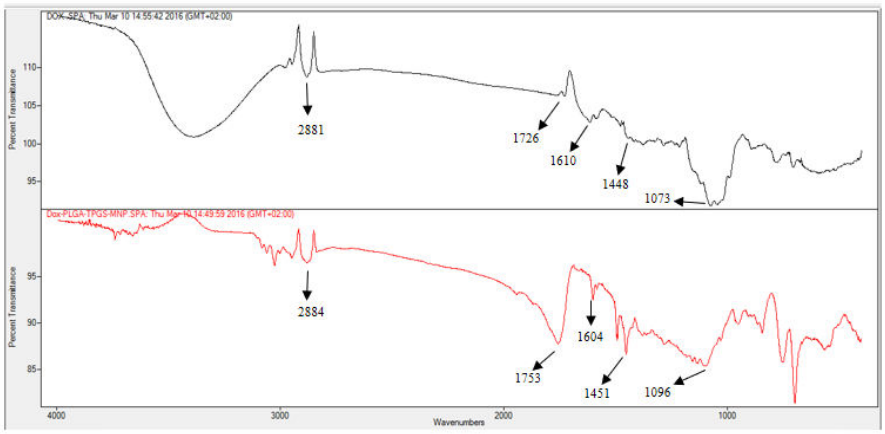

Figure 3.20 The FTIR spectra of (a) free doxorubicin and (b) Dox NPT20

The FTIR spectra of the free doxorubicin, Dox NPT20, PLGA-TPGS MNP and PLGA-TPGS NP were given in the same scheme as shown in Figure 3.21. Doxorubicin loading was confirmed by comparing Dox and Dox NPT20 spectra. On the other hand, loading of MNP, presence of PLGA and TPGS in the nanoparticle could be proved by this scheme. (The analysis of PLGA-TPGS NP and PLGA-TPGS-MNP spectra was explained in section 3.2.1.)

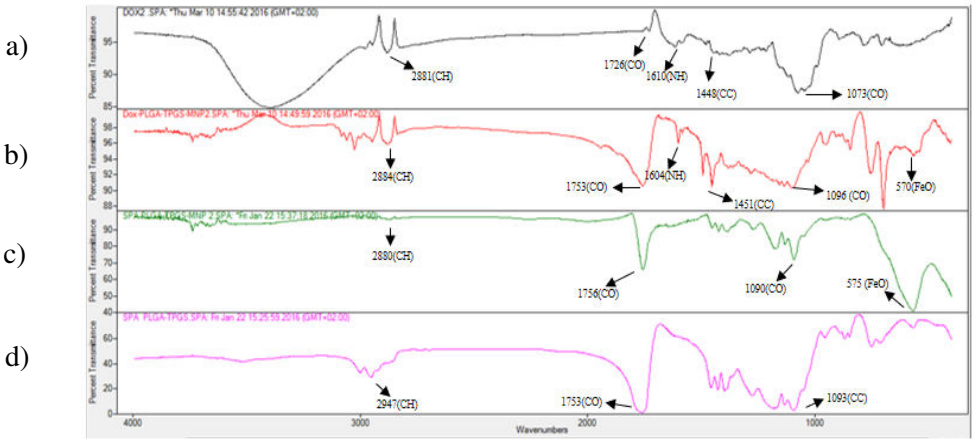

Figure 3.21 The FTIR spectra of (a) free doxorubicin, (b) Dox NPT20, (c) PLGA-TPGS-MNP and (d) PLGA-TPGS NP

3.3.3 Scanning Electron Microscopy (SEM)

The morphology of the synthesized Dox NPT20 was imaged by scanning electron microscopy as shown in Figure 3.22. Dox NPT20s were spherical shaped, but their surfaces were not smooth due to presence of TPGS on the surface. The component TPGS was used as additive in organic solution and surfactant in aqueous solution during the synthesis procedure. Thus, it was located at both inside and surface of the nanoparticle.

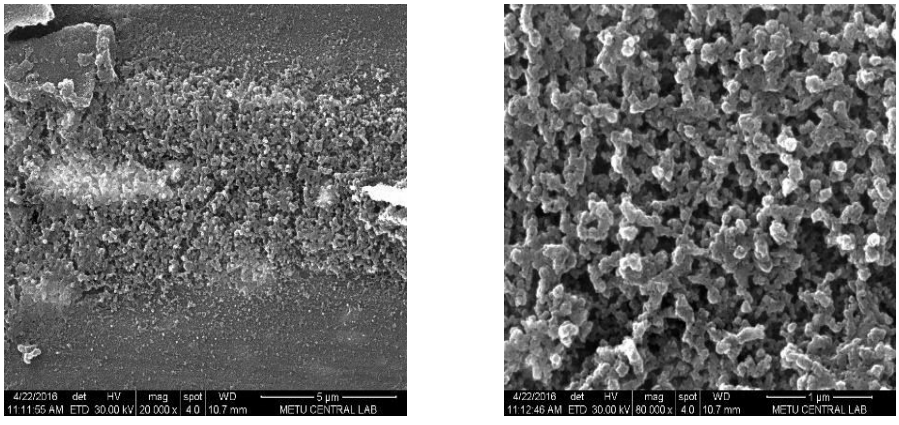

Figure 3.22 SEM images of Dox NPT20

3.3.4 Zeta Potential Analysis

The zeta potential of the Dox NPT20 was determined as -26.7 mV (Figure 3.23) by measuring the surface charge of the nanoparticles. In section 3.1.6 it was explained that the magnitude of the zeta potential gives information about the stability of the nanoparticles. Therefore, the nanoparticles having potential greater than +25 mV or less than -25 mV was confirmed as stable. Thus, the synthesized Dox NPT20 could be considered as stable. Consequently, it could be used in the future *in vitro* or *in vivo* studies.

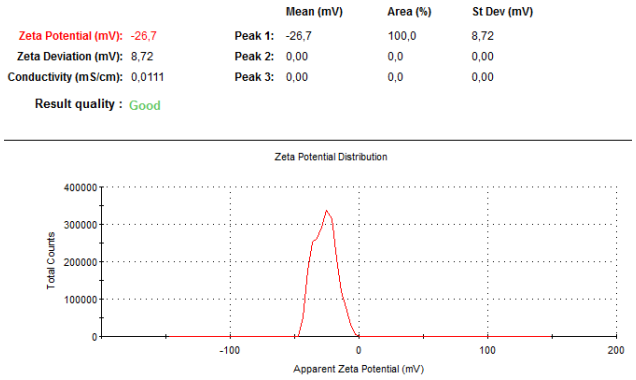

Figure 3.23 Zeta potential of Dox NPT20

The surface charges of the nanoparticles affect circulation lifetime and accumulation in the body. Neutral and negatively charged nanoparticles reduce the adsorption by serum proteins, so increase circulation half-life (Duan & Li, 2013). Blanco *et al.* showed that negatively charged nanoparticles having longer circulation time in blood and lower accumulation ability in monocyte phagocytic system (MPS); lung, liver and spleen (Blanco, Shen, & Ferrari, 2015). From this knowledge, it was concluded that the synthesized negatively charged nanoparticles could have long circulation time and high ability for avoiding body clearance.

3.3.5 Dynamic Light Scattering (DLS) Analysis

After the coating and drug loading process, the overall size of the nanoparticles is important because nanoparticles smaller than 5.5 nm are removed through renal clearance whereas the ones larger than 200 nm are trapped by the phagocytic cells of the spleen (Choi *et al*., 2007).

The average hydrodynamic diameter of the Dox NPT20 was found 121 nm with DLS analysis as shown in Figure 3.24. Moreover, it was observed that the size distribution was uniform. The average size of NPT20 was found as 125 nm in section 3.2.3. Hence, there was no difference between the size of the drug free and drug loaded form of the nanoparticle. This could be due to efficient binding of the doxorubicin having positively charged amino group to PLGA having negatively charged hydroxyl group. Thus, a condensed structure was formed and the size changed slightly. On the other hand, loading of drug on the pores formed by TPGS might prevent the increase the size of nanoparticles (Yoo, Lee, Oh, & Park, 2000).

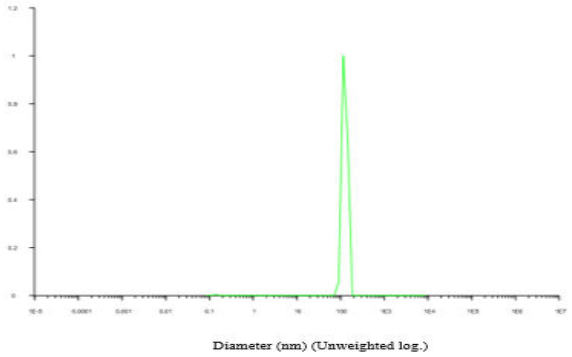

Figure 3.24 Hydrodynamic size distribution of Dox NPT20

The nanoparticles between 100 and 150 nm extravasate through vascular fenestrations of tumors due to EPR effect and escape from liver and spleen filtration (Blanco *et al*., 2015). Moreover, Hobbs *et al.* confirmed that nanoparticles around 100 nm sized were long-lasting in the circulation (Hobbs *et al*., 1998). In this study, the size of drug loaded

nanoparticles was 125 nm, so they could be delivered to tumor site without liver and kidney obstacles being cleared.

3.3.6 Thermal Gravimetric Analysis (TGA)

Thermal gravimetric analysis was performed to determine the phase of the doxorubicin which is encapsulated in Dox NPT20. The thermogram was given in Figure 3.25.

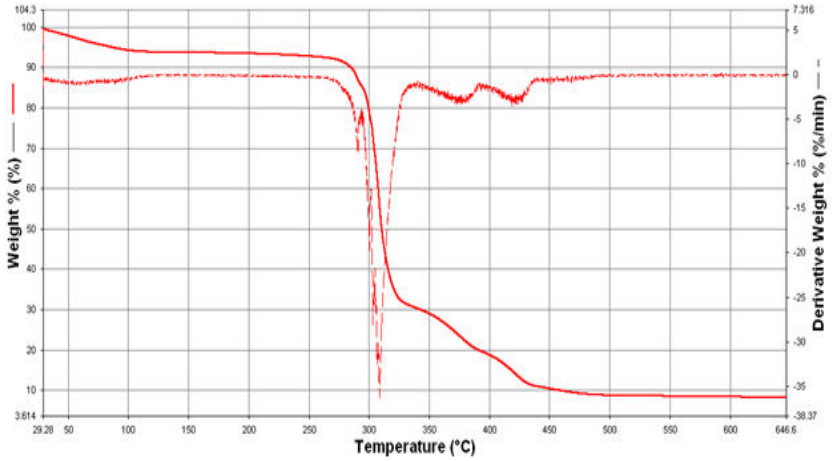

Figure 3.25 Thermogram of Dox NPT20 between 25 and 650°C

The melting point of the doxorubicin crystalline is 230°C, but there was no sharp weight loss point at that temperature for Dox NPT20. Hence, it could be determined that doxorubicin was present in the NP as an amorphous or disordered crystalline phase or in the solid solution state, but not in crystalline phase (Gulati, Aw, & Losic, 2012).

3.4 Drug Loading

There is an electrostatic interaction between amine group of doxorubicin and carboxyl group of PLGA (Qi *et al.*, 2016). In order to determine drug loading and entrapment capacities of the nanoparticles, different amounts of doxorubicin were added during the Dox NPT20 synthesis. The unloaded drug amount was calculated by measuring the

absorbance of the supernatant and loaded amount was determined by using standard calibration curve given in Figure A.5.

Encapsulation efficiency, loading content and loading efficiency of the nanoparticles were determined by using the Equations 2.1, 2.2 and 2.3, respectively.

Encapsulation efficiency was found 97.3 % from the Eqn. 2.1;

$$\text{EE \%} = \frac{(2000 \mu g\ Dox) - (53\ \mu g\ Dox\ in\ supernatant)}{(2000\ \mu g\ Dox)}\ x\ 100 = 97.3\ \%$$

When 2 mg (2000 µg) of doxorubicin was added during synthesis, 53 µg of doxorubicin was present in supernatant meaning that 1947 µg of doxorubicin loaded on nanoparticles. Moreover, 11 mg of Dox NP was obtained. Therefore, 177 µg of doxorubicin was loaded in 1 mg nanoparticle which is called loading content found from the Eqn. 2.2;

$$\text{Loading content} = \frac{(2000\ \mu g\ Dox) - (53\ \mu g\ Dox)}{(11\ mg\ Dox\ NPT20)} = 177\ \mu g.$$

Loading efficiency was found as 88.5% from the Eqn. 2.3;

$$\text{Loading efficiency (\%)} = \frac{(1947\ \mu g\ Dox)/(11\ mg\ NP)}{(2000\ \mu g\ Dox)/(10\ mg\ NP)}\ \text{x}\ 100 = 88.5\ \%$$

The average encapsulation efficiency, loading content and efficiency of the nanoparticles depending on drug amount was summarized in Table 3.1 and drug loading efficiencies were showed in Figure 3.26. The loaded drug amount increased until a certain value as more drug added during synthesis. The encapsulation efficiency was 97.3 % for 2 mg whereas 80.9% for 2.5 mg. Thus, 2 mg doxorubicin addition was preferred for further experiments to obtain efficient results.

Table 3.1 Entrapment efficiency, loading content and loading efficiency depending on the drug during synthesis

The amount of drug (mg)	Encapsulation Efficiency (%)	Loading Content (µg) ± SEM of 1 mg NP	Loading Efficiency (%) ± SEM
0.7	97.4	62 ± 3.68	88.5 ± 5.25
1.0	97.9	89 ± 6.11	89 ± 6.11
1.5	96.8	132 ± 5.79	88 ± 3.86
2.0	**97.3**	**177 ± 4.58**	**88.5 ± 2.29**
2.5	80.9	184 ± 2.94	73.6 ± 1.18

The drug loading profile with the increase in the amount of initial drug used in nanoparticle synthesis process was shown in Figure B.1. 177 µg of Dox was loaded in 1 mg of Dox NPT20 with 88.5% loading efficiency. This loading results were sufficient to use these nanoparticles in cancer treatment since studies showed that even 78 µg of doxorubicin loaded in 1 mg of nanocomposite was efficient to kill cancer cells (Chen *et al.*, 2011).

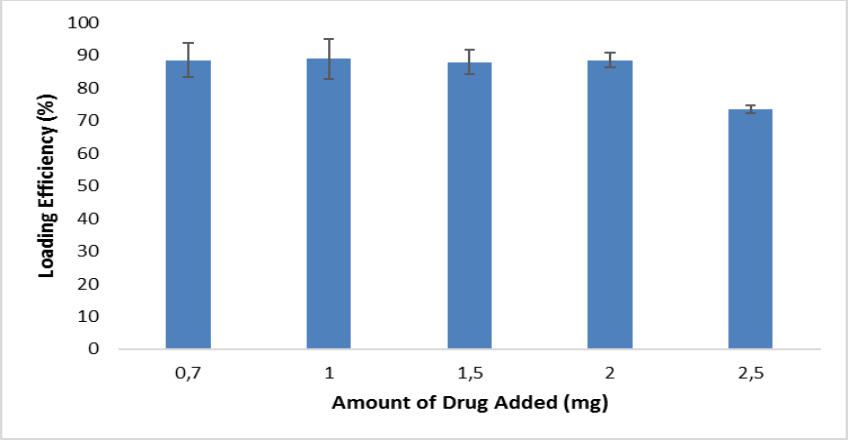

Figure 3.26 The drug loading efficiency depending on drug amount (Experiments were performed in triplicates.)

On the other hand, for determination of the relation between the loading capacity and TPGS amount in the nanoparticle, the nanoparticles not containing TPGS as core material, i.e. containing 100% PLGA (called Dox NPT0), were synthesized. 2 mg drug was added during synthesis period. Therefore, the comparison with the Dox NPT20 which produced by adding the same amount drug in the synthesis procedure could be done. Then, the loading content of these nanoparticles was calculated in the same way. The summary was given in the Table 3.2. Finally, it was found that 155 µg of Dox loaded in 1 mg of Dox NPT0 and the EE% was 85.7%. It could be seen that presence of TPGS in core material increased the loading capacity and entrapment efficiency of the nanoparticles. Other studies also reported that TPGS increased the drug loading capacity of the nanoparticles was confirmed, too (Zhu *et al.*, 2014a).

Table 3.2 Comparison of Dox NPT0 and Dox NPT20 in terms of EE (%), loading content and loading efficiency (%)

Nanoparticle Type	Entrapment Efficiency (%)	Loading Content (µg) ± SEM of 1 mg NP	Loading Efficiency (%) ± SEM
Dox NPT0	85.7	155 ± 1.17	77.9 ± 3.34
Dox NPT20	97.3	177 ±4.58	88.5 ±2.29

3.5 Drug Release

The *in vitro* release of doxorubicin from Dox NPT20 was followed over 35 days. For release study, the nanoparticles having highest encapsulation efficiency were used. 1 mg of Dox NPT20 was suspended in 1 ml of phosphate buffer (PBS 0.01 M, pH 7.4) and the released drug amount was determined with UV spectrophotometer by which the absorbance coming from drug in PBS was measured. Afterwards, the absorbance value was converted to concentration by using the calibration curve for doxorubicin that is plotted with standard concentration of doxorubicin in PBS (pH 7.4) (Figure 3.27).

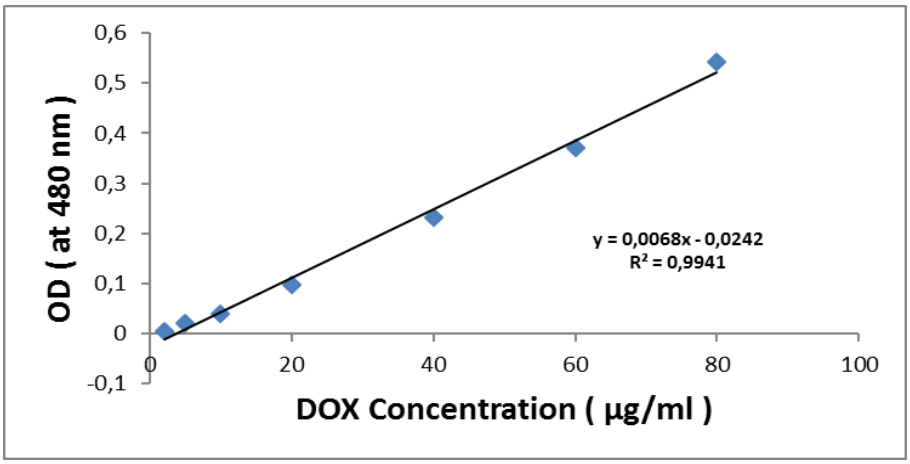

Figure 3.27 Calibration curve for doxorubicin in pH 7.4 buffer

The cumulative drug release from Dox NPT20 at pH 7.4 is shown in Figure 3.28. pH 7.4 was preferred to mimic intracellular part of breast cancer cells which was mentioned in section 1.1.2 because drug loaded PLGA nanoparticles escape the endo-lysosome and enter cytoplasm, and then drug release occurs. At first day, 27% of the total encapsulated drug was released. At the end of day 7, 47% of total drug released until the last day 55% of total released. Moreover, a burst release was present during first day since 27% of the drug released. During burst release phase, drug loaded in the cavities on the surface of PLGA and TPGS polymers, and drug entrapped in the regions close to the nanoparticle surface were released by diffusion. After that, during other two zones sustained release profile obtained and 55% of the total drug was released at the end of 35 days. This slowed down release could be due to decrease in drug amount loaded in the available diffusion distance from the surface. Thus, drug located at the inner layers of nanoparticle began to release after burst time. By comparing the drug amounts in burst release and sustained release phases, and considering the unreleased drug located at the inner site, it could be said that the most of the drug was loaded at the internal part of polymer matrix than the outer part.

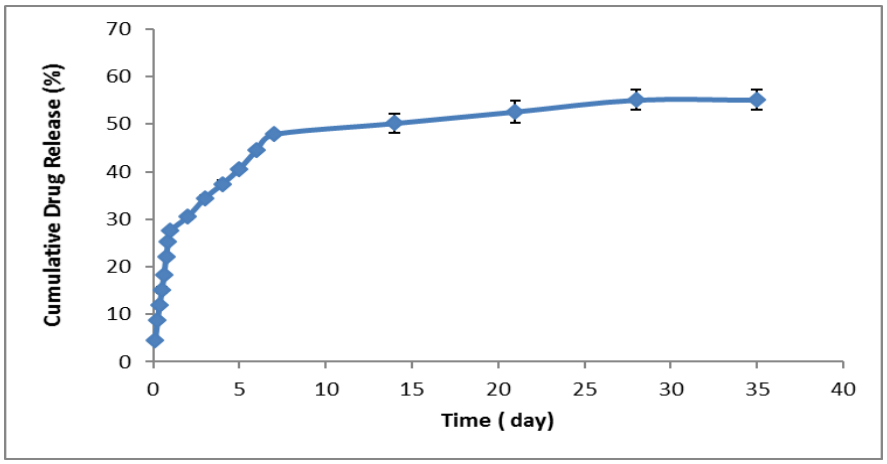

Figure 3.28 Cumulative drug release profile of Dox NPT20 at pH 7.4 (Experiments were performed in triplicates.)

Generally, the drug release from the polymeric nanoparticles occurs by diffusion which controls the releasing rate that is why the type of the polymer affects the release rate due to its degradation rate. Moreover, the physiological environment such as temperature and pH could influence this profile. For this purpose, doxorubicin release from Dox NPT20 was also studied at pH 4.2 and 5.2 which mimics endosomal conditions (Figures A.2 and A.4). Drug was released at lower rated at pH 4.2 and 5.2 than pH 7.4 (Figure 3.29) was because of protonated NH_2 group of doxorubicin in acidic environment. However, negativity of PLGA decreased due to proton addition to OH^- group of PLGA. Thus, there was no electrostatic effect for diffusion of drug from polymeric nanoparticle in acidic conditions (Guo *et al*., 2014a). As a result, there was no increase in drug release rate at acidic conditions for Dox NPT20.

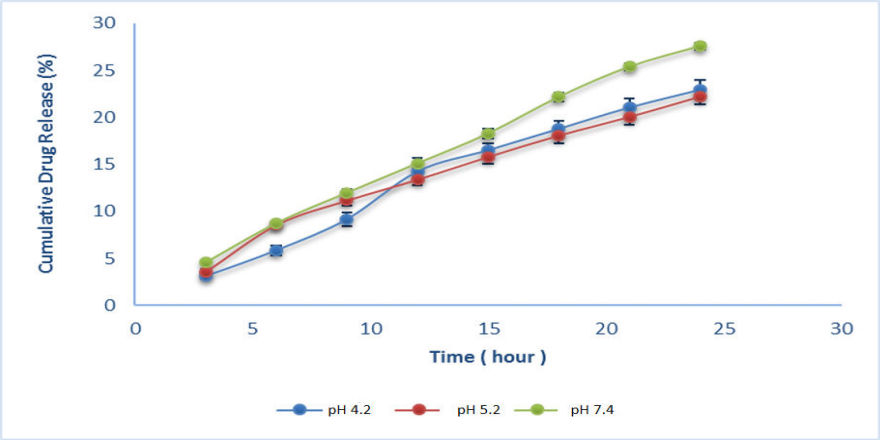

Figure 3.29 Cumulative drug release of Dox NPT20 at pH 4.2, 5.2 and 7.4 in 24 hours (Experiments were performed in triplicates.)

On the other hand, the drug release profile for Dox NPT0 was studied in the same way. As shown in Figure 3.30, 41% of the total loaded drug was released in 35 days. However, this value was 55% for Dox NPT20. From the previous studies, it is known that, TPGS forms pore on the surface of nanoparticles (Zhu *et al.*, 2014a). The porous structure increases the release of drug because water could enter from the pores into inner parts of the nanoparticle, so degradation rate elevated. Interaction of polymer with water is necessary for degradation since this process occurs by hydrolysis of ester bonds. Zhu *et al.* (2014) confirmed that the release rate improved with the increase in amount of TPGS in nanoparticle matrix. Our study was also showed that the increase in drug release owing to presence of TPGS as core material.

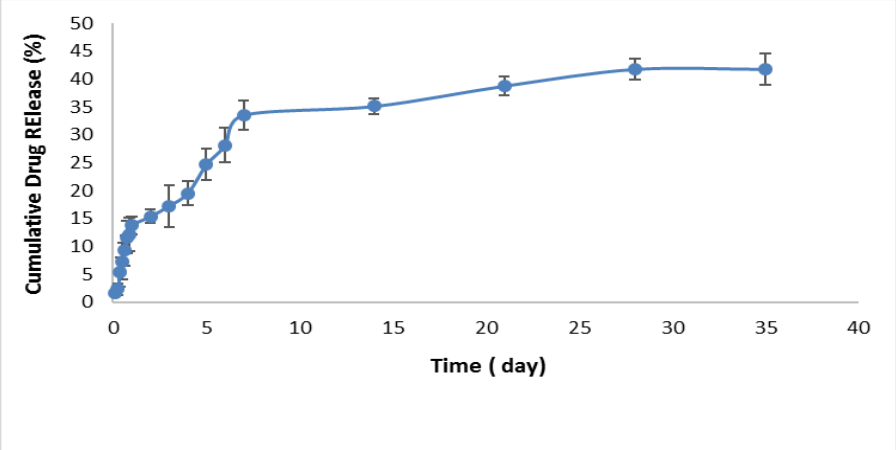

Figure 3.30 Cumulative drug release profile of Dox NPT0 at pH 7.4 (Experiments were performed in triplicates.)

3.6 Cell Culture Studies

3.6.1 Development of Drug Resistant Cell Line

Drug resistant cells were developed as explained in section 2.2.9.8. In order to confirm resistance to doxorubicin, XTT cell proliferation assay was performed. Hence, the half maximal inhibitory concentration (IC_{50}) of doxorubicin was determined in MCF-7 and MCF-7/Dox cells.

The cell proliferation profile of MCF-7 and MCF-7/Dox cells in the presence of various amounts of doxorubicin concentration are shown in Figure 3.31 and 3.32, respectively. IC_{50} value was found 2.5 µM in MCF-7 cells whereas it was 173 µM in MCF-7/Dox cells (Figure C1 and C2). Thus, it was concluded that MCF-7/Dox cells were 69-fold resistant to doxorubicin than MCF-7 cells, that its resistant index (R) was 69.

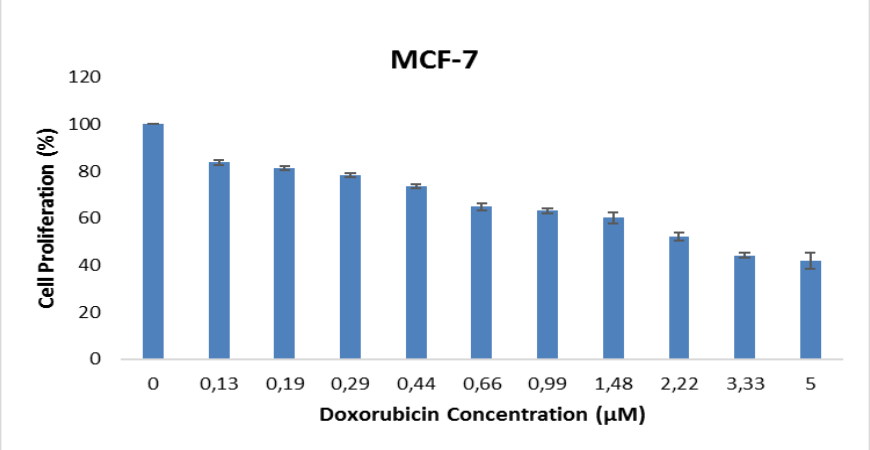

Figure 3.31 Cell proliferation profile of MCF-7 cells treated with increased concentration of doxorubicin (Experiments were performed in duplicates.)

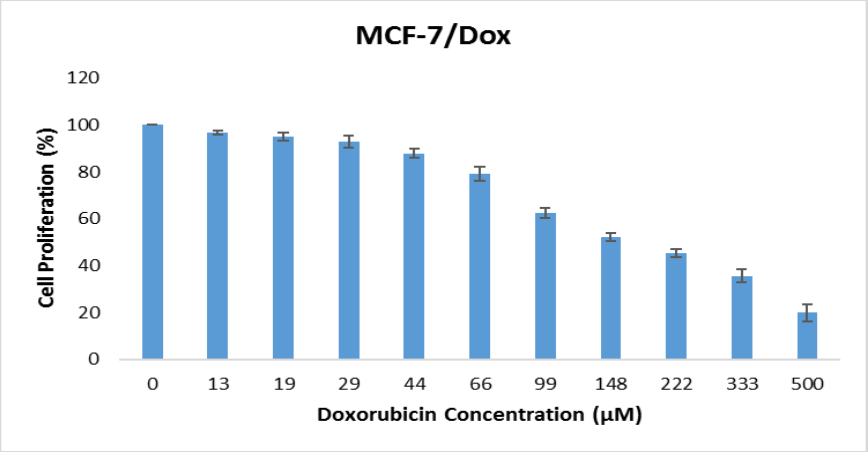

Figure 3.32 Cell proliferation profile of MCF-7/Dox cells treated with increased concentration of doxorubicin (Experiments were performed in duplicates.)

In addition, our previous lab members found that the cells having doxorubicin resistance also developed resistance to some other drugs such as paclitaxel, docetaxel and tamoxifen (Darcansoy, 2009) . Hence, MCF-7/Dox cells could represent the multidrug resistant cell model in this study.

3.6.2 Prussian Blue Staining for Detection of Nanoparticle Internalization

Dönmez *et al* showed that the uptake of free doxorubicin and accumulation in the cell was higher in MCF-7 cells than MCF-7/Dox cells due to overexpression of P-gp pump in resistant ones (P-gp is responsible for drug efflux in resistant cells.) (Donmez, Akhmetova, Iseri, Kars, & Gunduz, 2011). Although there was low level of nanoparticle efflux in resistant cells, NPs could not be effluxed easily as free drugs (Unsoy, 2013). For detection of NPT0 and NPT20 internalization by the cells, Prussian blue staining method was used. The principle of this technique is that ferric ion combines with the ferrocyanide and dark colored Prussian blue pigment is formed. Consequently, the magnetic nanoparticles could be stained dark. Moreover, this staining kit contains pararosaniline which interacts with the cell compartments, so pink color is formed in that regions. To show the cellular internalization of the nanoparticles and to determine the effect of TPGS on internalization, the same concentrations (50 µg/ml) of NPT0 and NPT20 were given to MCF-7 and MCF-7/Dox cells, then 5 h incubation was performed at 37°C. After that, they were observed under light microscope. The non-treated control cells were only pink colored while nanoparticle treated ones were both pink and dark. When cells were incubated with TPGS containing nanoparticles, more amount of nanoparticle internalized by the cells than NPT0 treated ones as shown in Figure 3.33 and 3.34. It was seen that more nanoparticles were located in the NPT20 treated resistant cells than NPT0 treated ones. Hence, resistance could be reduced by adding TPGS in core material of nanoparticles. Even though more nanoparticle internalized by MCF-7 cells than MCF-7/Dox cells, the cellular uptake of the nanoparticles by resistant ones was increased by using TPGS as additional core material. Hence, it could be used to enhance the cellular internalization of nanoparticles by both cell types. Zhu *et al.* also confirmed that TPGS presence on nanoparticle enhanced the cellular uptake of the nanoparticles (Zhu *et al.*, 2014a). It is known that TPGS increased the aqueous solubility of nanoparticles and membrane permeability due to hydrophilic PEG tail (Z. Zhang, Tan, & Feng, 2012). Thus, cellular internalization was improved by adding TPGS to nanoparticle core material.

a) b) c)

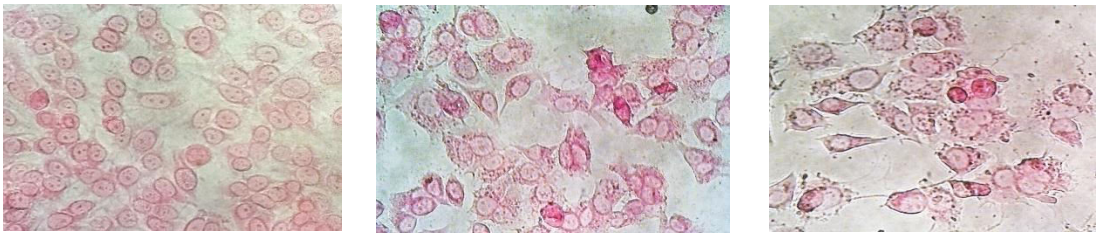

Figure 3.33 Light microscope imaging of MCF-7 cells (a) non-treated, treated with (b) NPT0 and (c) NPT20

a) b) c)

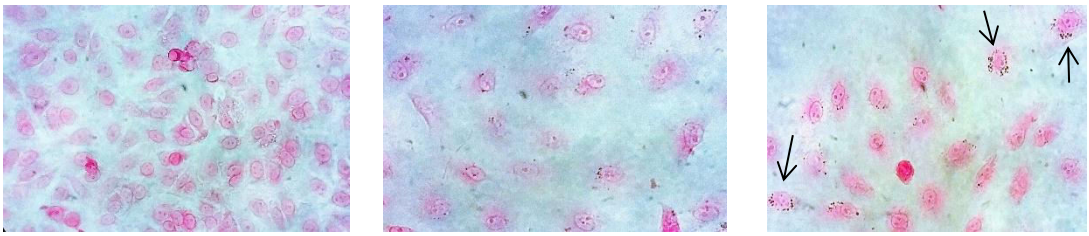

Figure 3.34 Light microscope imaging of MCF-7/Dox cells (a) non-treated, treated with (b) NPT0 and (c) NPT20

3.6.3 Magnetic Targeting of NPT20 by External Field

The targetable properties of NPT20 were detected by using the three well canal-connected slide. The behaviors of the nanoparticles in the presence or absence of magnetic field are shown in Figure 3.35.

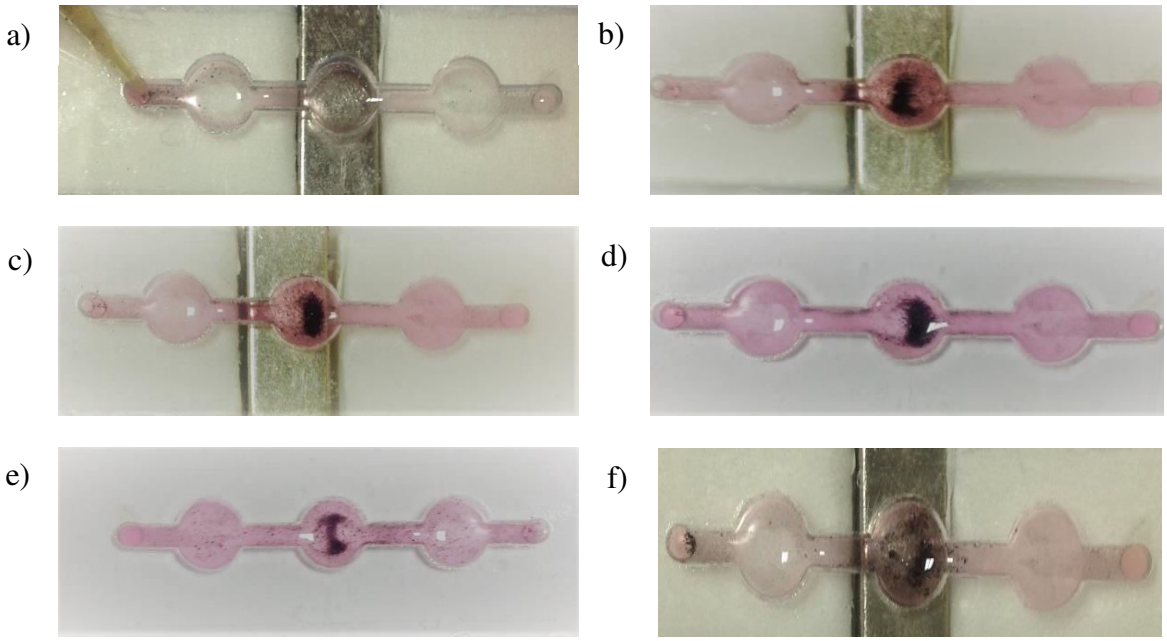

Figure 3.35 Magnetic targeting of NPT20; (a) injection NPs to the canal, (b) and (c) accumulation of NPs, (d) removal of magnetic field, (e) dispersion of NPs and (f) re-accumulation of NPs when magnetic field returned

When the magnetic field was applied to middle well, nanoparticles accumulated in that well and they could not pass to third well due to their sensitivity to magnetic exposure. On the other hand, in the absence of magnetic field nanoparticles began to disperse to other wells; but when magnetic field was returned. Re-accumulation of NPs was observed in the middle well. Thus, their superparamagnetic and targetable properties were confirmed by this test. Moreover, the cells were exposed to magnetic field were imagined with light microscope after 5 h incubation (Figure 3.36).

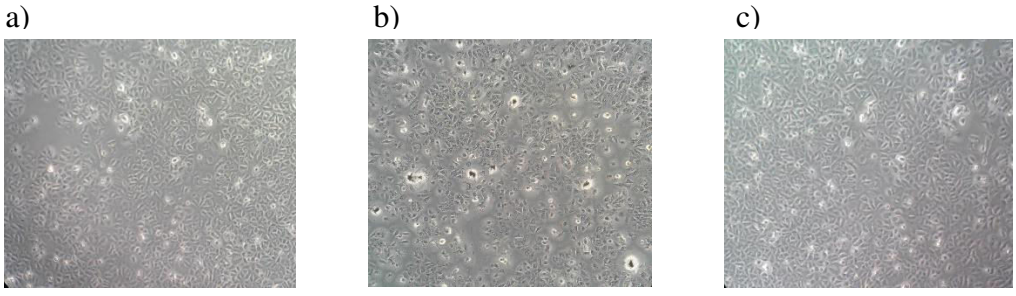

Figure 3.36 Light microscope images of the cells on (a) the left, (b) middle and (c) right well after 5 h

All nanoparticles were accumulated in the middle well due to magnetic field application at that side and they could not move onto the other wells. Hence, only the cells could uptake the nanoparticles. As a conclusion, the targetable property of NPT20 was shown.

3.6.4 Determination of Drug Accumulation

P-gp is a transmembrane protein functional in transport of the intracellular drug out of the cell for which ATP is necessary. Doxorubicin resistant cells (MCF-7/Dox) overexpress P-gp on their membrane (Iseri *et al.*, 2011) Hence, MCF-7/Dox cells were studied to determine drug accumulation in cells after treatment with NPT20, NPT0 and TPGS. The accumulation implies the drug efflux ability of cells, so more drug accumulation in cell meaning less P-gp efflux activity. After 1 hour of doxorubicin treatment, the cells were observed under florescence (FLoid) microscope (Figure 3.37).

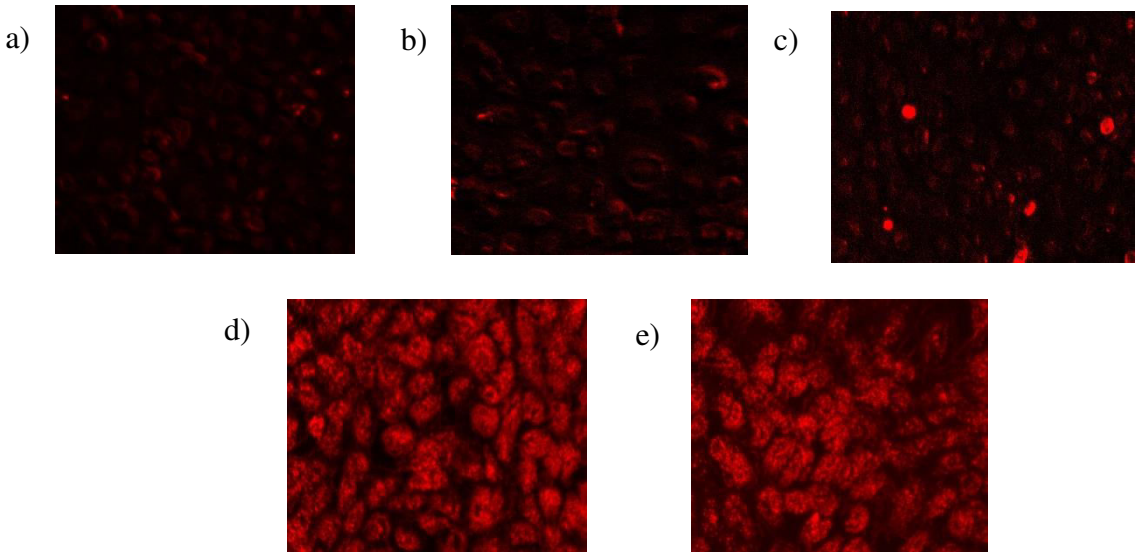

Figure 3.37 Florescence microscope images of MCF-7/Dox cells treated with (a) 5 µM Dox, (b) 20 µg/ml NPT0 and 5 µM Dox, (c) 20 µg/ml NPT20 and 5 µM Dox, (d) 200 µg/ml NPT20 and 5 µM Dox, (e) 5 µg/ml TPGS and 5 µM Dox

The intensity of red florescence showed the drug accumulation. In untreated cells (negative control) and treated with NPT0, there was no drug accumulation in the nucleus and slight amount of drug located on cell periphery. In the cells treated with 20 µg/ml of NPT20, there was an increase in drug accumulation in cell. Thus, some of the cells had high amount of red florescence. As the NPT20 concentration increased to 200 µg/ml, all cells were seen red due to drug accumulation in cells, indicating drugs were taken by cells and not effluxed outside. Thus, the increased concentration of NPT20 was more effective on the enhancement of drug accumulation and prevention of the drug efflux by P-gp pump. On the other hand, 10 µg/ml of TPGS treated cells (positive control) gave high florescence signal which was almost the same the intensity came from cells treated with 200 µg/ml of NPT20; hence, the same inhibition effect was obtained by increasing the concentration of NPT20. As a result, the inhibition effect of TPGS on P-gp pump was confirmed. From the other studies, it is known that TPGS is neither a substrate of P-gp nor a competitive inhibitor in efflux (Collnot *et al.*, 2010). It was determined that ATPase activity of P-gp was inhibited by TPGS, so ATP dependent drug efflux process was prevented (Hoosain *et al.*, 2015). As a conclusion, TPGS could be delivered with therapeutic drug to cancer cells to overcome drug resistance.

3.6.5 Anti-proliferative Effect of Nanoparticles on Cells

For determination of cytotoxic effects of drug loaded (Dox NPT20) and unloaded forms of NPT20 on MCF-7 and MCF-7/Dox cells, XTT cell proliferation assay was performed. However, it was not possible to show the long-term effects of nanoparticles due to cell culture limitation. Thus, only cytotoxicity of nanoparticles for 72 h was determined by XTT. Moreover, to access the reversal effect of TPGS on drug resistance; NPT0 and drug loaded form Dox NPT0 were also applied to cells for 72 h in the same way. Hence, the analysis results for Dox NPT0 and Dox NPT20 could be compared to show the effect of TPGS on resistance.

3.6.5.1 *In Vitro* Cytotoxicity of NPT20 and Dox NPT20 on MCF-7 Cells

The cytotoxic effects of NPT20 and Dox NPT20 on MCF-7 cells were determined by XTT cell proliferation assay and the profile was presented in the Figure 3.38.

In Figure D.1, cell proliferation profile of MCF-7 cells is shown after 72 h incubation with different concentrations of Dox NPT20 from 0.013 mg/ml (containing 3.92 μM Dox) to 0.5 mg/ml (containing 150 μM Dox) was determined. As seen from Figure 3.38, doxorubicin was released from the nanoparticles and triggered cell death. Hence, it could be concluded that the bioactivity of drug was not affected from conversion and encapsulation process where Dox-HCl reacted with TEA in acetone to be converted to Dox and then to be encapsulated. This proliferation profile suggested that the concentration 0.013 mg/ml led to slight toxicity whereas concentration at 0.5 mg/ml concentrations killed almost 20% of the cells. The IC_{50} value of Dox NPT20 after 72 h incubation was determined as 0.127 mg/ml. This showed that the release of Dox in 72 h was enough to kill MCF-7 cells with very low dose of nanoparticles.

Under the same conditions, drug free NPT20s were given to MCF-7 cells for 72 h. The cell proliferation is shown in Figure 3.38 and D.2. This was done to determine cytotoxicity of empty nanoparticles given between 0.013 mg/ml and 0.5 mg/ml of concentrations. There was no cytotoxic effect of NPT20 after 72 h since PLGA is biodegradable polymer. Lactic acid and glycolytic acid are formed at the end of degradation in the body and eliminated by the normal metabolic pathways. Thus, it could be also defined as biocompatible. In addition, during the synthesis process, acetone was used as organic solvent which is harmful for the body; however, NPT20s were not toxic for cells showing that solvent evaporation step was done successfully.

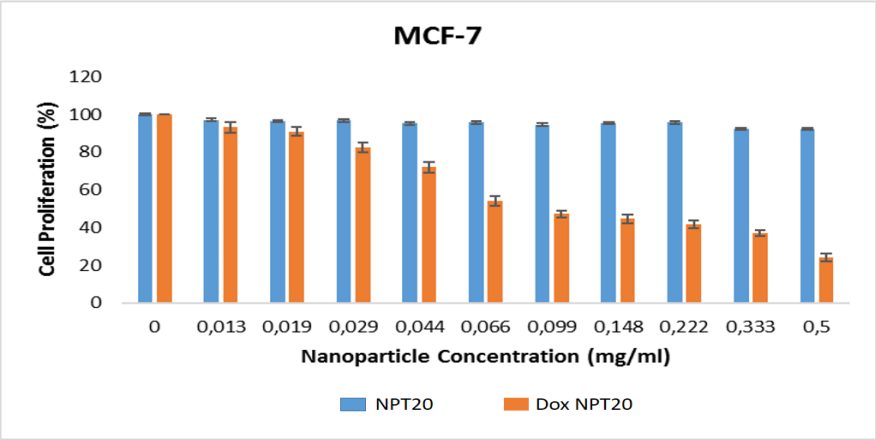

Figure 3.38 Cell proliferation profile of MCF-7 cells treated with NPT20 and Dox NPT20 (Experiments were performed in duplicates.)

3.6.5.2 *In Vitro* Cytotoxicity of NPT0 and Dox NPT0 on MCF-7 Cells

The cytotoxic effects of Dox NPT0 (100% PLGA on matrix) on MCF-7 cells were also identified by XTT assay to determine the effect of TPGS on nanoparticle cytotoxicity.

The cell proliferation profile of MCF-7 cells after 72 h of Dox NPT0 treatment was shown in Figure 3.39. Higher concentration of Dox NPT0 nanoparticles was given to cells than concentration of Dox NPT20 treatment since it had been determined that less amount of drug was encapsulated in Dox NPT0 than Dox NPT20. Hence, IC_{50} value of Dox NPT0 was found 2.03 mg/ml (Figure E1). The IC_{50} value was 15-fold higher than IC_{50} of Dox NPT20. However, only by looking this result, it could not be claimed that presence of TPGS decreased the IC_{50} value of Dox NP. Therefore, the same assay was performed with Dox NPT0 containing the same amount doxorubicin with that amount loaded in Dox NPT20, i.e. loaded amount of doxorubicin on nanoparticles were equalized by increasing the concentration of Dox NPT0, as shown in Figure E2.

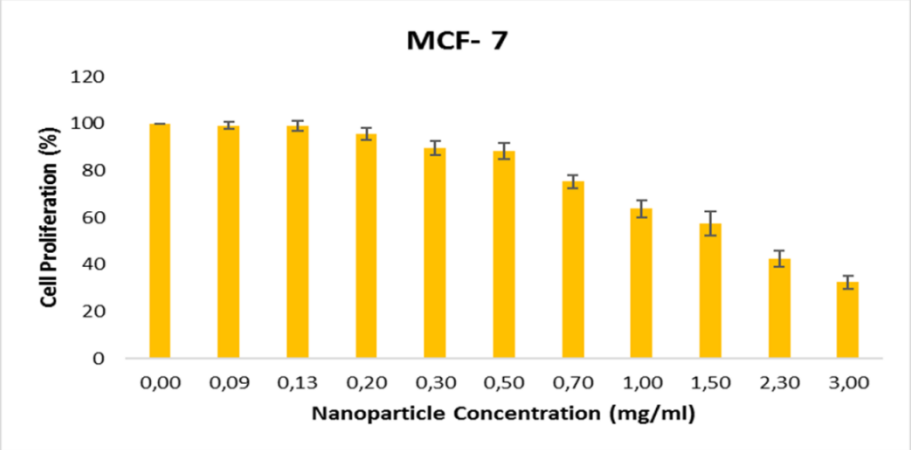

Figure 3.39 Cell proliferation profile of MCF-7 treated with Dox NPT0 (Experiments were performed in duplicates.)

After that, the cell killing effects of Dox NPT0 and Dox NPT20 encapsulating identical quantity of drug was compared in Figure 3.40. It could be seen that when MCF-7 cells treated with Dox NPT20 containing 88.5 µg drug, 75% of the cells were killed whereas only 25% of cells killed treated with Dox NPT0 containing same amount of drug. The reason of this situation could be pore forming ability of TPGS, so the drug release rate from nanoparticles was increased since drug could diffuse from the pores easily. Moreover, TPGS is a water-soluble polymer; hence, nanoparticles containing TPGS on their core could be degraded faster than nanoparticles containing only PLGA; thus, higher amount of drug was released (Tang *et al.*, 2015). This water solubility feature of TPGS due to hydrophilic PEG tail also increases the water solubility of nanoparticles and membrane permeability. Hence, the enhancement in cellular internalization of nanoparticles also could be another reason of this cell proliferation profile difference between Dox NPT0 and Dox NPT20 (Win & Feng, 2005).

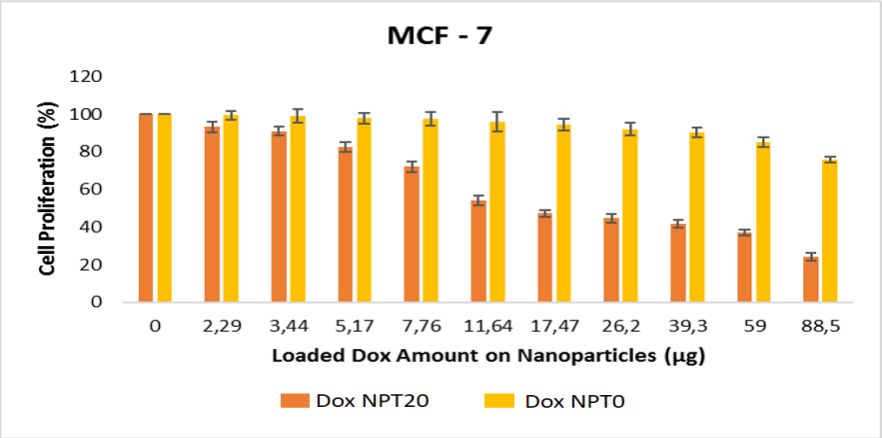

Figure 3.40 Cell proliferation profile of MCF-7 treated with Dox NPT20 and Dox NPT0 containing the same amount of loaded doxorubicin (Experiments were performed in duplicates.)

3.6.5.3 *In Vitro* Cytotoxicity of NPT20 and Dox NPT20 on MCF-7/Dox Cells

The same analyses were also performed for drug resistant cell line as shown in Figure 3.41. When the MCF-7/Dox cells incubated with NPT20 from 0.08 mg/ml to 3 mg/ml concentrations for 72 h, there was no cytotoxic effects observed in the cells. Consequently, cell proliferation was about 93% at highest amount of nanoparticle treatment, (Figure F1) because of biocompatible and biodegradable properties of PLGA.

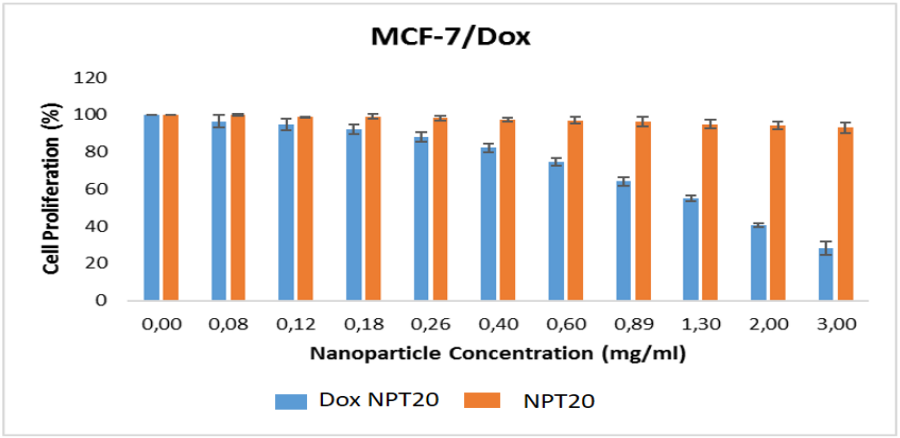

Figure 3.41 Cell proliferation profile of MCF-7/Dox cells treated with NPT20 and Dox NPT20 (Experiments were performed in duplicates.)

The cell proliferation of the MCF-7/Dox cells incubated with 0.08 mg/ml to 3 mg/ml of Dox NPT20 is shown in Figure F2. It could be seen that almost 70% of the cells were killed at 3 mg/ml nanoparticle incubation for 72 h. This amount was not very low, but only short-term effect of the nanoparticles could be studied with this assay. Hence, high concentration of nanoparticles was given to cells. Otherwise, the killing effect could not be seen by incubating the cells with lower concentration of nanoparticles for 72 h. IC_{50} value of Dox NPT20 for 72 h was found 1.52 mg/ml which would be lower in long term assay since the principle of drug release from PLGA nanoparticle is degradation of polymer. Hence, longer time period like 4-5 weeks is needed to release of drugs and to show real cytotoxic effects. On the other hand, the IC_{50} values in sensitive and resistant cells could be compared; IC_{50} of Dox NPT20 was 0.127 mg/ml in MCF-7 whereas 1.52 mg/ml in MCF-7/Dox.

3.6.5.4 *In Vitro* Cytotoxicity of NPT0 and Dox NPT0 on MCF-7/Dox Cells

The other aim of this assay was to study the effect of TPGS on reversal of drug resistance. Therefore, nanoparticles having no TPGS in core materials were given to resistant cell line. Several studies reported that TPGS could be used to overcome MDR and the presence of TPGS in nanoparticle significantly decreases the IC_{50} value of nanoparticle (Zhu *et al.*, 2014b ; Guo *et al.*, 2014). Therefore, higher concentration of nanoparticles was given to cells to determine the cytotoxicity and IC_{50} values. In Figure 3.42 the cell proliferation of MCF-7/Dox cells after 72 h could be seen and IC_{50} of Dox NPT0 was found 29.42 mg/ml (Figure G1) which was almost 19 times of that of Dox NPT20.

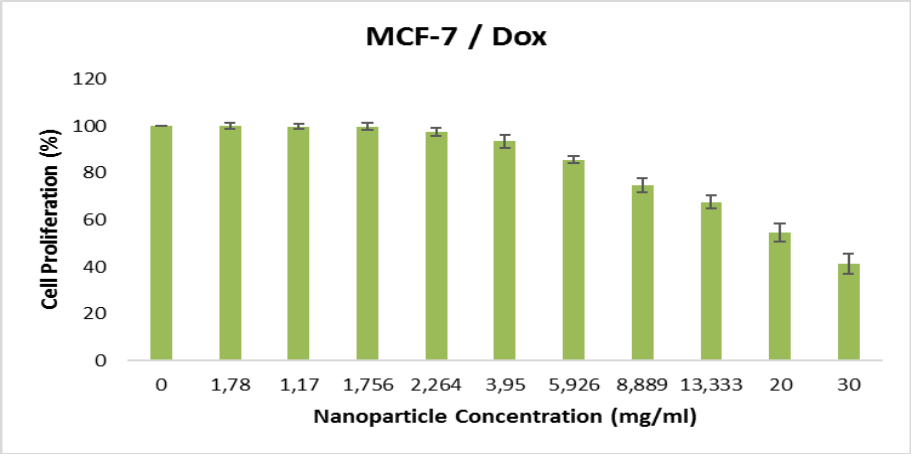

Figure 3.42 Cell proliferation profile of MCF-7/Dox treated with Dox NPT0 (Experiments were performed in duplicates.)

However, to confirm the reversal effect of TPGS, the cells were incubated with Dox NPT0 and Dox NPT20 containing the same concentration of loaded drugs (Figure 3.43). When the nanoparticles containing 530 µg doxorubicin were compared, it could be observed 23% of the cells were killed by Dox NPT0 while 72% of that killed by Dox NPT20. Therefore, the reversal effect of TPGS on resistance was confirmed with XTT results.

It had been found that TPGS increased the cellular uptake of nanoparticles in sensitive and drug resistant cells. Moreover, it was seen that TPGS has a combinational effect for increase in P-gp efflux inhibition and drug accumulation in cell. Zhang *et al.* also confirmed that TPGS increased drug accumulation in nuclear part (Zhang *et al.*, 2012). These properties of TPGS could be reason for the increase in cytotoxicity of Dox NPTs with TPGS addition in core material.

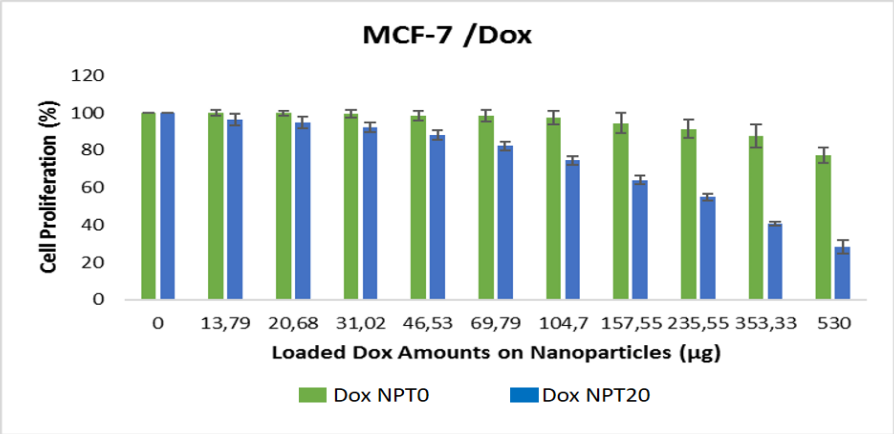

Figure 3.43 Cell proliferation profile of MCF-7/ Dox cells treated with Dox NPT0 and Dox NPT20 containing the same amount of loaded doxorubicin (Experiments were performed in duplicates.)

In Table 3.3, IC_{50} values of MCF-7 and MCF-7/Dox cells treated with Dox NPT20 and Dox NPT0 were compared. Thus, the higher cytotoxic effect of TPGS containing ones and their reversal effect on resistance could be seen. 0.127 mg/ml Dox NPT20 had the same cytotoxic effect with 2.03 mg/ml Dox NPT0 on MCF-7 cells whereas 1.52 mg/ml Dox NPT20 had the same cytotoxic effect with 29.42 mg/ml Dox NPT0 on MCF-7/Dox cells.

Table 3.3 Comparison of IC_{50} values of MCF-7 and MCF-7/Dox cells treated with Dox NPT20 and Dox NPT0

Type of Cells	**IC_{50} for Dox NPT 20**	**IC_{50} for Dox NPT0**
MCF-7	0.127 mg/ml	2.03 mg/ml
MCF-7/Dox	1.52 mg/ml	29.42 mg/ml

Resistance index for Dox NPT20 is $\frac{1.52}{0.127} = 12$

Resistance index for Dox NPT0 is $\frac{29.42}{2.03} = 14.5$

By comparing the resistance index of Dox NPT0 and Dox NPT20, it could be said that presence of TPGS in core material of Dox NPs decreased the resistance. Thus, Dox NPT20s could be used for reversal of drug resistance in the breast cancer cells.

3.6.6 Stability of Dox NPT20s

In the cell proliferation assays, fresh nanoparticles, i.e. 2 or 3 days later from the nanoparticle synthesis, were used and their cytotoxic effects were determined. However, to show the stability of the drug loaded nanoparticles, long-term stored (5 weeks) ones were used for XTT assay. The cytotoxic effects of the stored and fresh nanoparticles are shown in Figure 3.44.

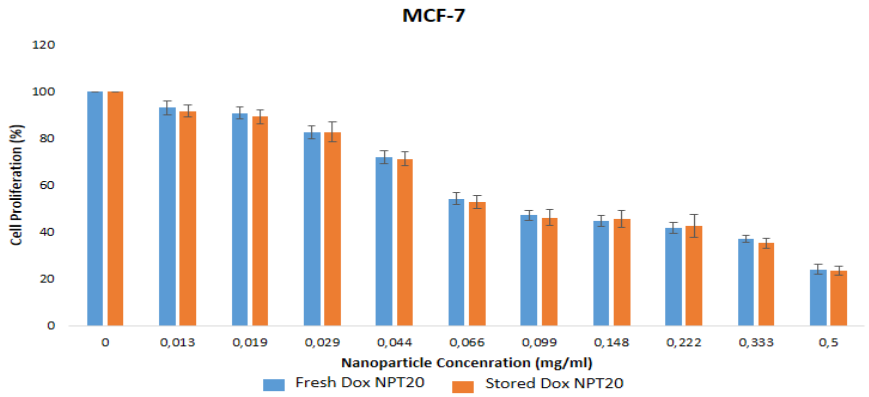

Figure 3.44 Cell proliferation profile of MCF-7 cells treated with fresh and stored Dox NPT20 (Experiments were performed in duplicates.)

As seen in Figure 3.44, there was no difference between the cell proliferation profiles of MCF-7 treated with fresh and stored nanoparticles. Thus, it could be said that the nanoparticles were stable during this period (5 week), so the efficacy of encapsulated drug did not change due to storage conditions (4°C and dark). On the other side, the stability of that nanoparticles had been confirmed by zeta potential analysis. TPGS was used as not only core material but also emulsifier during nanoparticle production process. Therefore, it could provide a protective layer for encapsulated drug and some

portion of the PLGA polymer (Esmaeili, Atyabi, & Dinarvand, 2007). As a result, it was showed that Dox NPT20s maintained the pharmacological activity of doxorubicin for 5 weeks.

CHAPTER 4

CONCLUSION

The main purpose of this study was to synthesize PLGA coated magnetic nanoparticles for targeted delivery of Vitamin E TPGS and doxorubicin to breast cancer cells. TPGS is known as P-gp inhibitor, so its reversal effect on drug resistance was also studied.

Magnetic nanoparticles were synthesized and then their surfaces were coated with oleic acid to prevent agglomeration and to make them compatible with polymer coating and drug loading. OA coating was confirmed by hydrophobicity test, FTIR, XPS and zeta potential analysis. To show the superparamagnetic property of OA-MNPs in room and body temperatures, VSM analysis was done. MNPs and OA-MNPs were spherical and 8-16 nm sized which was determined with TEM imaging.

Drug free and drug loaded form of polymeric magnetic nanoparticles containing TPGS on core, NPT20, were synthesized. (To study the effect of TPGS on the parameters which are drug loading and release profile and cytotoxicity, NPT0 was also produced).

The spherical shaped drug free NPT20 were 125 nm whereas drug loaded ones were 121 nm which was determined by SEM and DLS analysis. The size of the nanoparticles was suitable for application in targeted drug delivery.

On the other hand, by thermal gravimetric analysis it was proved that TPGS was a remnant in NPT20. In drug loaded nanoparticles, presence of doxorubicin was shown by UV-vis absorbance spectrophotometer, TGA and FTIR analysis.

By measuring the zeta potential of Dox NPT20, -26.7 mV, it was determined that drug loaded nanoparticles were stable and could be used in future *in vivo* studies since negatively charged nanoparticles have longer circulation time and lower accumulation ability in monocyte phagocytic system organs.

177 µg of doxorubicin was loaded in 1 mg of Dox NPT20 whereas 155 µg of doxorubicin was loaded in Dox NPT0. Consequently, TPGS increased drug loading efficiency of the nanoparticles.

Drug release studies showed that Dox NPs had a burst release at first day and then a sustainable release profile was observed in Dox NPs through 35 days. 55% of total loaded drug was released from Dox NPT20 while the value was 41% in Dox NPT0. Hence, it could be said that the presence of TPGS in core material enhanced the drug releasing rate.

Doxorubicin resistant MCF-7 cells (MCF-7/Dox) were about 70-fold resistant to doxorubicin than sensitive MCF-7 cells which was proved by comparing IC_{50} values determined by XTT cell proliferation assay.

The internalization of NPT0 and NPT20 by sensitive and resistant cells was observed by Prussian blue staining method. It was shown that NPs were successfully internalized by MCF-7 and MCF-7/Dox cells. TPGS increased the cellular internalization. This might be due to the fact that it increases aqueous stability of NP and membrane permeability by the presence of a hydrophilic PEG tail.

The targetable features of NPT20 were tested by exposing external magnetic field to a three well canal-connected slide on which cells were seeded and treated with NPT20. It was seen that only the cells exposed to the magnetic field could uptake the nanoparticles whereas the cells on the other wells could not reach any nanoparticle due to absence of magnetic field.

In addition, the effect of TPGS on drug accumulation was determined. When MCF-7/Dox cells were treated with NPT20, doxorubicin was accumulated in cells while in NPT0 treated cells there was no drug in intracellular parts. Thus, the inhibitory effect of TPGS on P-gp pump was confirmed, so it could be used to overcome MDR.

Drug free polymeric nanoparticles were not cytotoxic in cells, but drug loaded forms killed the cells with different degree of cytotoxicity; hence, NPT0 and NPT20 were

biocompatible. Killing effect of Dox NPT20 was higher than Dox NPT0 when they were applied to cells in the same concentrations of drug. IC_{50} value was 15-fold increased in Dox NPT0 treated MCF-7 while 18-fold increased in Dox NPT0 treated MC-7/Dox cells when compared with the Dox NPT20 treated cells.

In conclusion, polymeric magnetic nanoparticles were biocompatible and they could be used for targeted therapy by using external magnetic field. Doxorubicin was more efficiently loaded to Dox NPT20 than Dox NPT0 and the released drug ratio was higher in Dox NPT20 at the end of 35 days. Furthermore, Dox NPT20 has higher cytotoxic effect in MCF-7 and MCF-7/Dox cells. TPGS also inhibited the drug efflux mechanism in MCF-7/Dox cells. Consequently, doxorubicin loaded TPGS containing PLGA nanoparticles could be used to reverse the drug resistance.

REFERENCES

Akbarzadeh, A., Samiei, M., & Davaran, S. (2012). Magnetic nanoparticles: preparation, physical properties, and applications in biomedicine, 1–13. https://doi.org/10.1186/1556-276X-7-144

Alimohammadi, Y., & Joo, S. (2014). PLGA-based nanoparticles as cancer drug delivery systems. *Asian Pac J Cancer Prev*, *15*, 517–535. https://doi.org/10.7314/APJCP.2014.15.2.517

American Cancer Society. (2013). Targeted Therapy What is targeted therapy? *American Cancer Society*, 27. Retrieved from http://www.cancer.org/treatment/treatmentsandsideeffects/treatmenttypes/targetedtherapy/targeted-therapy-what-is

Arias, J. L., Gallardo, V., Gómez-Lopera, S. a, Plaza, R. C., & Delgado, a V. (2001). Synthesis and characterization of poly(ethyl-2-cyanoacrylate) nanoparticles with a magnetic core. *Journal of Controlled Release: Official Journal of the Controlled Release Society*, *77*, 309–321. https://doi.org/10.1016/S0168-3659(01)00519-3

Bhatt, A., & Goswami, L. (2013). Current and Future Trend in Nanotechnology: A Review. *International Journal of Pharmacy and Research Science*, *2*(7), 859–884.

Bini, R. A., Marques, R. F. C., Santos, F. J., Chaker, J. A., & Jafelicci, M. (2012). Synthesis and functionalization of magnetite nanoparticles with different amino-functional alkoxysilanes. *Journal of Magnetism and Magnetic Materials*, *324*(4), 534–539. https://doi.org/10.1016/j.jmmm.2011.08.035

Blanco, E., Shen, H., & Ferrari, M. (2015). Principles of nanoparticle design for overcoming biological barriers to drug delivery. *Nature Biotechnology*, *33*(9), 941–951. https://doi.org/10.1038/nbt.3330

Botchkarev, V. A., & Sharov, A. A. (2016). Modeling Chemotherapy- Induced Hair Loss: From Experimental Propositions Toward Clinical Reality. *Journal of Investigative Dermatology*, *136*(3), 557–559. https://doi.org/10.1016/j.jid.2015.10.068

Chen, D., Xia, X., Gu, H., Xu, Q., Ge, J., Li, Y., … Lu, J. (2011). pH-responsive polymeric carrier encapsulated magnetic nanoparticles for cancer targeted imaging and delivery. *Journal of Materials Chemistry*, *21*(34), 12682. https://doi.org/10.1039/c1jm11195g

Chiang, W. L., Ke, C. J., Liao, Z. X., Chen, S. Y., Chen, F. R., Tsai, C. Y.,Sung, H. W. (2012). Pulsatile drug release from PLGA hollow microspheres by controlling the permeability of their walls with a magnetic field. *Small*, *8*(23), 3584–3588. https://doi.org/10.1002/smll.201201743

Chlebowski, R. T., & Anderson, G. L. (2012). Changing concepts: Menopausal hormone therapy and breast cancer. *Journal of the National Cancer Institute*, *104*(7), 517–527. https://doi.org/10.1093/jnci/djs014

Choi, H. S., Liu, W., Misra, P., Tanaka, E., Zimmer, J. P., Itty Ipe, B., Frangioni, J. V. (2007). Renal clearance of nanoparticles. *Nat. Biotechnol.*, *25*(10), 1165–1170. https://doi.org/10.1038/nbt1340.Renal

Coates, A. S., Winer, E. P., Goldhirsch, A., Gelber, R. D., Gnant, M., Piccart-Gebhart, M. J., Xu, B. (2015). Tailoring therapies-improving the management of early breast cancer: St Gallen International Expert Consensus on the Primary Therapy of Early Breast Cancer 2015. *Annals of Oncology*, *26*(8), 1533–1546. https://doi.org/10.1093/annonc/mdv221

Collnot, E. M., Baldes, C., Schaefer, U. F., Edgar, K. J., Wempe, M. F., & Lehr, C. M. (2010). Vitamin e TPGS P-glycoprotein inhibition mechanism: Influence on conformational flexibility, intracellular ATP levels, and role of time and site of access. *Molecular Pharmaceutics*, *7*(3), 642–651. https://doi.org/10.1021/mp900191s

Colombo, M., Carregal-Romero, S., Casula, M. F., Gutierrez, L., Morales, M. P., Bohm, I. B., Parak, W. J. (2012). Biological applications of magnetic nanoparticles. *Chemical Society Reviews*, *41*(11), 4306–4334. https://doi.org/10.1039/c2cs15337h

Cruz-Acuña, M., Maldonado-Camargo, L., Dobson, J., & Rinaldi, C. (2016). From oleic acid-capped iron oxide nanoparticles to polyethyleneimine-coated single-particle magnetofectins. *Journal of Nanoparticle Research*, *18*(9), 268. https://doi.org/10.1007/s11051-016-3577-9

Cuperus, F. J. C., Claudel, T., Gautherot, J., Halilbasic, E., & Trauner, M. (2014). Special Section on Transporters in Toxicity and Disease — Minireview The Role of Canalicular ABC Transporters in Cholestasis, *2014*(April), 546–560. https://doi.org/dmd.113.055806

Donmez, Y., Akhmetova, L., Ozlem Darcansoy, Kars, M. D., & Gunduz, U. (2011). Effect of MDR modulators verapamil and promethazine on gene expression levels of MDR1 and MRP1 in doxorubicin-resistant MCF-7 cells. *Cancer Chemotherapy and Pharmacology*, *67*(4), 823–828. https://doi.org/10.1007/s00280-010-1385-y

Damaghi, M., Wojtkowiak, J. W., & Gillies, R. J. (2013). pH sensing and regulation in cancer. *Frontiers in Physiology*, *4 DEC*(December), 1–10. https://doi.org/10.3389/fphys.2013.00370

Danhier, F., Ansorena, E., Silva, J. M., Coco, R., Le Breton, A., & Préat, V. (2012). PLGA-based nanoparticles: An overview of biomedical applications. *Journal of Controlled Release*, *161*(2), 505–522. https://doi.org/10.1016/j.jconrel.2012.01.043

Darcansoy, Ö. (2009). Investigation of docetaxel and doxorubicin resistance in MCF-7 breast carcinoma cell line. *Breast*, (February).

Datasheet, P. (2015). Doxorubicin hydrochloride, (12), 1–3.

Dost, S. (2014). Delivery of doxorubicin using protein nanocarriers, 34–38.

Duan, X., & Li, Y. (2013). Physicochemical characteristics of nanoparticles affect circulation, biodistribution, cellular internalization, and trafficking. *Small*, *9*(9–10), 1521–1532. https://doi.org/10.1002/smll.201201390

Esmaeili, F., Atyabi, F., & Dinarvand, R. (2007). Preparation of PLGA nanoparticles using TPGS in the spontaneous emulsification solvent diffusion method. *Journal of Experimental Nanoscience*, *2*(3), 183–192. https://doi.org/10.1080/17458080701393137

Estoration, F. O. R., & Awai, I. N. H. (2009). T He E Mission -Reduction Potential of Native, 1–6.

Fukumura, D., & Jain, R. K. (2007). Tumor microenvironment abnormalities: Causes, consequences, and strategies to normalize. *Journal of Cellular Biochemistry*, *101*(4), 937–949. https://doi.org/10.1002/jcb.21187

Gabriel, A., & Maxwell, G. P. (2016). Breast Anatomy. *Medscape*, 82194.

Gulati, K., Aw, M. S., & Losic, D. (2012). Nanoengineered drug-releasing Ti wires as an alternative for local delivery of chemotherapeutics in the brain. *International Journal of Nanomedicine*, *7*(November 2016), 2069–2076. https://doi.org/10.2147/IJN.S29917

Guo, Y., Chu, M., Tan, S., Zhao, S., Liu, H., Otieno, B. O.,Zhang, Z. (2014a). Chitosan-g-TPGS nanoparticles for anticancer drug delivery and overcoming multidrug resistance. *Molecular Pharmaceutics*, *11*(1), 59–70. https://doi.org/10.1021/mp400514t

Guo, Y., Chu, M., Tan, S., Zhao, S., Liu, H., Otieno, B. O., Zhang, Z. (2014b). Chitosan ‐ g ‐ TPGS Nanoparticles for Anticancer Drug Delivery and Overcoming Multidrug Resistance. *Molecular Pharmaceutics*, *11*, 59–70.

Guo, Y., Luo, J., Tan, S., Otieno, B. O., & Zhang, Z. (2013). The applications of Vitamin e TPGS in drug delivery. *European Journal of Pharmaceutical Sciences*, *49*(2), 175–186. https://doi.org/10.1016/j.ejps.2013.02.006

Hanahan, D., & Weinberg, R. A. (2011). Hallmarks of cancer: The next generation. *Cell*, *144*(5), 646–674. https://doi.org/10.1016/j.cell.2011.02.013

Harmer, V. (2011). Surgery for Breast Cancer. *Breast Cancer Nursing Care and Management*, 81–102.

Hobbs, S. K., Monsky, W. L., Yuan, F., Roberts, W. G., Griffith, L., Torchilin, V. P., & Jain, R. K. (1998). Regulation of transport pathways in tumor vessels: role of tumor type and microenvironment. *Proceedings of the National Academy of Sciences of the United States of America*, *95*(8), 4607–12. https://doi.org/10.1073/pnas.95.8.4607

Hoosain, F. G., Choonara, Y. E., Tomar, L. K., Kumar, P., Tyagi, C., Du Toit, L. C., & Pillay, V. (2015). Bypassing P-Glycoprotein Drug Efflux Mechanisms: Possible Applications in Pharmacoresistant Schizophrenia Therapy. *BioMed Research International*, *2015*(i). https://doi.org/10.1155/2015/484963

Institute, N. C. (2016). Breast cancer. Retrieved from http://www.cancer.org/cancer/breastcancer/detailedguide/breast-cancer-risk-factors

Issa, B., Obaidat, I. M., Albiss, B. A., & Haik, Y. (2013). Magnetic nanoparticles: Surface effects and properties related to biomedicine applications. *International Journal of Molecular Sciences*, *14*(11), 21266–21305. https://doi.org/10.3390/ijms141121266

Kars, M. D., Iseri, O., & Gunduz, U. (2011). A microarray based expression profiling of paclitaxel and vincristine resistant MCF-7 cells. *European Journal of Pharmacology*, *657*(1–3), 4–9. https://doi.org/10.1016/j.ejphar.2011.02.001

Khosroshahi, M. E., & Ghazanfari, L. (2010). Preparation and characterization of silica-coated iron-oxide bionanoparticles under N2 gas. *Physica E: Low-Dimensional Systems and Nanostructures*, *42*(6), 1824–1829. https://doi.org/10.1016/j.physe.2010.01.042

Kuehn, T., Bauerfeind, I., Fehm, T., Fleige, B., Hausschild, M., Helms, G., Untch, M. (2013). Sentinel-lymph-node biopsy in patients with breast cancer before and after neoadjuvant chemotherapy (SENTINA): A prospective, multicentre cohort study. *Lancet Oncology*, *14*(7), 609–618. https://doi.org/10.1016/S1470-2045%2813%2970166-9

Kumar, R., Kulkarni, A., Nagesha, D. K., & Sridhar, S. (2012). In vitro evaluation of theranostic polymeric micelles for imaging and drug delivery in cancer. *Theranostics*, *2*(7), 714–722. https://doi.org/10.7150/thno.3927

Lai, P., Daear, W., Löbenberg, R., & Prenner, E. J. (2014). Overview of the preparation of organic polymeric nanoparticles for drug delivery based on gelatine, chitosan, poly(d,l-lactide-co-glycolic acid) and polyalkylcyanoacrylate. *Colloids and Surfaces B: Biointerfaces*, *118*, 154–163. https://doi.org/10.1016/j.colsurfb.2014.03.017

Lakshmanan, S., Gupta, G. K., Avci, P., Chandran, R., Sadasivam, M., Jorge, A. E. S., & Hamblin, M. R. (2014). Physical energy for drug delivery; poration, concentration and activation. *Advanced Drug Delivery Reviews*, *71*(June), 98–114. https://doi.org/10.1016/j.addr.2013.05.010

Lammers, T., Kiessling, F., Hennink, W. E., & Storm, G. (2012). Drug targeting to tumors: Principles, pitfalls and (pre-) clinical progress. *Journal of Controlled Release*, *161*(2), 175–187. https://doi.org/10.1016/j.jconrel.2011.09.063

Lee, N., & Hyeon, T. (2012). Designed synthesis of uniformly sized iron oxide nanoparticles for efficient magnetic resonance imaging contrast agents. *Chemical Society Reviews*, *41*(7), 2575–2589. https://doi.org/10.1039/C1CS15248C

Lin, G. G., & Scott, J. G. (2012). NIH Public Access, *100*(2), 130–134. https://doi.org/10.1016/j.pestbp.2011.02.012.Investigations

Liu, K., Markakis, J. P., & Smith, D. (1990). Trypsin Inhibition by Free Fatty Acids and Stearoyl-COAT, 1988–1991.

Liu, Y., Huang, L., & Liu, F. (2010). Paclitaxel nanocrystals for overcoming multidrug resistance in cancer. *Molecular Pharmaceutics*, *7*(3), 863–869. https://doi.org/10.1021/mp100012s

Ma, Y., Zheng, Y., Liu, K., Tian, G., Tian, Y., Xu, L., … Mei, L. (2010). Nanoparticles of poly(Lactide-Co-Glycolide)-d-a-Tocopheryl polyethylene glycol 1000 succinate random copolymer for cancer treatment. *Nanoscale Research Letters*, *5*(7), 1161–1169. https://doi.org/10.1007/s11671-010-9620-3

Mahdavi, M., Ahmad, M. Bin, Haron, M. J., Namvar, F., Nadi, B., Ab Rahman, M. Z., & Amin, J. (2013). Synthesis, surface modification and characterization of biocompatible magnetic iron oxide nanoparticles for biomedical applications. *Molecules*, *18*(7), 7533–7548. https://doi.org/10.3390/molecules18077533

McCall, R. L., & Sirianni, R. W. (2013). PLGA nanoparticles formed by single- or double-emulsion with vitamin E-TPGS. *Journal of Visualized Experiments: JoVE*, (December), 51015. https://doi.org/10.3791/51015

Meschino, J. P. (2010). How Chemotherapy Drugs Work. *Dynamic Chiropractic Canada*, *3*(5), 1–7. Retrieved from http://www.dynamicchiropractic.ca/mpacms/dc_ca/article.php?id=54916

Mody, V. V., Cox, A., Shah, S., Singh, A., Bevins, W., & Parihar, H. (2013). Magnetic nanoparticle drug delivery systems for targeting tumor. *Applied Nanoscience*, *4*(4), 385–392. https://doi.org/10.1007/s13204-013-0216-y

Mohammed, L., Gomaa, H. G., Ragab, D., & Zhu, J. (2016). applications: A review. *Particuology*, 1–14. https://doi.org/10.1016/j.partic.2016.06.001

Nanocomposix. (2012). Zeta Potential Analysis of Nanoparticles. *Nanocomposix Publications*, 1–6.

Nguyen, H. N., Hoang, T. M. N., Mai, T. T. T., Nguyen, T. Q. T., Do, H. D., Pham, T. H., … Ha, P. T. (2015). Enhanced cellular uptake and cytotoxicity of folate decorated doxorubicin loaded PLA-TPGS nanoparticles. *Advances in Natural Sciences: Nanoscience and Nanotechnology*, *6*(2), 1–8. https://doi.org/10.1088/2043-6262/6/2/025005

Not, D. (2016). Doxorubicin, 1–4.

Okassa, L. N., Marchais, H., Douziech-Eyrolles, L., Hervé, K., Cohen-Jonathan, S., Munnier, E., … Chourpa, I. (2007). Optimization of iron oxide nanoparticles encapsulation within poly(d,l-lactide-co-glycolide) sub-micron particles. *European Journal of Pharmaceutics and Biopharmaceutics*, *67*(1), 31–38. https://doi.org/10.1016/j.ejpb.2006.12.020

Page, R., & Takimoto, C. (2005). Principles of chemotherapy. *Cancer Management: A Multidisciplinart Approach*, 21–37. https://doi.org/10.1016/j.paed.2009.10.003

Pan, L., Liu, J., He, Q., Wang, L., & Shi, J. (2013). Biomaterials Overcoming multidrug resistance of cancer cells by direct intranuclear drug delivery using TAT-conjugated mesoporous silica nanoparticles. *Biomaterials*, *34*(11), 2719–2730. https://doi.org/10.1016/j.biomaterials.2012.12.040

Parsian, M., Unsoy, G., Mutlu, P., Yalcin, S., Tezcaner, A., & Gunduz, U. (2016). Loading of Gemcitabine on chitosan magnetic nanoparticles increases the anti-cancer efficacy of the drug. *European Journal of Pharmacology*, *784*, 121–128. https://doi.org/10.1016/j.ejphar.2016.05.016

Pérez-herrero, E., & Fernández-medarde, A. (2015). European Journal of Pharmaceutics and Biopharmaceutics Advanced targeted therapies in cancer: Drug nanocarriers, the future of chemotherapy, *93*, 52–79. https://doi.org/10.1016/j.ejpb.2015.03.018

Prabhakar, U., Maeda, H., K. Jain, R., Sevick-Muraca, E. M., Zamboni, W., Farokhzad, O. C., … Blakey, D. C. (2013). Challenges and key considerations of the enhanced permeability and retention effect for nanomedicine drug delivery in oncology. *Cancer Research*, *73*(8), 2412–2417. https://doi.org/10.1158/0008-5472.CAN-12-4561

Qi, R. ling, Tian, X. jiao, Guo, R., Luo, Y., Shen, M. wu, Yu, J. yong, & Shi, X. yang. (2016). Controlled release of doxorubicin from electrospun MWCNTs/PLGA hybrid nanofibers. *Chinese Journal of Polymer Science (English Edition)*, *34*(9), 1047–1059. https://doi.org/10.1007/s10118-016-1827-z

Rawat, P., Manglani, K., Gupta, S., Kalam, A., Vohora, D., Ahmad, F. J., & Talegaonkar, S. (2015). Design and Development of Bioceramic Based Functionalized PLGA Nanoparticles of Risedronate for Bone Targeting: In-vitro Characterization and Pharmacodynamic Evaluation. *Pharmaceutical Research*, *32*(10), 3149–3158. https://doi.org/10.1007/s11095-015-1692-4

Rouhollah, K., Pelin, M., Serap, Y., Gozde, U., & Ufuk, G. (2013). Doxorubicin loading, release, and stability of polyamidoamine dendrimer-coated magnetic nanoparticles. *Journal of Pharmaceutical Sciences*, *102*(6), 1825–1835. https://doi.org/10.1002/jps.23524

Ruddon, R. W. (2007). *Cancer Biology. Vasa.* Retrieved from http://medcontent.metapress.com/index/A65RM03P4874243N.pdf

Sagnella, S. M., McCarroll, J. A., & Kavallaris, M. (2014). Drug delivery: Beyond active tumour targeting. *Nanomedicine: Nanotechnology, Biology, and Medicine*, *10*(6), 1131–1137. https://doi.org/10.1016/j.nano.2014.04.012

Saraswathy, M., & Gong, S. (2013). Different strategies to overcome multidrug resistance in cancer. *Biotechnol Adv*, *31*(8), 1397–1407. https://doi.org/10.1016/j.biotechadv.2013.06.004

Schrefl, T., Hrkac, G., Suess, D., Scholz, W., & Fidler, J. (2003). Coercivity and remanence in self-assembled FePt nanoparticle arrays. *Journal of Applied Physics*, *93*(10 2), 7041–7043. https://doi.org/10.1063/1.1557398

Sedlmayer, F., Sautter-Bihl, M. L., Budach, W., Dunst, J., Fastner, G., Feyer, P., Sauer, R. (2013). DEGRO practical guidelines: Radiotherapy of breast cancer I: Radiotherapy following breast conserving therapy for invasive breast cancer. *Strahlentherapie Und Onkologie*, *189*(10), 825–833. https://doi.org/10.1007/s00066-013-0437-8

Seyfried, T. N., & Huysentruyt, L. C. (2013). On the origin of cancer metastasis. *Critical Reviews in Oncogenesis*, *18*(1–2), 43–73. https://doi.org/10.1016/S0306-9877(96)90136-X

Shabir, A., Alhusban, F., Perrie, Y., & Mohammed, A. R. (2011). Effects of ball-milling on PLGA polymer and its implication on lansoprazole-loaded nanoparticles. *Journal of Basic and Clinical Pharmacy*, (2), 71–82.

Si, S. (2015). iMedPub Journals Synthesis and Characterization of Carrageenan Coated Magnetic Nanoparticles for Drug Delivery Applications Abstract, 1–5.

Siegel, R. L., Miller, K. D., & Jemal, A. (2016). Cancer statistics. *CA Cancer J Clin*, *66*(1), 7–30. https://doi.org/10.3322/caac.21332.

Sirdeshmukh, D. B., Sirdeshmukh, L., Subhadra, K. G., & Sunandana, C. S. (2014). *Electrical, Electronic and Magnetic Properties of Solids* (Vol. 207). https://doi.org/10.1007/978-3-319-09985-9

Sonali, Agrawal, P., Singh, R. P., Rajesh, C. V., Singh, S., Vijayakumar, M. R., Muthu, M. S. (2015). Transferrin receptor-targeted vitamin E TPGS micelles for brain cancer therapy: preparation, characterization and brain distribution in rats. *Drug Delivery*, *7544*(October), 1–11. https://doi.org/10.3109/10717544.2015.1094681

Sun, C., Lee, J. S. H., & Zhang, M. (2008). Magnetic nanoparticles in MR imaging and drug delivery. *Advanced Drug Delivery Reviews*, *60*, 1252–1265. https://doi.org/10.1016/j.addr.2008.03.018

Tamariz, E., & Rios-ramírez, A. (2013). Biodegradation of medical purpose polymeric materials and their impact on biocompatibility. *Biodegradation-Life of Science* 3–30. https://doi.org/http://dx.doi.org/10.5772/56220

Tang, X., Liang, Y., Feng, X., Zhang, R., Jin, X., & Sun, L. (2015). Co-delivery of docetaxel and Poloxamer 235 by PLGA-TPGS nanoparticles for breast cancer treatment. *Materials Science and Engineering C*, *49*, 348–355. https://doi.org/10.1016/j.msec.2015.01.033

Tansik, G., Yakar, A., & Gündüz, U. (2014). Tailoring magnetic PLGA nanoparticles suitable for doxorubicin delivery. *Journal of Nanoparticle Research*, *16*(1). https://doi.org/10.1007/s11051-013-2171-7

Thorn, Caroline; Oshiro, Connie; Marsh, Sharon; Hernandez-Boussard, Tina; McLeod, Howard; Klein, Teri; Altman, R. (2012). Doxorubicin pathways: pharmacodynamics and adverse effects. *Pharmacogenet Genomics*, *21*(7), 440–446. https://doi.org/10.1097/FPC.0b013e32833ffb56.

Ug, A. L. I. (2006). Development of Rational in Vitro Models for Drug Resistance in Breast Cancer and Modulation of MDR by Selected Compounds, *4568*, 4559–4568.

Upreti, M., Jyoti, A., & Sethi, P. (2013). Tumor microenvironment and nanotherapeutics. *Translational Cancer Research*, *2*(4), 309–319. https://doi.org/10.3978/j.issn.2218-676X.2013.08.11

Vaupel, P. (2004). Tumor microenvironmental physiology and its implications for radiation oncology. *Seminars in Radiation Oncology*, *14*(3), 198–206. https://doi.org/10.1016/j.semradonc.2004.04.008

Veronese, F. M., Schiavon, O., Pasut, G., Mendichi, R., Andersson, L., Tsirk, A., Duncan, R. (2005). PEG-doxorubicin conjugates: Influence of polymer structure on drug release, in vitro cytotoxicity, biodistribution, and antitumor activity. *Bioconjugate Chemistry*, *16*(4), 775–784. https://doi.org/10.1021/bc040241m

Win, K. Y., & Feng, S. S. (2005). Effects of particle size and surface coating on cellular uptake of polymeric nanoparticles for oral delivery of anticancer drugs. *Biomaterials*, *26*(15), 2713–2722. https://doi.org/10.1016/j.biomaterials.2004.07.050

Wu, W., He, Q., & Jiang, C. (2008). Magnetic iron oxide nanoparticles: Synthesis and surface functionalization strategies. *Nanoscale Research Letters*, *3*(11), 397–415. https://doi.org/10.1007/s11671-008-9174-9

Xu, X., Chen, X., Ma, P., Wang, X., & Jing, X. (2008). The release behavior of doxorubicin hydrochloride from medicated fibers prepared by emulsion-electrospinning. *European Journal of Pharmaceutics and Biopharmaceutics*, *70*(1), 165–170. https://doi.org/10.1016/j.ejpb.2008.03.010

Yadav, K. S., & Sawant, K. K. (2010). Modified nanoprecipitation method for preparation of cytarabine-loaded PLGA nanoparticles. *AAPS PharmSciTech*, *11*(3), 1456–1465. https://doi.org/10.1208/s12249-010-9519-4

Yallapu, M. M., Foy, S. P., Jain, T. K., & Labhasetwar, V. (2011). PEG-Functionalized Magnetic Nanoparticles for Drug Delivery and Magnetic Resonance Imaging Application. *Pharmaceutical Research*, *27*(11), 2283–2295. https://doi.org/10.1007/s11095-010-0260-1.PEG-Functionalized

Yoo, H. S., Lee, K. H., Oh, J. E., & Park, T. G. (2000). In vitro and in vivo anti-tumor activities of nanoparticles based on doxorubicin-PLGA conjugates. *J. Control. Release*, *68*(3), 419–431. https://doi.org/10.1016/S0168-3659(00)00280-7

Yu, J., Huang, D.-Y., Yousaf, M. Z., Hou, Y.-L., & Gao, S. (2013). Magnetic nanoparticle-based cancer therapy. *Chinese Physics B*, *22*(2), 27506. https://doi.org/10.1088/1674-1056/22/2/027506

Zeng, X., Tao, W., Mei, L., Huang, L., Tan, C., & Feng, S. S. (2013). Cholic acid-functionalized nanoparticles of star-shaped PLGA-vitamin E TPGS copolymer for docetaxel delivery to cervical cancer. *Biomaterials*, *34*(25), 6058–6067. https://doi.org/10.1016/j.biomaterials.2013.04.052

Zhang, L., He, R., & Gu, H. C. (2006). Oleic acid coating on the monodisperse magnetite nanoparticles. *Applied Surface Science*, *253*(5), 2611–2617. https://doi.org/10.1016/j.apsusc.2006.05.023

Zhang, L., Li, Y., & Yu, J. C. (2014). Chemical modification of inorganic nanostructures for targeted and controlled drug delivery in cancer treatment. *Journal of Materials Chemistry B*, *2*(5), 452. https://doi.org/10.1039/c3tb21196g

Zhang, Z., & Feng, S. S. (2006). Nanoparticles of poly(lactide)/vitamin E TPGS copolymer for cancer chemotherapy: Synthesis, formulation, characterization and in vitro drug release. *Biomaterials*, *27*(2), 262–270. https://doi.org/10.1016/j.biomaterials.2005.05.104

Zhang, Z., Tan, S., & Feng, S. S. (2012). Vitamin E TPGS as a molecular biomaterial for drug delivery. *Biomaterials*, *33*(19), 4889–4906. https://doi.org/10.1016/j.biomaterials.2012.03.046

Zhao, F., Zhang, B., & Feng, L. (2012). Preparation and magnetic properties of magnetite nanoparticles. *Materials Letters*, *68*(1), 112–114. https://doi.org/10.1016/j.matlet.2011.09.116

Zhu, H., Chen, H., Zeng, X., Wang, Z., Zhang, X., Wu, Y., Feng, S. S. (2014a). Co-delivery of chemotherapeutic drugs with vitamin E TPGS by porous PLGA nanoparticles for enhanced chemotherapy against multi-drug resistance. *Biomaterials*, *35*(7), 2391–2400. https://doi.org/10.1016/j.biomaterials.2013.11.086

Zhu, H., Chen, H., Zeng, X., Wang, Z., Zhang, X., Wu, Y., Feng, S. S. (2014b). Co-delivery of chemotherapeutic drugs with vitamin E TPGS by porous PLGA nanoparticles for enhanced chemotherapy against multi-drug resistance. *Biomaterials*, *35*(7), 2391–2400. https://doi.org/10.1016/j.biomaterials.2013.11.086

APPENDICES

APPENDIX A

Calibration Curves and Cumulative Drug Releases

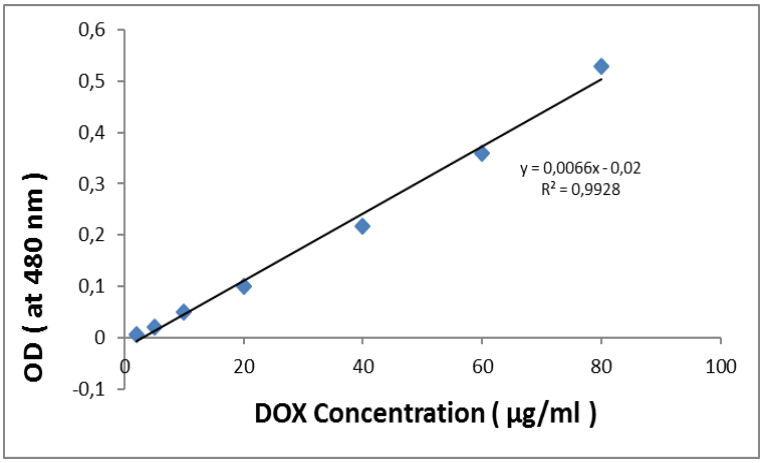

Figure A.1 Calibration curve for doxorubicin in pH 4.2 buffer

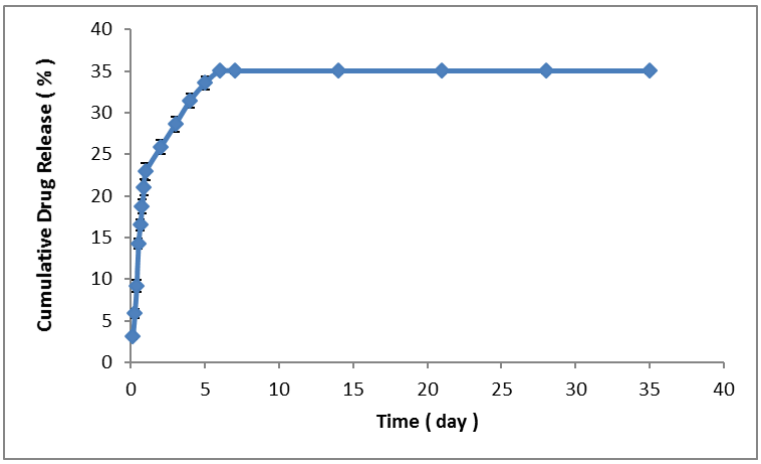

Figure A.2 Cumulative drug release at pH 4.2 (Experiments were performed in triplicates.)

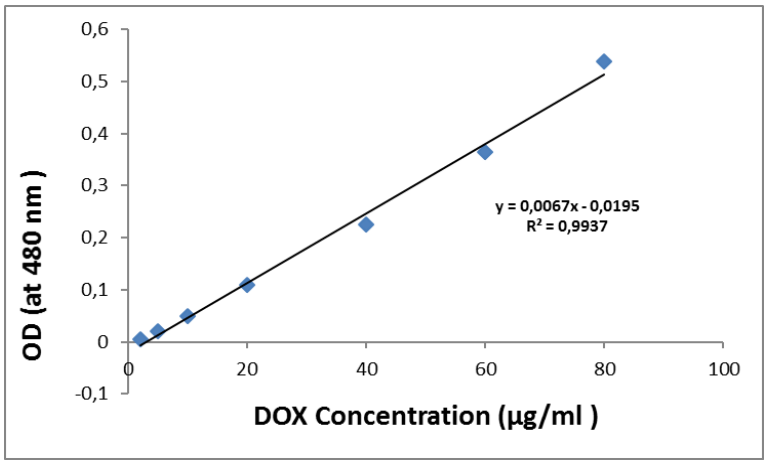

Figure A.3 Calibration curve for doxorubicin in pH 5.2 buffer

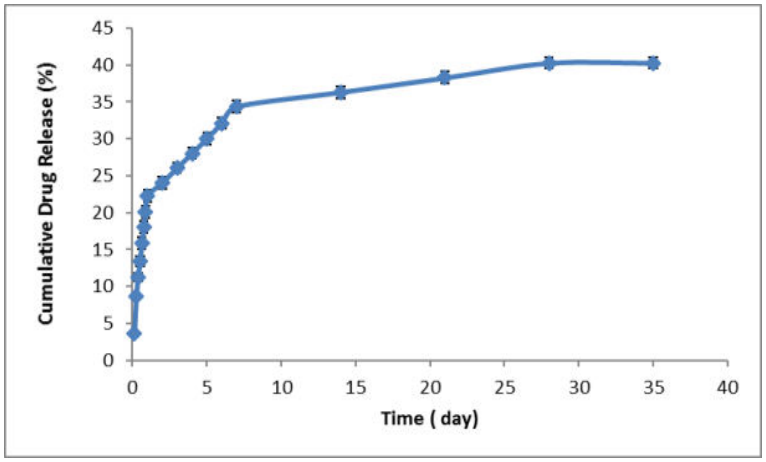

Figure A.4 Cumulative drug release at pH 5.2 (Experiments were performed in triplicates.)

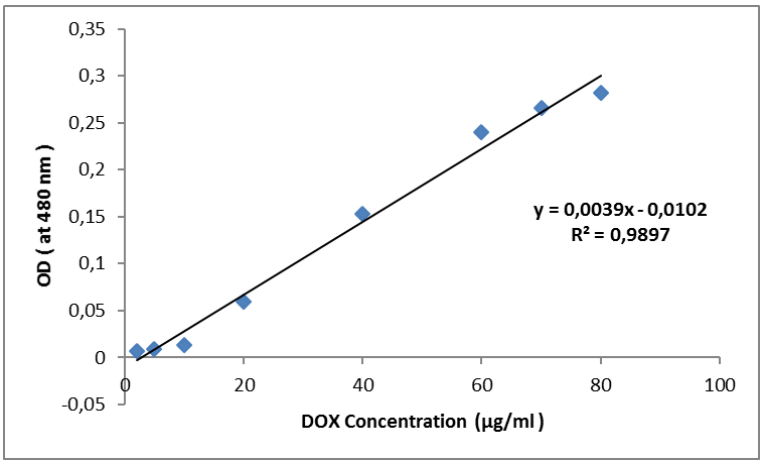

Figure A.5 Calibration curve for doxorubicin in water

APPENDIX B

Drug Loading

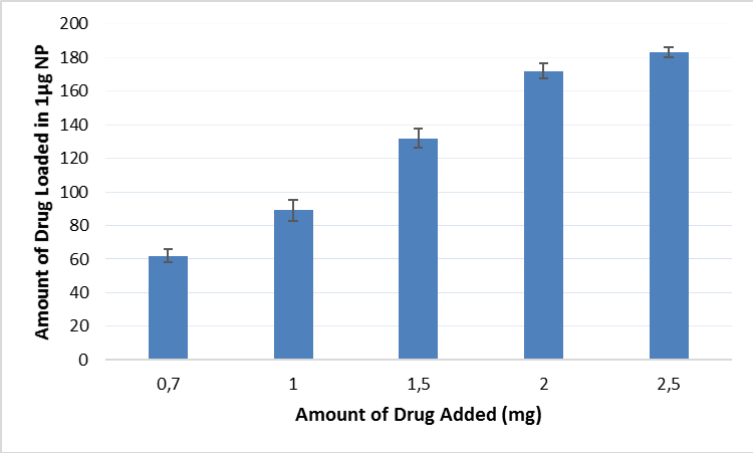

Figure B.1 Drug loading to nanoparticles depending on added drug amount (Experiments were performed in triplicates.)

APPENDIX C

Cytotoxicity of Doxorubicin on MCF-7 and MCF-7/Dox Cells

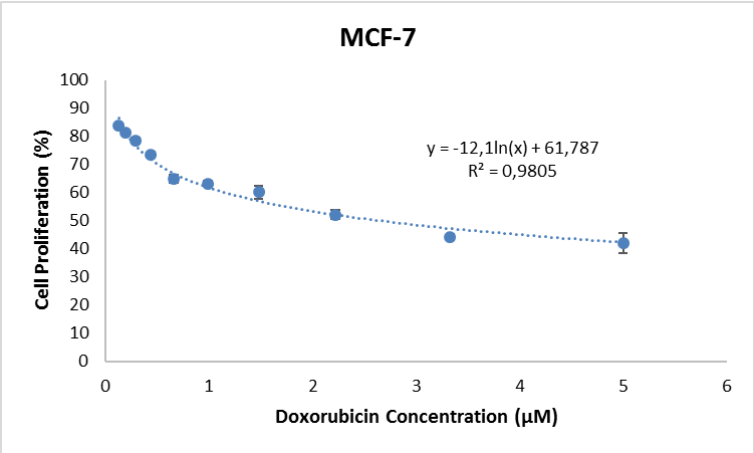

Figure C.1 Cell proliferation profile of MCF-7 treated with doxorubicin (Experiments were performed in duplicates.)

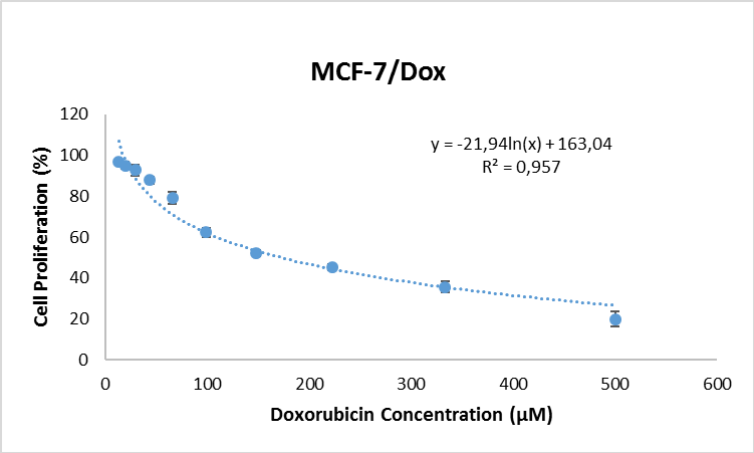

Figure C.2 Cell proliferation profile of MCF-7/Dox treated with doxorubicin (Experiments were performed in duplicates.)

APPENDIX D

Cytotoxicity of NPT20 and Dox NPT20 on MCF-7 Cells

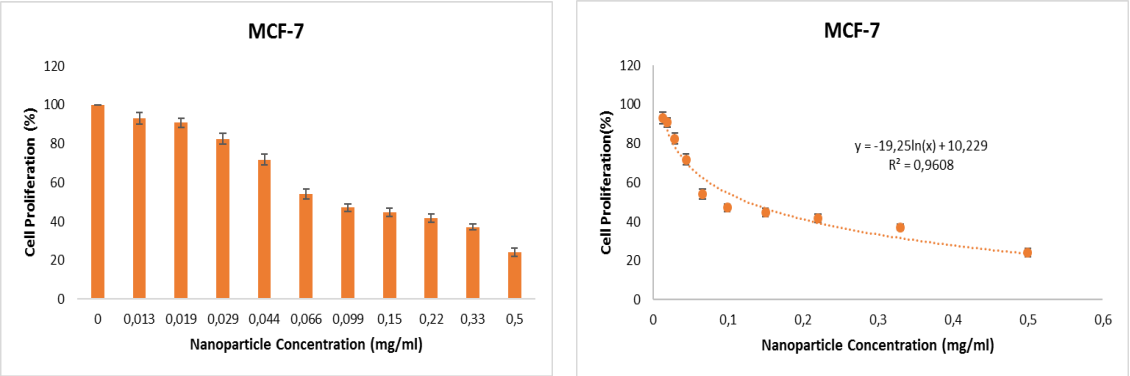

Figure D.1 Cell proliferation profile of MCF-7 treated with Dox NPT20 (Experiments were performed in duplicates.)

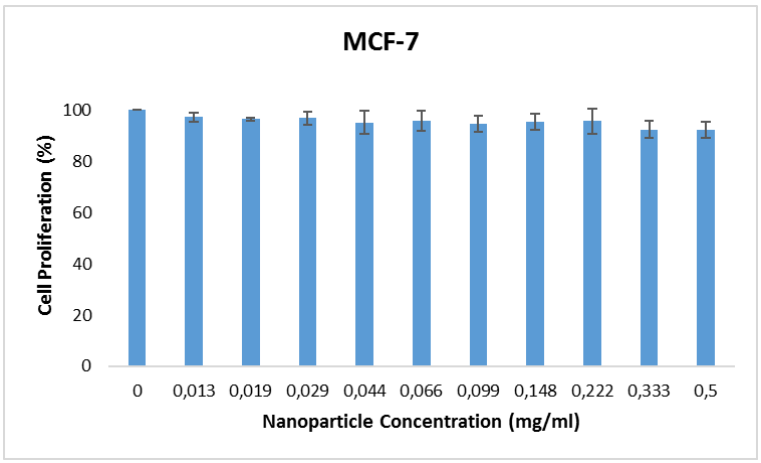

Figure D.2 Cell proliferation profile of MCF-7 treated with NPT20 (Experiments were performed in duplicates.)

APPENDIX E

Cytotoxicity of NPT0 and Dox NPT0 on MCF-7 Cells

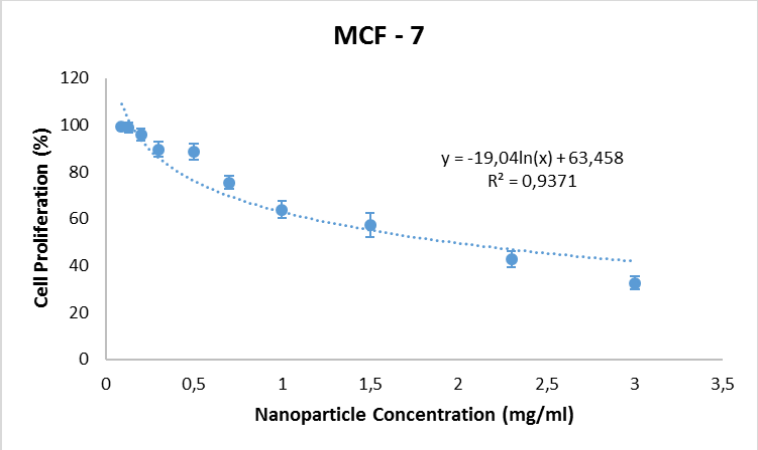

Figure E.1 Cell proliferation profile of MCF-7 treated with Dox NPT0 (Experiments were performed in duplicates.)

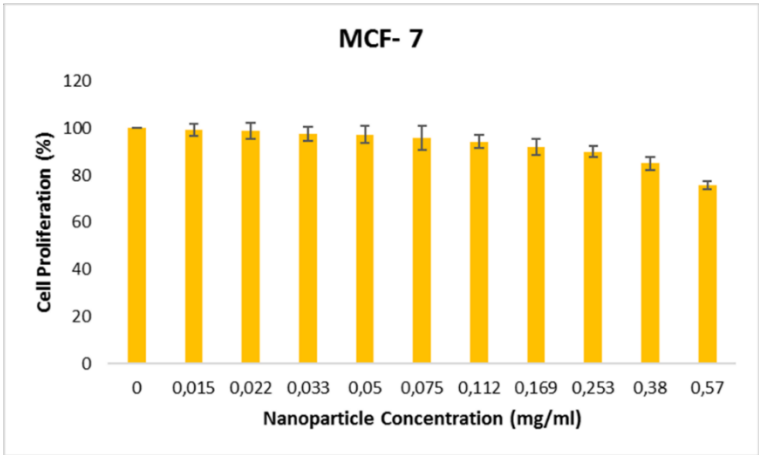

Figure E.2 Cell proliferation profile of MCF-7 treated with Dox NPT0 containing same amount dox with Dox NPT20 (Experiments were performed in duplicates.)

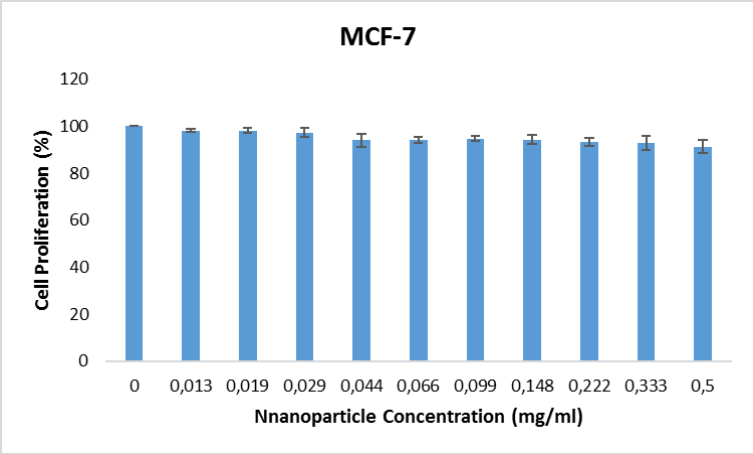

Figure E.3 Cell proliferation profile of MCF-7 treated with NPT0 (Experiments were performed in duplicates.)

APPENDIX F

Cytotoxicity of NPT20 and Dox NPT20 on MCF-7/Dox Cells

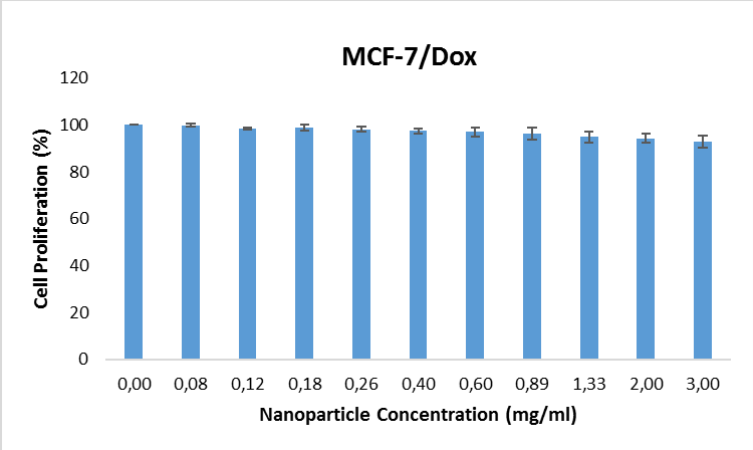

Figure F.1 Cell proliferation profile of MCF-7/Dox treated with NPT20 (Experiments were performed in duplicates.)

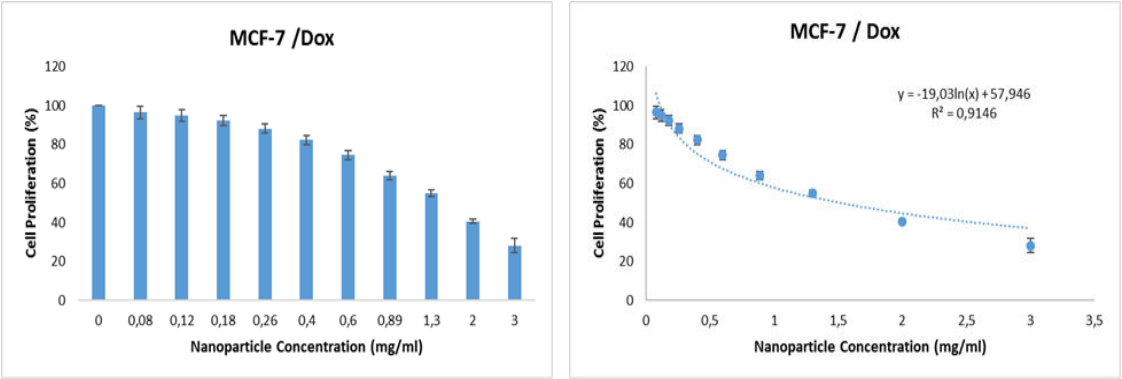

Figure F.2 Cell proliferation profile of MCF-7/Dox treated with Dox NPT20 (Experiments were performed in duplicates.)

APPENDIX G

Cytotoxicity of NPT0 and Dox NPT0 on MCF-7/Dox Cells

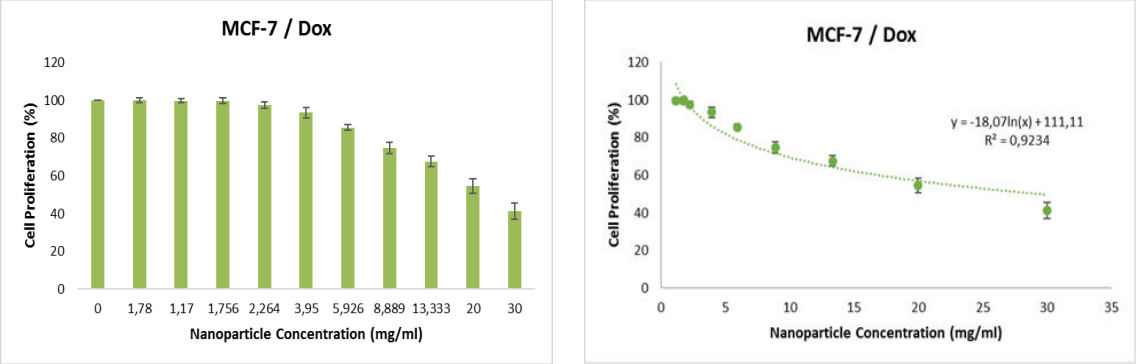

Figure G.1 Cell proliferation profile of MCF-7/Dox treated with Dox NPT0 (Experiments were performed in duplicates.)

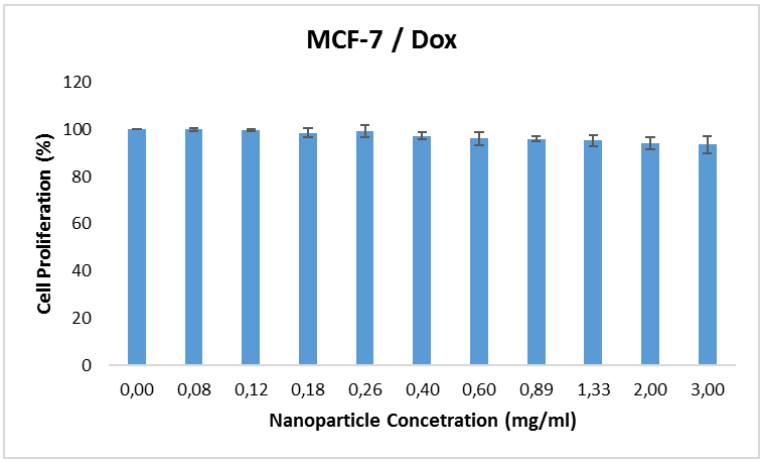

Figure G.2 Cell proliferation profile of MCF-7/Dox treated with NPT0 (Experiments were performed in duplicates.)

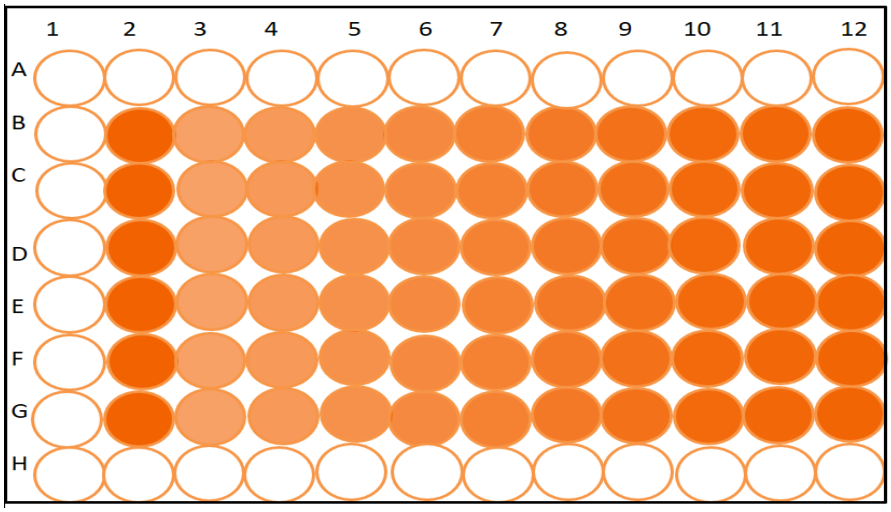

Figure G.3 96-well plate image at the end of XTT cell proliferation assay performed.

The intensity of florescence is proportional with live cell number. Column 1 is medium control and 2 is cell control. Line A and H contain only drug/ nanoparticle and medium. Column 3 contains highest dose of drug, and columns other than 1,2,3 composed of cell, medium and serially diluted drug/nanoparticle.